UNIVERSITA' DEGLI STUDI DI TORINO

Dipartimento di Biotecnologie Molecolari e Scienze per la Salute

Dottorato di ricerca in

MEDICINA MOLECOLARE

Ciclo XXIX

miR-148b as a candidate for targeted cancer therapy

Candidato: **Lorena QUIRICO**

Tutor: **Prof. Daniela TAVERNA**

Coordinatore del dottorato: **Prof. Francesco NOVELLI**

Anni Accademici 2014-2017

This work was performed at the Molecular Biotechnology Center (MBC), at the Università degli Studi di Torino (Torino).

I am grateful to my PhD Tutor Prof. Daniela Taverna, for allowing me to work in her lab, to start this project and for her expert guidance, encouragement and advice she has provided throughout these years.
I also would like to acknowledge all the members of Daniela Taverna's group, who shared with me happy moments and alwayso support me even in difficult moments. You are nice collegues and friend!. Dr. Francesca Orso, for teaching me many things, for assisting me with my experiments (in particular for performing the in vivo part), her help and advices were fundamental for my work. I gratefully thank also the other members of the group: Federico Virga, Annamaria Massa, Désirée Baruffaldi, Sofia Bertone, Alberto Dalmasso and past members Daniela Dettori and Roberto Coppo who both helped me for the in vivo experiments, Monica Raimo, Irene Vercellino, Camilla Paoletti, Elisa Penna and Daniela Cimino.

I thank my PhD advisors Prof. Enzo Calautti, Prof. Giorgio Merlo, Prof. Valeria Poli and Prof. Emilia Turco for the scientific feedback and suggestions that they gave me every year.

Thank to Alessandro Fatica and Gerolama Condorelli for reviewing this thesis.

This work was made possible thanks to the collaboration with many people: Michael Stadler (FMI, Basel, CH) for miR-148b sponges design; Elena Grassi and Prof. Paolo Provero (MBC, Torino, IT) for bioinfomatics analyses on miR-148b; Dr Marco Forni (MBC, Torino, IT) for the help with the histology interpretation; Angela Elia (MBC, Torino, IT) for GFP FACS analysis; Laura Conti and Prof. Federica Cavallo (MBC, Torino, IT) for FACS analysis on mammosphere; Emiliano Panieri and Stefania Rocca (MBC, Torino, IT) for FACS analysis; Lei Xu and Prof. Richard Hynes (MIT, Cambridge, MA, USA) for the melanoma metastatic cell variants; Prof. Luca Primo (IRCC, Candiolo, Torino, IT) and Prof. Maria Felice Brizzi (Molinette hospital, Torino, IT) for the HUVECs for transendothelial migration experiments. A special thank goes to Prof. Vittorio de Franciscis and Carla Lucia Esposito (CNR, Napoli, IT) for the constant advices, help, optimism and even reagent support they put in collaborating with me for the aptamer part of this work.

SUMMARY

ABSTRACT

MicroRNAs (miRNAs) are small non-coding RNAs that act as negative regulators of gene expression and play a central role in tumor progression, in fact, aberrant miRNA levels influence gene networks involved in tumorigenesis and metastasis formation. Therefore, a therapeutic intervention that controls miRNA expression could be powerful in the treatment of neoplasia. We previously demonstrated the prometastatic role of miR-214 in malignant melanomas via the coordination of a novel pathway including, among several players, the small non-coding RNA, miR-148b. In parallel, we evidenced an antimetastatic function of miR-148b in breast cancers, due to direct targeting of adhesion-molecules and their signaling players. Based on those findings, we explored the possibility to block melanoma and breast cancer dissemination by simultaneous miR-214 inhibition and miR-148b overexpression in cells. Here, I present results showing that the dual miR-214/miR-148b targeting successfully reduced extravasation and metastasis dissemination of tumor cells *in vivo*, by impairing the expression of the adhesion receptors ALCAM and ITGA5 and some of their downstream players. Our investigation underlines the relevance of the molecular network involving miR-214 and miR-148b-direct targets in the control of metastasis formation, therefore modulation of these miRNAs offers considerable therapeutic potential. To this aim, we explored the use of nucleic acid aptamers as carriers for cell-targeted delivery of miR-148b. Precisely, we used an aptamer that binds to and antagonizes the oncogenic receptor tyrosine kinase axl (highly overexpressed in various tumor cells) to deliver miR-148b to breast, melanoma and lung cancer cell lines. The efficacy of the conjugated chimeric aptamers was appreciated when migration of tumor cells through a porous membrane or an endothelial cell monolayer or invasion of a matrigel layer resulted impaired compared to controls. Moreover, expression of known miR-148b direct target genes was reduced. Relevantly, axl-148b chimeric aptamers inhibited mammosphere formation *in vitro*, promoted apoptosis and necrosis in primary tumors and blocked tumor cell dissemination in mice. In conclusion, our data demonstrate that the cascade of events involving miR-214 and miR-148b in the control of melanoma and breast cancer progression can be exploited for therapeutic interventions with specific delivery. We believe chimeric aptamers are promising targeted therapy tools that can help to inhibit metastatic traits on their own or in combination with traditional anti-cancer therapies.

INTRODUCTION

1. What are miRNAs?

miRNAs are short (20-22 nt), non-coding RNAs that have emerged as important post-transcriptional negative regulators of gene expression *via* binding to the 3'untranslated region (3' UTR) of their target mRNAs, causing a block of translation and/or mRNA degradation.

The history of miRNA started in 1993 with the characterization of lin-4 in the control of developmental timing of larval *C. elegans* (1). For seven years, there were no other hints that a similar regulatory mechanism mediated by non-coding RNAs was present in *C. elegans* or other metazoans. However, things changed in 2000, when another *C. elegans* small RNA regulatory molecule, let-7, was characterized by the Ruvkun's lab. Similarly to lin-4, let-7 was essential for cell fate transitions from the larval to adult stages (2). Nowadays, we know that miRNAs are present not only in *C. elegans*, but also in other metazoas, plants, protozoa and helmints (3–5).

Today, almost 2000 miRNAs have been identified in the human genome and it is estimated that 1-4% of genes encode miRNAs, and that, as reported by predictions, can control the activity of nearly 60% of the protein-coding genes (6–8). Such abundance made necessary to have a proper miRNA nomenclature. miRNAs name can be preceded by three letters specific for the organism, with "hsa" referring to human and "mmu" to mouse. Then, they have a prefix, miR, followed by a unique identifying number that is sequential, meaning that a newly discovered miRNA has a higher number. A lower case letter following the number denotes closely related mature sequences. Few exceptions were described before the advent of the naming system, such as lin-4 and let-7 from *C. elegans*. Moreover, miRNAs that come from the same pre-miR, but originate either from the 3' or 5' end are denoted with -3p or -5p suffix (9).

2. miRNAs biogenesis and mechanism of action

miRNA sequences are found in intergenic positions of the genome or are portions of introns or exons of protein-coding genes and can also be organized in families of redundant genes (10).

Their biogenesis is a complex process (Fig. intro 1). miRNAs genes are mainly transcribed by RNA polymerase II (in this case they are capped and polyadenylated) or III into primary transcript precursors (pri-miRNA) (7,11). A pri-miRNA may be hundreds to thousands nucleotides long, often contains sequences for different miRNAs and includes a ~33 base-pairs hairpin stem, a terminal loop and two single-stranded flanking regions located upstream and downstream of the hairpin (12,13).

The pri-miRNA is next endonuclealitically cleaved by the nuclear complex formed by the RNase III type enzyme Drosha and Pasha and in this way the long pri-miRNA is processed as ~70 nt hairpin called pre-miRNA (8,10,11). Some pre-miRNAs bypass Drosha cleavage because they are produced from very short introns (mirtrons) (8,10,11).

The resulting precursor is then actively exported from the nucleus into the cytoplasm by Exportin-5 (XPO5) that acts in complex with its cofactor Ran-GTP. In the cytoplasm, the RNase III Dicer recognizes the pre-miRNA, cleaves off its loop and generates a 20-22-nt miRNA duplex with two nucleotides protruding at each 3'end. Generally, the -5p strand, also called the "guide" strand, works as mature miRNA, whereas the -3p strand (the "passenger") is degraded, but, sometimes, both arms of the pre-miRNA may generate functional miRNAs (12).

At this point, the functional strand of the mature miRNA is loaded into ribonucleoprotein complexes called miR-induced silencing complexes (miRISC) together with the proteins from the Argonaute family (Ago 1-4 in mammals). AGO2 is the only AGO that functions in RNAi: its RNaseH-like P-element induced wimpy testis (PIWI) domain can cleave the mRNA at the center of the duplex (8,11,14). Apart from AGO family, miRISC contains other components, that act as translation modulators or as regulatory factors, or are important during complex assembly (11). Once loaded onto the miRISC complexes, mRNA is silenced by cleavage, translational repression or deadenylation (3,13).

The complementarity of the miRNA to the mRNA determines whether the mRNA is cleaved or productive translation is inhibited. With a high degree of complementarity, RISC complex will cleave the mRNA; in contrast, if the complementarity is not enough for cleavage but still fitting,

translation will be repressed. It is also important which specific Ago protein incorporates the miRNA, for example Ago2 is responsible for RISC cleavage activity (15).

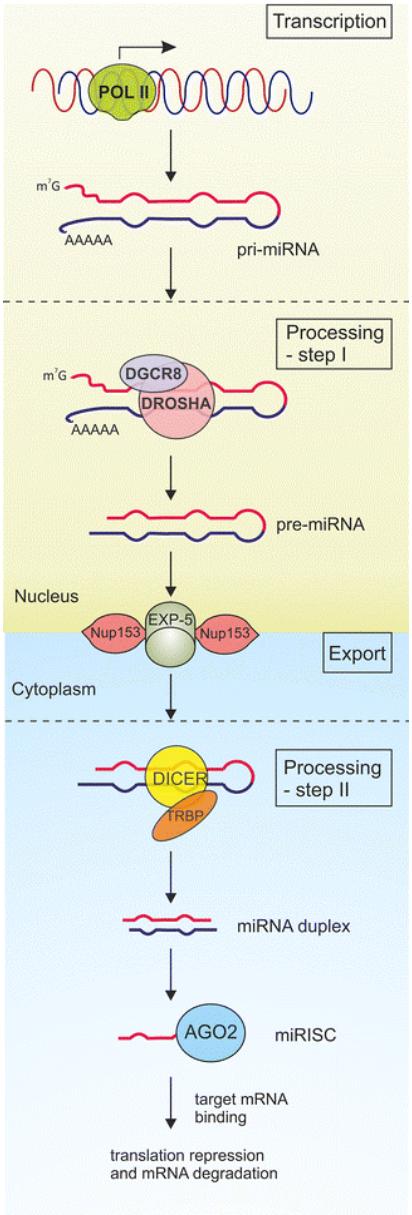

Figure intro 1 - The biogenesis of miRNA begins with RNA polymerase II-dependent transcription that generates pri-miRNA. During the first processing step, pri-miRNAs are cropped to pre-miRNAs by the microprocessor complex composed of Drosha and DGCR8. Next, pre-miRNAs are transported from the nucleus to the cytoplasm by Exportin - 5/RanGTP complex where they undergo processing by the RNase III protein—Dicer with the cofactor protein TRBP. Stem-loop structure of pre-miRNA is cleaved to the short miRNA duplex that is approximately 22 nt in length. In the next step, the miRNA is incorporated into the RNA-induced silencing complex (RISC), and following unwinding and strand selection, the mature miRNA can recognize the target sequence that is localized mainly in the 3′ UTRs of transcripts. Binding of the miRISC to the target results in translational repression and/or deadenylation and degradation. (Modified from Olejniczak et al., 2018)

miRNAs and their mRNA targets interact by base pairing (Fig. intro 2). In plants, miRNAs bind to mRNAs with nearly perfect complementarity, thus inducing endonucleolytic cleavage and mRNA degradation by a RNAi-like mechanism (8,11). Conversely, in metazoan miRNAs match with their targets imperfectly (8,11). There is a perfect and contiguous canonical base pairing of miRNA nucleotides 2-8 that represent the 'seed' region, that allows the miRNA–mRNA association. Repression is strongly affected by GU pairs or mismatches and bulges in this region. An A residue across position 1 of the miRNA, and an A or U across position 9 improves efficiency, although they do not need to base pair with miRNA nucleotides. Furthermore, bulges or mismatches must be present in the central region of the miRNA-mRNA duplex, precluding the Argonaute-mediated endonucleolytic cleavage of mRNA. Finally, reasonable complementarity to the miR 3′ half is necessary to stabilize the interaction. Mismatches and bulges are generally tolerated in this region, although good base pairing, particularly to residues 13–16 of the miRNA, becomes optimal when matching of the seed region is suboptimal. There are other factors that can improve site efficacy including an AU-rich neighborhood and, for long 3′ UTRs, a position that is not too far away from the poly(A) tail or the termination codon (11).

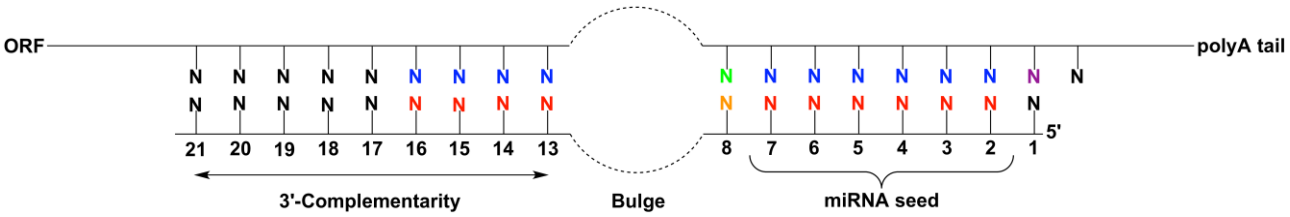

Figure intro 2 - Key structural features of an miRNA binding site. Of critical importance is a region that is highly complementary to the seed region (nucleotides 2 through 7, shown in red and blue) of the miRNA. Greater efficacy is obtained if the mRNA bears an A across from miRNA position 1 (shown in purple), and if the mRNA and miRNAs are also complementary at miRNA position 8 (shown in green and orange). An uncomplementary bulge is usually present in the region corresponding to miRNA positions 9 through 12, followed by a second region of complementarity in the 3' end of the miRNA, especially corresponding to positions 13 through 16 (shown in red and blue). (https://www.vanderbilt.edu/vicb/DiscoveriesArchives/microRNAs_gene_expression.html)

Several mechanisms through which miRISC can inhibit the expression of target mRNA have been proposed: (a) miRISC can prevent mRNA circularization; (b) miRISC can compete with translation factor eukaryotic initiation factor 4E (EIF4E) for binding to the mRNA 5′ cap structure; (c) miRISC can inhibit the assembly of the 60S ribosomal subunit with the 40S preinitiation complex causing ribosome stalling (11,16). AGO-bound miRNA/mRNA complexes are then stored and degraded in sub-cytoplasmatic granular compartments (P-bodies) that are involved in mRNA catabolism, deadenylation and degradation (11,17).

Besides functioning inside the cells, miRNAs are also present and abundant in the bloodstream and can act in neighbouring cells or at more distant sites in a hormone-like fashion, so they are involved in short- and long-range cell-cell communication. In the past few years, the "competing endogenous RNA" (ceRNA) hypothesis was developed, according to which these ceRNAs act as sponges for a miRNA thorough their miRNA response elements (MRE), as a consequence, all the target genes of the respective miRNA family, are de-repressed. The first hint for such a ceRNA crosstalk has been found for the tumor suppressor gene PTEN and its pseudogene PTENP1 which are targeted by and thus can compete for the same set of miRNAs (miR-17, -21, -214, -9, and -26 families) (18).

3. miRNAs and diseases

Taking into account that each miRNA is able to regulate the expression of approximately several hundred target genes, the miRNA apparatus is involved in controlling gene expression of a large quota of mammalian transcriptomes and proteomes. Consequently, miRNAs may be involved in developmental and physiological processes, such as the development and function of many tissues and organs. As a consequence of miRNAs impact on biological processes, mutations affecting miRNA function are expected to have a pathogenic role in human genetic diseases, similar to protein-coding genes. The main kinds of these mutations are: (a) mutations affecting miRNA sequences (e.g. point mutations, deletions or duplications); (b) mutations in in the 3' UTR of mRNAs that remove or generate a new target recognition site for a specific miRNA; and (c) mutations in genes involved in miRNA processing and function (19). It has been shown that miRNA do indeed play a strong pathogenic role in the development of several genetic diseases such as Tourette's syndrome (20) and Fragile X syndrome (21).

miRNAs are also involved in the regulation of heart function and cardiovascular system in general (22). Their role in the heart has been addressed by conditionally inhibiting miRNA maturation in the murine heart, and has revealed that miRNAs play an essential role during its development. miRNA expression profiling studies demonstrate that levels of specific miRNAs change in diseased human hearts, pointing to their involvement in cardiomyopathies. Furthermore, studies on specific miRNAs in animal models have identified distinct roles for miRNAs both during heart development and under pathological conditions, including the regulation of key factors

important for cardiogenesis, the hypertrophic growth response, and cardiac conductance (23,24). In particular, in adult cardiac tissue, miR-1, miR-16, miR-27b, miR-30d, miR-126, miR-133, miR-143, and the let-7 family are abundantly expressed (25). Studies have shown that miR-1, miR-133, and miR-208 are important regulators of heart development and myocyte differentiation (26,27). Furthermore, deregulation of miR-1 and miR-133 was reported in heart failure (28,29).

miRNA are also able to regulate the nervous system. Neural miRNAs are involved at various stages of synaptic development, including dendritogenesis, synapse formation and synapse maturation (30). miRNAs expression in brain changes during brain development: some miRNAs are more abundant during early development in mammalian brain, other are less during later development (31). Recent progresses from studies characterizing miRNA functions in neurodegenerative diseases (ND) have shed new light on disease pathogenesis. A systemic miRNA profiling in peripheral blood mononuclear cells from patients suffering of Parkinson's disease, associated miR-30b, miR-30c, and miR-26a with the susceptibility of the pathology (32). Similarly, the expression of miR-29a, miR-29b-1 and miR-9 was significantly decreased in patients with Alzheimer's disease (AD) (33), resulting in abnormally high expression of their target BACE1, a protein with an important role in AD pathogenesis (34).

Studies have shown that replication of hepatitis C virus (HCV) depends on liver-specific miR-122 expression (35). This miRNA regulates HCV by binding directly to two adjacent sites (seed site S1 and S2) in the 5'UTR of HCV RNA. miRNAs generally repress gene expression by binding to 3'UTR sites, this positive regulation of viral replication via a 5'UTR represents a novel function for miR-122 (36,37). It acts by moderately stimulating viral protein translation (38) and, in concert with Argonaute (AGO), by stabilizing and protecting the uncapped HCV RNA genome from degradation (39–41).

There are also evidences that miRNAs have a role in the regulation of immune functions and prevention of autoimmunity, but the precise mechanisms by which miRNA dysregulation could lead to pathogenesis in an autoimmune disease are still not clear. An abnormal expression of miR-155 and miR-146 was reported in patients with Rheumatoid Arthritis (RA). In particular the level of these two microRNAs was higher in synovial tissues and fibroblasts isolated from patients with RA, compared to healthy controls (42). Another significant autoimmune disease is represented by Systemic Lupus Erythematosus (SLE). In a microarray analysis on miRNAs in SLE patients, seven miRNAs (miR-196a, miR-17-5p, miR-409- 3p, miR-141, miR-383, miR-112, and miR-184) were found to be downregulated while nine (miR-189, miR-61, miR-78, miR-21, miR-142-3p, miR-342, miR-299-3p, miR-198, and miR-298) upregulated relative to healthy people (43).

miRNA expression patterns can be disease-specific and hold great prognostic value. miRNAs were found to play key roles in important biological processes such as cell division and death (44), cellular metabolism (45), immunity (46) and cell movement (47). Alterations of these conditions, are frequent in cancer, the most prominent human disease with a clear role for miRNAs regulation. Next paragraph will focus on miRNAs and cancer.

4. miRNAs and cancer

Cancer is a multistep disease in which normal cells undergo genetic changes starting from a premalignant state (initiation), passing into invasive cancer (progression) that can disseminate throughout the body (metastatization). In particular, cancer cells acquire different biological capability: sustaining proliferative signaling, evading growth suppressors, resisting cell death, enabling replicative immortality, inducing and sustaining angiogenesis and activating invasion and metastasis (48). Specifically, metastasis is a complex process by which primary tumor cells invade adjacent tissue, enter the systemic circulation (intravasate), translocate through the vasculature, arrest in distant capillaries, extravasate into the surrounding tissue parenchyma, and finally proliferate from microscopic growths (micrometastases) into macroscopic secondary tumors (49).

miRNAs are involved in controlling a huge number of biological processes such as differentiation, proliferation, and apoptosis. Since the deregulation of these steps is a hallmark of cancer, it was hypothesized that mutations affecting miRNAs or their interactions with genes linked with cancer development (oncogenes and tumor suppressor genes) might bring to tumorigenesis (50). As a consequence, miRNAs can also behave as oncogenes or tumor suppressor genes, depending on the role of their target genes. Onco-miRs are generally gained in tumors and target tumor-suppressor genes and, *viceversa*, tumor suppressor miRNAs are downregulated or lost in cancer leading to the upregulation of their oncogenic targets (50,51). However, it is difficult to classify miRNAs as oncogenes or tumor suppressors due to the fact that their expression patterns vary in specific tissues and differentiation state. Moreover, it may not always be clear if altered miRNA patterns are a direct cause of cancer or rather an indirect effect of changes in the cellular phenotype. Additionally, the observation that a single miRNA controls several targets and that its effect depends on the pool of target genes that specific cells expresses (the ceRNA theory) could implicate that a single miRNA may act as a tumor suppressor in one context and as an oncogene in another (52,53).

Genome-wide studies have shown that human miRNA genes are frequently located in fragile chromosomal regions that are susceptible to amplification, deletion, or translocation during the course of tumor development (54).

miRNA misexpression has been well documented in cancer. In 2002, the first evidence about the involvement of miRNAs in cancer established that miR-15a/16-1 cluster is frequently deleted in patients with chronic lymphocytic leukemia (CLL). As a consequence, the antiapoptotic gene B-cell lymphoma 2 (BCL-2) was overexpressed, suggesting the potential role of the cluster as a tumor suppressor (55). After this first study, a great number of miRNAs have been found deregulated in various cancers (Fig. intro 3) including pancreatic (56,57), colorectal (56), prostate (58), cervical (59) and ovarian cancer (60), sarcomas (61) and neuroblastoma (62).

Figure intro 3 - miRNA abnormally expressed in human cancers - examples from several different publications (Giza et al., 2014)

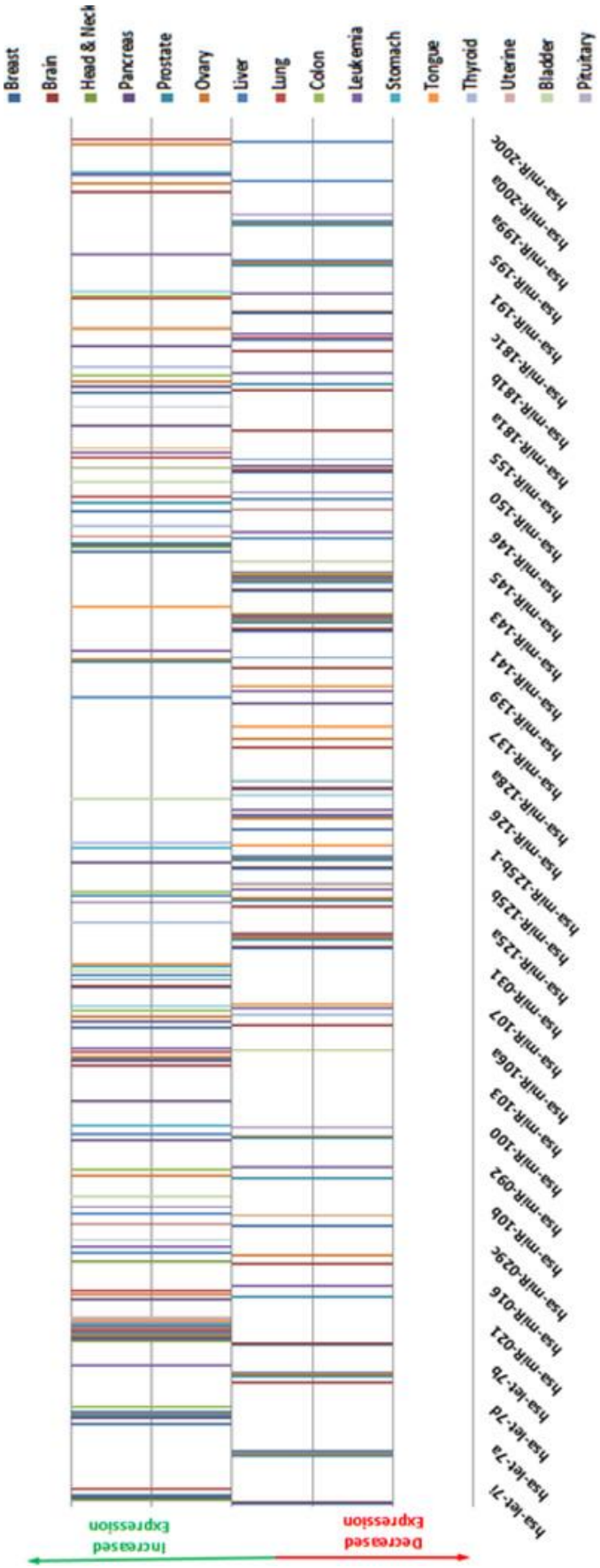
Breast
Brain
Head & Neck
Pancreas
Prostate
Ovary
Liver
Lung
Colon
Leukemia
Stomach
Tongue
Thyroid
Uterine
Bladder
Pituitary
hsa-let-7i
hsa-let-7a
hsa-let-7d
hsa-let-7b
hsa-miR-021
hsa-miR-016
hsa-miR-029c
hsa-miR-10b
hsa-miR-092
hsa-miR-100
hsa-miR-103
hsa-miR-106a
hsa-miR-107
hsa-miR-031
hsa-miR-125a
hsa-miR-125b-1
hsa-miR-126
hsa-miR-128a
hsa-miR-137
hsa-miR-139
hsa-miR-141
hsa-miR-143
hsa-miR-145
hsa-miR-146
hsa-miR-150
hsa-miR-155
hsa-miR-181a
hsa-miR-181b
hsa-miR-181c
hsa-miR-191
hsa-miR-195
hsa-miR-199a
hsa-miR-200a
hsa-miR-200c
Decreased Expression
Increased Expression

miRNAs may control primary tumors by targeting cell-cycle components, but also by extensively regulating multiple signaling pathways. Indeed, miR-486, downregulated in non-small-cell lung cancer, was demonstrated to alter cell proliferation and migration through insulin growth receptor (IGF) and PI3K signaling pathways by targeting IGF1, IGF1R and p85α (63). Evasion of apoptosis is another significant hallmark of tumor progression, which is believed to be regulated by miRNAs (64). In fact, cancer cells developed a variety of strategies to limit or circumvent apoptosis: among them, the loss of p53 tumor suppressor is very common. For example, Pichiorri *et al.* identified three miRNAs (miR-192, miR-194 and miR-215) transcriptionally activated by p53 to suppress Mdm2 expression via directly binding to its mRNA, thereby protecting p53 from degradation (65). The three miRNAs are positively regulated by p53 and their downregulation is fundamental in multiple myeloma development. A negative feedback regulation occurs between miR-122 and p53. In particular, miR-122 promotes p53 activity by targeting cyclin G1 (66). miR-34 family, which targets CDK4/6, cyclinE2 and MET and it is downregulated in pancreatic, colon, breast and liver cancers (67). miR-34a is a key regulator of tumor suppression. It controls the expression of a plethora of target proteins involved in cell cycle, differentiation and apoptosis, and antagonizes processes that are necessary for basic cancer cell viability as well as cancer stemness, metastasis, and chemoresistance (68).

Besides their role in promoting primary tumors, miRNAs have also been implicated in affecting tumor progression, including the lethal metastatic phase of the disease (69). Considering all the prometastatic miRNAs, miR-10b and miR-373 are particularly interesting. miR-10b is directly transcriptionally regulated by Twist1, a well-known inducer of the epithelial to mesenchymal transition (EMT). Overexpression of miR-10b in non-metastatic breast cancer cell lines promotes cell invasion and metastatic spread of transplanted tumors, as a consequence of targeting of the homeobox protein HOXD10. The miR-373 prometastatic potential has been validated in tumor transplantation experiments using breast cancer cells and has also been identified as a potential oncogene (together with miR-372) in testicular germ cell tumors (70). The miR-200 family was shown to affect EMT by inhibiting the expression of E-cadherin transcriptional repressors ZEB1 and ZEB2 (71). Other miRNAs involved in regulating metastasis include miR-9 and miR-212. miR-9 is activated by c-Myc and n-Myc, both of which directly bind to the *miR-9-3* locus. The expression level of miR-9 closely correlates with *MYCN* amplification, tumor grade and metastatic status in neuroblastoma tumors. In primary breast tumors of patients with metastatic disease, miR-9 expression is higher than in metastasis-free patients. miR-9 reduces the expression of E-cadherin in breast cancer cells via directly binding to its 3′-untranslate region (72). Inhibition of miR-9 using a ‘sponge’ suppresses metastasis formation in animal model,

implying that miR-9 silencing may represent a new therapeutic approach (73). miR-212 is significantly downregulated in human CRC tissues as a consequence of promoter hypermethylation and loss of heterozygosity (74). Comparing their differential expression in non-metastatic versus metastatic breast cancer cell lines, miR-126, miR-206, and miR-335 were also proposed to inhibit tumor progression: overexpression of these miRNAs can inhibit metastasis in a cell transplantation model, and reduced expression of miR-126 and miR-335 correlates with poor metastasis-free survival of breast cancer patients (75).

miRNAs are also involved in melanoma tumorigenesis (76) and malignant melanoma (77). In a previous work of our group, Penna, Orso et al. identified a new pathway, coordinated by miR-214 and including TFAP2C, ITGA3 as well as multiple surface molecules, which controls melanoma metastasis dissemination by increasing migration, invasion, extravasation and survival of melanoma cells (78). miR-211, miR-18b, miR-26, miR-573, miR-126-3p and -5p and miR-196a are poorly expressed during melanoma progression (79,80). In another work, miR-146a was identified as a key double-acting player in melanoma malignancy exerting a dual role in melanoma cells, favoring tumor cell growth, while inhibiting cell invasion. miR-146a expression was found strictly modulated across the various steps of melanoma progression: it was high in primary and distant-site tumors, where it promoted cell growth, but it dropped in circulating tumor cells (CTCs), suggesting the necessity for miR-146a expression to fluctuate during tumor progression in order to favor tumor growth and allow dissemination (81).

A growing list of reports suggests that miRNAs play an important role in breast cancer. Altered miRNAs expression in breast cancer was discovered by Iorio *et al*, who identified 29 miRNAs with aberrant expression patterns in breast cancer tissue compared to normal one. Among the most significantly deregulated miRNAs, miR-10b, miR-125b and miR-145 were down-regulated and miR-21 and miR-155 were up-regulated (82). In our group, miR-148b was demonstrated to be downregulated in aggressive breast tumors, resulting a major coordinator of malignancy. In particular, miR-148b controls malignancy by coordinating a pathway involving the players of the integrin signaling, such as ITGA5, ROCK1, PIK3CA/p110α, and NRAS, as well as CSF1, a growth factor for stroma cells (83). Another work from our group used computational analysis of cancer gene expression datasets to identify microRNAs involved in cancer progression. From this study miR-223 demonstrated a prominent role in breast malignancy by decreasing migration, increasing cell death in anoikis conditions and sensitivity to chemotherapy when overexpressed. The analysis of miR-223 predicted targets revealed enrichment in cell death and survival-related genes and in pathways frequently altered in breast cancer (84).

In conclusion, emerging evidences suggest that miRNAs can function as crucial nodes within metastasis regulatory pathways. Due to their implication in tumor formation and progression, they may be considered as biomarkers for diagnostic or prognostic purposes and as targets for the development of therapeutic tools for cancer treatment.

5. miRNAs as therapeutic tools

miRNA-based therapy field is expanding as showed by the growing literature about this topic. Considering that the main issue of the targeted therapy is the *in vivo* delivery, it is essential to identify safe, selective and efficient delivery of miRNA modulators to the tumor sites avoiding the off-target effects generated when miRNAs entered in non-target tissues. The main problems to overcome are the degradation by serum RNases, the half-life in circulation due to renal and liver clearance and lysosomal degradation (85). Moreover, interactions between miRNAs and the cell membrane are hampered by charge repulsion, causing poor cellular uptake. Consequently, translating *in vivo* miRNA delivery either requires a chemical modification or formulation into delivery systems (Fig. intro 4).

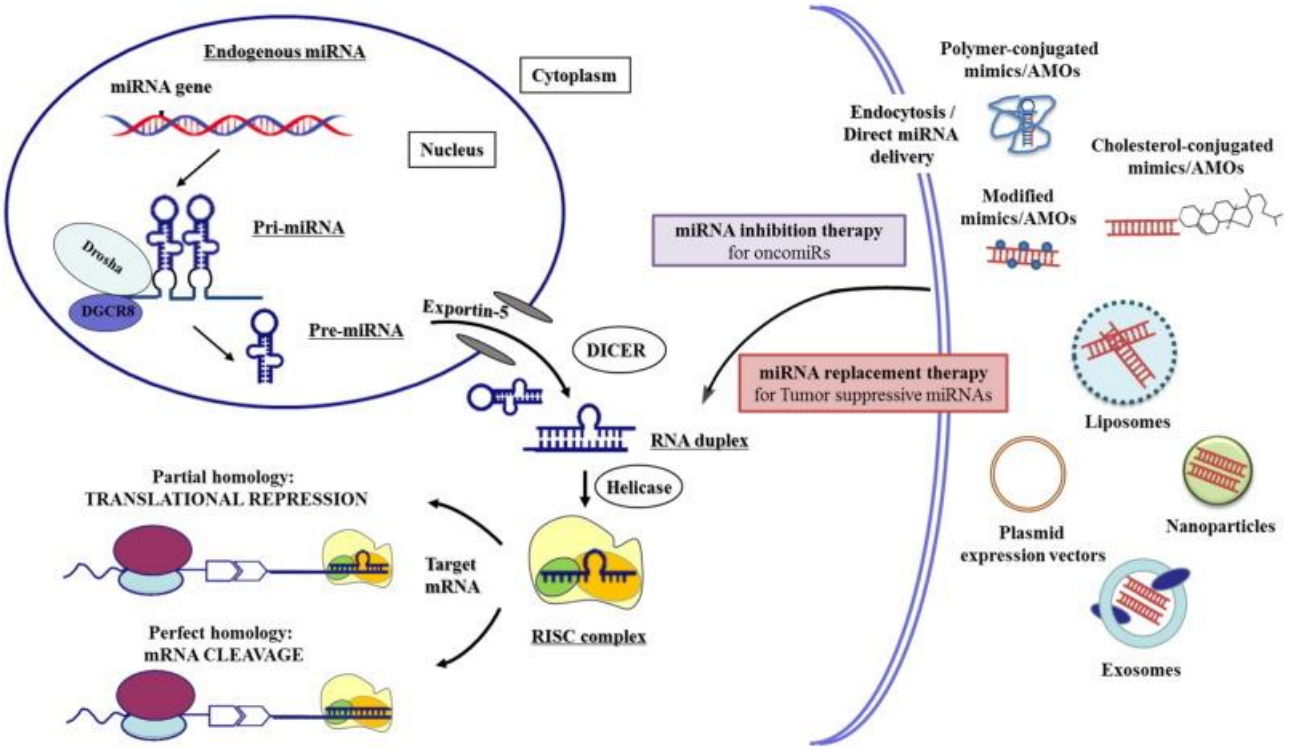

Figure intro 4 - miRNA mechanism and modulation. Canonical biogenesis and processing of miRNAs and mechanism of RNAi-regulated gene silencing is presented. Additionally, the several mechanisms of delivery of miRNA and therapeutic agents are also presented. (Shah et el., 2016)

The most common approaches employed to increase miRNAs function are miRNA mimics and expression vectors coding-miRNAs (86,87). Conversely, the strategies to block oncogenic miRNAs are ASO (antisense oligonucleotides), LNA (Locked Nucleic Acids)-antimiR, AMO (anti-miR oligonucleotides), antagomiR (88) and miRNA-sponges (89). The small size of miRNAs inhibitors and their possibility to be chemically modified, made possible the development of naked antagomirs. In particular, two different miR-122 inhibitors were developed to treat chronic hepatitis C: single locked nucleic acid molecules (Miravirsen, Santaris Pharma) and an antagomiR conjugated to a hepatocyte-specific ligand acting as a targeting mojety (GalNac-miR122 or RG-101, Regulus Therapeutics). Specifically, the compound of Regulus Therapeutics was tested in patients with chronic HCV genotype 1, 3, and 4 infection. The results showed that a dose of 2 mg/kg or 4 mg/kg was well tolerated and suggested an antiviral effect in HCV genotype 1, 3, and 4 infection. Importantly, three patients had undetectable HCV RNA level at 76 weeks after a dose of RG-101. This study was the first to suggest that an anti-miRNA oligonucleotide linked to an N-acetylgalactosamine structure might have clinical efficacy (90). In June 2016, RG-101 was placed on clinical hold following the Company's submission of a serious adverse event (SAE) of jaundice. On January 27, 2017 the company announced that it received written communication from the U.S. Food and Drug Administration (FDA) that the clinical development program for RG-101 remains on clinical hold (http://ir.regulusrx.com/news-releases/news-release-details/regulus-announces-continuation-rg-101-clinical-hold). Miravirsen, the other compound in clinical trial for Chronic Hepatitis C (CHC), various doses of administration resulted in a substantial and prolonged decrease in plasma miR-122 levels and did not affect plasma levels of other miRNAs in CHC patients (91). Fig. intro 5 shows miRNAs molecules that are in preclinical and/or clinical trial and their status of clinical trial.

Figure intro 5 - Status of various miRNA Therapeutics under Clinical Trials (Modified from Chakraborty et al., 2017).

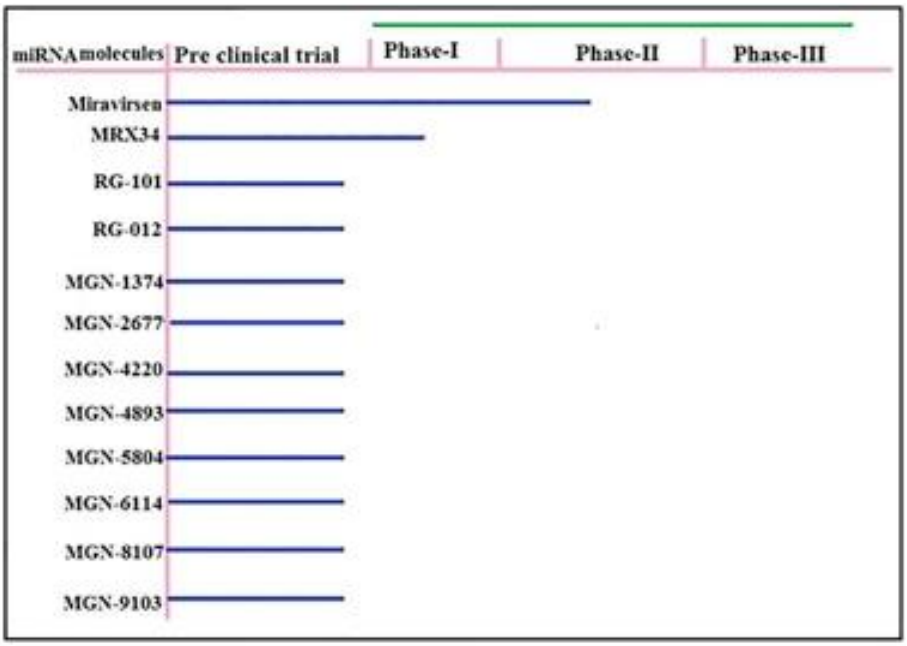

In order to make more effective the mentioned molecules, delivery systems based on viral or non-viral moiety are currently under investigation. Lentiviral, Adenoviral or Adeno Associated viral (AAV) vectors expressing miRNA antagonists or mimics were tested in several cancer models (92). They can transfer miRNAs sequences that enter into the target cells, then are transcribed and processed. Although efficient cellular delivery, viral vectors worry because of genomic integration of Lentiviruses that can trigger the expression of oncogenes, or immunogenicity and the transient nature of miRNA expression for adeno or adeno-associated viruses (93).

Non-viral delivery systems rely on the miRNA inability to cross biological membranes due to their hydrophilicity and negative charge. Therefore, a widely used system is the incorporation of the miRNAs in positively charged vehicles such as cationic lipids or polymers resulting in a positively charged final complex. Liposomes are amphiphilic molecules composed of phopsholipids that resemble the membrane of a human cell. This enable them to pass through cell membranes and release their cargo (94). The main issues of liposomes are low specificity or toxicity. To overcome these problems, liposomes are modified in their surface by coating with PEG or poLysaccharides (hyaluronan) (95,96). Ando et al., used liposomes modified with a PEG chain bearing the antiangiogenic vessel targeting peptide Ala-Pro-Arg-Pro-Gly (APRPG) conjugated with miR-499 to inhibit tumor growth of colon cancer cell xenograft (97). PEGylate liposome-polycation-hyaluronic acid (LHP) nanoparticles conjugated with a cyclic RGD peptide were used as carrier system for anti-miR-296 in vivo delivery (98). In order to repress neovascularization in breast tumors, Anand and colleagues used anti-miR-132 conjugated with liposomal nanoparticles composed of distearoylphosphatidilcoline (DSPC), cholesterol, dileoylphosphatidylethnolamine (DSPE)-

mPEG2000 modified with a DSPE-cRGD, targeting $\alpha_v\beta_3$ (99). To note, the first miRNA replacement therapy that arrived to clinical testing is represented by customized liposomes containing a miR-34 mimic (MRX34, Mirna Therapeutics). MRX34 delivery restores miR-34 expression in cancer cells, antagonizing self-renewal, migratory potential and chemo-resistance. On 20th September 2016, Mirna Therapeutics announced its decision to close the ongoing Phase 1 study of MRX34, its investigational microRNA therapy for multiple cancers. The Company voluntarily halted enrollment and dosing in the clinical study following multiple immune-related severe adverse events (SAE) observed in patients dosed with MRX34 over the course of the trial. The decision of to close the study came after a fifth, immune-related serious adverse event. This patient experienced severe (Grade 4) cytokine release syndrome and is undergoing treatment (https://www.businesswire.com/news/home/20160920006814/en/Mirna-Therapeutics-Halts-Phase-1-Clinical-Study). In April 2017 came out a a phase I study to assess the maximum tolerated dose (MTD), safety, pharmacokinetics, and clinical activity of MRX34 in patients with advanced solid tumors. Adult patients with solid tumors refractory to standard treatment were enrolled in a dose escalation trial. MRX34 was given intravenously twice weekly for three weeks in 4-week cycles. The study showed that MRX34 treatment with dexamethasone premedication was associated with acceptable safety and showed evidence of antitumor activity in a subset of patients with refractory advanced solid tumors (100).

Polymeric carriers are subdivided into natural or synthetic polymers. Naturally derived cationic polymers included atellocollagen, chitosan, protamine, dextran, gelatin, cellulose and cyclodextrin polymer (101–103). Synthetically derived cationic polymers include Polyethylenimine (PEI), poly L-lysin, poly amido amines, poly amino-co-ester and dendrimers (102,104). PEI-based delivery system is one of the most widely used polymers for gene delivery. It has the advantage of a rapid uptake and release of the nucleic acid (104); on the other hand this polymer in not biodegradable and cause cytotoxicity due to its interactions with blood components (105). It has been demonstrated that miR-7 loaded peptide/polymer-based delivery systems modified with a cRGP ligand targeting the integrins $\alpha_v\beta_3$ and $\alpha_v\beta_5$ systemically administered in mice bearing glioblastoma xenograft strongly reduced angiogenesis and tumor proliferation (106).

Another approach to deliver miRNAs into cells is the encapsulation inside biodegradable nanoparticles such as Poly (lactide-co-glycolide) (PLGA) or silica nanoparticles. This method allows the release of miRNAs after intracellular dissolution of the particles and has the advantage of being free from potentially toxic cationic materials (107). Nanoparticle-based systems have

achieved a limited effectiveness *in vivo* due to an accumulation in the liver, a toxicity that is dose-dependent and hepatotoxicity (108).

The major weakness of the mentioned miRNA delivery systems is the lack of specificity. It is necessary to find a tool that is able to recognize and deliver miRNAs exclusively to cancer cells or other pathological cells. Nowadays, thanks to the use of aptamers, it is possible to obtain a specific delivery.

6. Aptamers

Aptamers are short, single-stranded DNA or RNA oligonucleotides that selectively bind to their targets with high affinity and specificity by shape complementarity. In fact, the term "aptamer" derived from the latin word *aptus* (to fit) and the Greek one *meros* (part). (Fig. intro 6).

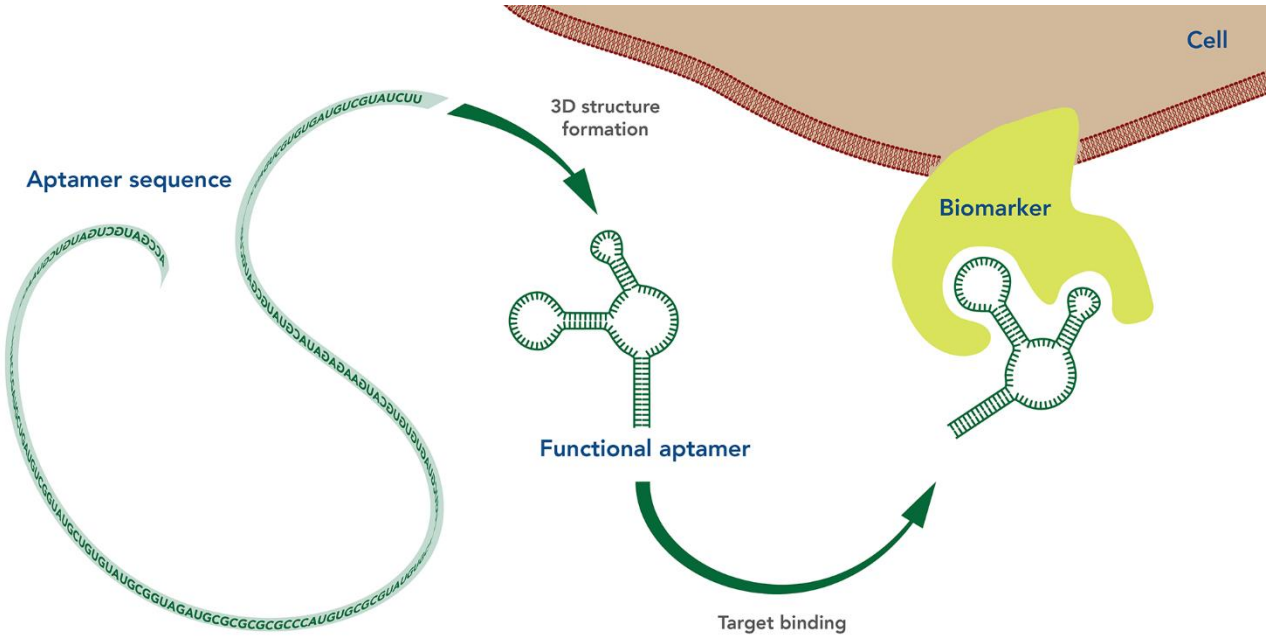

Figure intro 6 - Schematic representation of aptamers: aptamers sequence fold into its 3D structure and it binds its target molecules by shape compementarity (http://www.idtdna.com).

Aptamers were first isolated in 1990 by Ellington and Gold. Ellington reported a selection of RNA molecules that specifically bound to organic dyes (109), and Gold an RNA ligand that interacted with T4 DNA polymerase (110). Aptamers are 10-100 nucleotides long and they are generated

through a process called Systematic Evolution of Ligands by EXponential enrichment (SELEX). Over multiple rounds, SELEX allows the identification of functional oligonucleotides sequences able to recognize a specific target from a single-stranded DNA or RNA library. Some sequences of the library are folded into unique three-dimensional structures (stem, loops, hairpins, pseudoknots, bulges and G-quadruplexes). These three-dimensional interactions, together with hydrophobic and electrostatic interactions, hydrogen bonding, van der Waals forces, shape complementarity and base stacking, are fundamental for aptamer binding affinity and specificity (111).

Aptamers are very versatile molecules. RNA aptamers can sometimes substitute antibodies because they bind their targets with equal or better specificity (112,113). Therefore, aptamers conjugated to signaling molecules may be used in enzyme-linked immunosorbent assays (ELISAs), Western blot assays, and chip-based technologies (114–116). Davis et al. developed fluorophore-tagged RNA aptamers for flow cytometry (117). Another group reported a novel quantum dot–aptamer–doxorubicin conjugate as a targeted combined cancer imaging, therapy, and sensing system (118). Recently, Gold et al. created a new class of aptamers, the Slow Off-rate Modified Aptamer (SOMAmer). They contain chemically modified nucleotides and kinetic manipulations to support the construction of diagnostic tools. Multiplex SOMAmer affinity assays allow large-scale comparison of proteome profiles among discrete populations (119).

The capability of aptamers to virtually recognize any kind of biological molecules, make them tools able to rival antibodies as targeting agents (120,121). Aptamers against specific receptors of cell surface are emerging as powerful delivery tools able to drive, penetrate and accumulate therapeutic cargoes (siRNAs and miRNAs, toxins, radioisotopes, and chemotherapeutic agents) into receptor expressing target cancer cells. Several secondary reagent-aptamer chimeras have been created (Fig. intro 7).

Figure intro 7 - Aptamers as delivery agents. Aptamers can be used to selectively deliver secondary reagents to target cells that express aptamer targets on cell surface (left). Only this subset of cells will be exposed to the secondary reagent, whereas cells that do not express aptamer targets will not be affected (right) (Esposito et al., 2014).

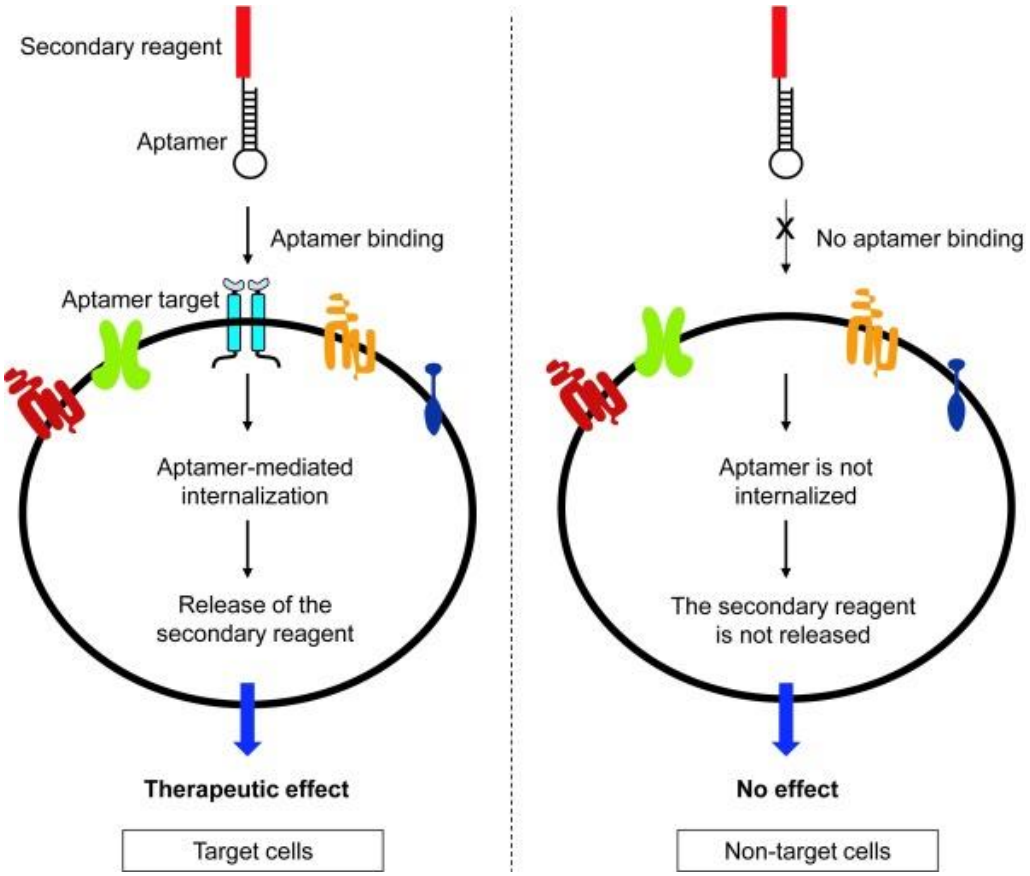

To date, aptamers against the extracellular domain of PSMA (A9 and A10) are well characterized to deliver siRNA to prostate cancer cells. PSMA–aptamers has been linked to siRNAs by approaches based either on non-covalent or covalent conjugation (122). Chu et al reported the development of a non-covalent approach employing a streptavidin bridge to link the A9 aptamer and the siRNA targeting laminin A/C and GAPDH. Treating LNCaP ($PSMA^{+}$) cells with the conjugates resulted in a inhibition of the genes comparable to those observed with conventional lipid reagents (123). Furthermore, the anti-nucleolin aptamer AS1411 was conjugated to siRNAs for snail family zinc finger 2 (SLUG) and neuropilin 1 (NRP1) genes (124). The number of aptamer-siRNA conjugates developed so far increased representing new promising therapeutic options (125).

Interestingly, some papers explored the use of aptamer to deliver microRNAs as cancer therapeutic Dai et al., developed a chimeric aptamer by binding MUC1 aptamer to miR-29b (Chi-29b) to increase chemosensitivity in an OVCAR-3 ovarian cancer model (126). In particular, intraperitoneal injections of the chimeras to tumor-bearing mice promoted apoptosis compared to controls. Rohde et al., reported a novel strategy to deliver miR-126 to endothelial and breast cancer cells by linking the miRNA to an aptamer for the ubiquitously expressed transferrin receptor (transferrin receptor aptamer, TRA). The conjugate was demonstrated to repress VCAM-1, a known miR-126 target,

improve endothelial cell sprouting, reduce proliferation and paracrine endothelial cell recruitment of breast cancer cells (127). Another aptamer used in a wide panel of studies was GL21.T that binds to the oncogenic tyrosine kinase receptor axl, which is expressed by various types of solid tumors (128). GL21.T is a well-characterized aptamer and was successfully linked to different miRNAs in order to overexpress (let-7g, miR-212, miR-137) them or downmodulate (miR-222) their levels (129–133).

Aptamers were not only used as carriers, but also to cover nanoparticles in order to target them to sick cells. Kim et al. developed a cancer targeting theranostics probe using an AS1411 aptamer - and miRNA 221 molecular beacon conjugated magnetic fluorescence (MF) nanoparticle (MFAS miR-221 MB) to simultaneously target cancer cells, image intracellularly expressed miRNA-221 and treat miRNA-221- involved carcinogenesis (134). Furthermore, the above mentioned anti-MUC1 aptamer in combination with miR-29 was also used to form an aptamer-hybrid nanoparticle bioconjugate delivery system to selectively deliver miRNA-29b to MUC1-expressing cancer cells. This functionalized nanoparticles led to antiproliferative effects and induction of apoptosis in a model of lung cancer (135).

The relatively new fields of aptamer chimeras is standing out as a new way to deliver therapeutic miRNAs with broad applicability to treat many human diseases. In particular, aptamer-miRNAs targeted therapy may become an effective weapon to treat cancer in the near future.

Considering that miRNAs are fundamental players in tumor progression, in the first part of this thesis we aimed to characterize miR-214-miR-148b axis for therapeutic interventions. We demonstrated a strong impairment of metastatization when miR-214 was inhibited and miR-148b was overexpressed. In the second part of this work, we selected miR-148b as a candidate for targeted cancer therapy. In particular, we explored the relevance for miR-148b based therapeutic interventions and used an aptamer to deliver it specifically to cancer cells.

AIM OF THE WORK

Cancer is among the most lethal diseases worldwide. In particular, the dissemination of primary tumor cells and the consequent metastasis formation at distant organs are the principal causes of cancer-related mortality. The currently available treatments (surgery, radio-, chemo-, and targeted therapy) mainly control primary tumors, but they only exert a mild effect on metastases, mostly because of resistance mechanisms activated by tumor cells. Thus, it is mandatory to identify key regulators of metastatic dissemination and develop new targeted therapies.

Research from our laboratory demonstrated that miR-214 promotes melanoma metastasis dissemination by increasing migration, invasion, extravasation, and survival of melanoma cells *via* a novel pathway involving over 70 direct or indirect targets, among them the metastasis suppressors, TFAP2 transcription modulators and ITGA3. In parallel, it was evidenced that another small non coding RNA, miR-148b opposes breast cancer progression, acting directly on the integrin signaling players such as ITGA5, ROCK1, and PIK3CA/p110α. More recently, a link between miR-214 and miR-148b was shown in the lab, for melanoma and breast cancer. In fact, it was demonstrated that miR-214 downregulates miR-148b in tumor cells partially via TFAP2C with the consequent upregulation of miR-148b direct targets.

The aims of work were:

1. To explore the relevance of miR-148b and miR-214 for miRNA- based therapeutic interventions
2. To find suitable methods for specific deliver of miRNA-based therapeutic tool to cancer cells

For our purposes we first transduced melanoma and breast cancer cells with engineered lentivirus vectors to obtain miR-148b overexpression or miR-214 downmodulation (miR-214 sponge). Dual interventions in the same cells were also attempted. Modified cells were used to evaluate metastatic traits and to investigate the molecular mechanisms involved. More importantly, dissemination of these cells was analyzed in mice. Since we demonstrated that single or combined modulations of miR-214 (inhibition) and miR-148b (overexpression) significantly inhibited metastatization, we attempted cell specific targeted therapy, focusing first on miR-148b for this purpose. We took advantage of an axl aptamer as a moiety to deliver miR-148b to cancer cells, and designed a multifunctional conjugate by binding the oncosuppressor miR-148b to the axl aptamer. To note that many cancer cells, but not their normal counterparts, overexpress the axl tyrosine kinase receptor on their surface. Specific delivery of the axl-148b chimeric aptamer was obtained for axl-expressing

cancer cells. Here, silencing of miR-148b direct targets (i.e. ITGA5 and ALCAM) was proved. Relevantly, metastatic traits and tumor cell dissemination resulted inhibited, proving the validity of specifically delivered miRNA-based therapeutic interventions.

MATERIALS AND METHODS

Cell culture

MA-2 and MC-1 cells were kindly provided by L. Xu and R.O. Hynes (136) and maintained as described in (78,137). Human HBL-100, MDAMB231 and SKBR3 were from American Type Culture Collection instead 4175-TGL, SK-MEL-28 and A549 were kindly provided respectively by J. Massagué (138), L. Poliseno and V. de Franciscis and maintained in standard conditions. Human umbilical vein endothelial cells (HUVECs) were kindly provided by L. Primo (with GFP) or generated by L. Brizzi and maintained as described in (78,137).

Reagents and antibodies

miR precursors: Pre-miR™ miRNA Precursor Negative Control #1, Pre-miR miRNA Precursor Hsa-miR-214 (PM12124), Pre-miR™ miRNA Precursor hsa-miR-148b (PM10264), Anti-miR miRNA Inhibitor Negative Control #1, Anti-miR miRNA Inhibitor Hsa-miR-214 (AM12124), Anti-miR miRNA Inhibitor hsa-miR-148b (AM10264) (all from Applied Biosystems, Foster City, CA). TaqMan® MicroRNA assays for miRNA detection: Hsa-miR-214 ID 002306, Hsa-miR-148b ID 000471, U6 snRNA ID001973, U44 snRNA ID001904 (all from Applied Biosystems, Foster City, CA). Qiagen miScript-SYBR Green PCR Kit and miScript Primer Assay: has-let-7g ID 218300, Axl ID 330001 (all from Qiagen, Milan, IT). Primary antibodies: anti-PIK3CA #4255, anti-Cleaved Caspase-3 (Asp175) #9661 (Cell Signaling Technology), anti-GFP ab290, anti-Ki67 ab15580 (Abcam), anti-ITGA5 pAb RM10 kindly provided by G. Tarone, anti-CD166/ALCAM mAb MOG/07 (Novocastra Laboratories, Newcastle, UK), anti-ROCK-1 pAb H-85, anti-hsp90 mAb F-8, anti-GAPDH pAb V-18, anti-ACTIN I-19 pAb (all from Santa Cruz Biotechnology, Santa Cruz, CA), anti-α-tubulin mAb B5-1-2 (Sigma, St Louis, MO), anti-CD31 pAb (Becton Dickinson). Secondary antibodies: HRP-conjugated goat anti-mouse IgG, goat anti-rabbit IgG, donkey anti-goat IgG (all from Santa Cruz Biotechnology, Santa Cruz, CA), goat anti-rat IgG Alexa-Fluor-568 and goat anti-rat IgG Alexa-Fluor-488 (Molecular Probes, Invitrogen Life Technologies). siRNAs: si-ITGA5 (Hs_ITGA5_5 siRNA), si-ALCAM (Hs_ALCAM_5 siRNA), and All Stars Negative Control siRNA were purchased from Qiagen.

Sponge design and recombinant vector preparations

miR-214 sponges were described in ref. (78). miR-148b-specific sponge sequences containing eight miRNA binding sites interrupted by 15-nts spacers were designed to be perfectly complementary to the miR-148b seed region, with a bulge position 9–12 to prevent undesired cleavage of the sponge RNA. Sponges were synthesized by DNA 2.0, cloned into pJ241 plasmids, excised using flanking *Hind*III sites, blunted and subcloned into blunted *Bam*HI and *Sal*I sites, downstream of EGFP into pLenti CMV-GFP-Puro (658-5) vector (Addgene), giving rise to pLenti148-spongeA/B. Nucleotides (in Table 1) were verified by sequencing. pLemiR-empty, pLemiR-214, and pLemiR-148b expression vectors were described in refs. (78) and (83). The same miR-148b expression cassette was also subcloned in a pLenti4/V5 expression vector (kindly provided by C.M. DiPersio, Albany Medical College, Albany, NY).

Aptamer-miRNA conjugate preparations.

GL21.T-sticky (axl aptamer):
5'AUGAUCAAUCGCCUCAAUUCGACAGGAGGCUCACXXXXGUACAUUCUAGAUAGCC 3'

3P of miR-148b: 5' AGUCAGUGCAUCACAGAACUUUGUCU**UU** 3'

5P-sticky of miR-148b: 5'
AGGUGAAGUUCUGUUAUACACUCAGGCUGGCUAUCUAGAAUGUAC 3'

All RNAs were modified with 2′-F pyrimidines and synthesized at the Synthetic and Biopolymer Chemistry Core at the Beckman Research Institute City of Hope (Duarte, CA). **UU** (in **bold**) in the guide strand of miR-148b are 3′-overhang. Sticky sequence, consisting of 2′-F-Py and 2′-OMe-Pu, is underlined. X indicated C3 carbon linker. To prepare axl-148b and axl-let-7g conjugates: 1) miR-148b or let-7g passenger and guide were annealed by incubating in annealing buffer at 95 °C for 10 min, at 55 °C for 10 min and then at 37 °C for 20 min; 2) sticky aptamers were refolded (5 min 85 °C, 3 min on ice, 10 min at 37 °C); 3) equal amounts (ratio 1:1) of sticky aptamer and annealed passenger-guide were then annealed by incubating together at 37 °C for 30 min

Transient transfections, vectors, and generation of stable cell lines

To obtain transient anti-miR or pre-miR or siRNA expression, cells were plated at 50% confluency and immediately transfected using HiPerFect Transfection Reagent (Qiagen), with 100 nmol/l anti-miR, 75 nmol/l pre-miR, or 100 nmol/l siRNA. For transient cDNA overexpression, cells were plated at 90% confluency and transfected 24 hours later using Lipofectamine^{TM}2000 reagent (Invitrogen Life Technologies, Carlsbad, CA). For ITGA5 or ALCAM overexepression pEGFP-N3-ITGA5 (83) or pLVX-ALCAM (137) expression vectors were used. All stable cell lines were generated via lentiviral infection. Sponge vectors were obtained as described above. The pLKO.1-shALCAM lentiviral vector was from Open Biosystems (RHS3979). Lentiviruses were produced by calcium phosphate transfection of 20-μg vector plasmid together with 15-μg packaging (pCMVdR8.74) and 6-μg envelope (pMD2.G-VSVG) plasmids in 293T cells, according to Trono's lab protocol (http://tronolab.epfl.ch), and supernatants were harvested 48 hours after transfection.

RNA isolation and qRT-PCR for miR or mRNA detection

Total RNA was isolated from cells using TRIzol® Reagent (Invitrogen Life Technologies). qRT-PCRs for miR detection were performed with the indicated TaqMan MicroRNA Assays (Applied Biosystems) on 10 ng total RNA, according to the manufacturer's instructions. For mRNA detection, 1 μg of DNAse-treated RNA (RQ1 RNase-Free DNase, Promega, Madison, WI) was retrotranscribed with High-Capacity cDNA Reverse Transcription Kit (Thermo Fisher Scientific, Waltham, MA) and qRT-PCRs were carried out using gene-specific primers for mRNA detection, using a 7900HT Fast Real Time PCR System (Thermo Fisher Scientific). Quantitative normalization was performed on the expression of the RNU44 or U6 small nucleolar RNAs or of RRN18S, for miR or mRNA detection, respectively. The relative expression levels between samples were calculated using the comparative delta Ct (threshold cycle number) method (2-ΔΔCt) with a control sample as the reference point (139).

Protein preparation and immunoblotting

Total protein extracts were obtained using a boiling buffer containing 0.125 M Tris/HCl, pH 6.8 and 2.5% sodium dodecyl sulphate (SDS) or in a cold JS buffer containing 50 mM HEPES, 150 mM NaCl, 1.5 mM $MgCl_2$, 1% Glycerol 1% Triton and 5mM EGTA. In all, 10-60 μg of proteins were

separated by SDS polyacrylamide gel electrophoresis (PAGE) and electroblotted onto polyvinylidene fluoride membranes (BioRad, Hercules, CA). Membranes were blocked in 5% non-fat milk phosphate-buffered saline (PBS)-Tween buffer (4.3 mM Sodium Phosphate, Dibasic Na2HPO4, 137 mM Sodium Chloride NaCl, 2.7 mM Potassium Chloride KCl, 1.4 mM Potassium Phosphate, Monobasic KH2PO4, pH 7.4, with 0.1% Tween-20) for 1 h at 37 °C, then incubated with appropriate primary and secondary antibodies in PBS-Tween buffer, respectively, overnight at 4°C or for 1 h at room temperature and visualized by enhanced chemiluminescence (ECL®, GE Healthcare).

Migration, invasion and transendothelial migration transwell assays

To measure migration and matrigel invasion $7.5x10^4$ MA-2, MC-1 or A549, 3×10^4 HBL-100, $5x10^4$ 4175-TGL, SK-MEL-28 or MDAMB231 and $1x10^5$ SKBR3 were seeded in serum-free medium in the upper chambers of cell culture transwells with 8.0 μm pore size membrane (BD Biosciences, NJ), pre-coated or not with 4 μg/well growth factor reduced matrigel (BD Biosciences, NJ) or in BioCoat Matrigel Invasion Chambers (Becton Dickinson). The lower chambers were filled with complete growth medium. After 18h or 24h, the migrated cells on the lower side of the membrane were fixed in 2.5% glutaraldehyde, stained with 0.1% crystal violet and photographed using an Olympus IX70 microscope. For transendothelial migration assay 10^5 HUVECs were seeded in complete medium in the upper part of transwell inserts with 5.0 μm pore size membrane (Costar, Corning Incorporated, NY) coated by 0.1% gelatin, and grown till confluency. Then, $5x10^4$ cells labeled with CellTracker™ Orange CMRA or Green CMFDA (Molecular Probes, Invitrogen Life Technologies, Carlsbad, CA), were seeded onto the HUVECs monolayer. 20h later HUVECs and non-transmigrated cells were removed and the red or green fluorescent cells that migrated on the lower side of the membrane were fixed in 4% paraformaldheyde and photographed using Zeiss Axiovert200M microscope. Migration, invasion and transendothelial migration were evaluated by measuring the area occupied by migrated cells using the ImageJ software (http://rsbweb.nih.gov/ij/).

Proliferation assays

$5x10^3$ MA-2, MC-1, MDAMB231 or 4175-TGL cells/well were plated in 96-well plates in complete medium and starved for 24 h. Complete medium was then added and cells were allowed

to grow for 1, 2, 3, 4 and 5 days, fixed with 2.5% glutaraldehyde and stained with 0.1% crystal violet. The dye was solubilized using 10% acetic acid and optical density was measured using Promega GloMax®-Multi Detection System (Promega, Madison, WI) at 600 nm wavelength.

Mammosphere formation assays

Mammosphere formation assays were performed as in https://www.stemcell.com/tumorsphere-culture-human-breast-cancer-cell-lines-lp.html. Briefly, 4175-TGL or SKBR3 breast cancer cell lines were first grown as monolayers. Then, they were trypsinized as single cells, counted and seeded in poly-HEMA (poly-2-hydroxyethyl-methacrylate)-coated 24 well plates following two different protocol.

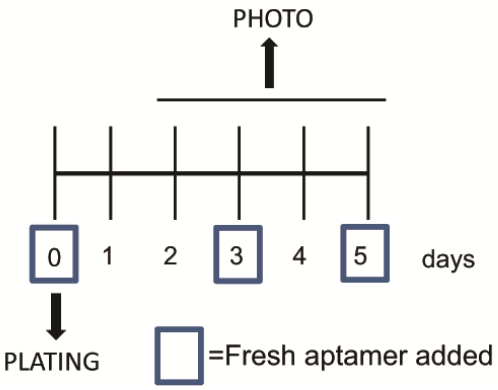

In one case, single breast cancer cells ($8x10^3$ cells/well for 4175-TGL, $1x10^4$ cells/well for SKBR3) were plated (day 0) and maintained in suspension in MammoCult Medium (StemCell Technologies, Vancouver, CA) and left untreated (controls=ctrl) or treated with 400 nmol/l of axl or axl-148b aptamers. Treatments were renewed at day 3 and 5 (200 nmol/l). At day 5 sphere size and number were evaluated using a Zeiss AxioObserver microscope and ImageJ Software (http://rsbweb.nih.gov/ij/). For size, a total of 30-40 spheres were measured for each experimental condition (long side of sphere was measured). For number, the total number of spheres present in 50 µl volume was counted for each treatment.

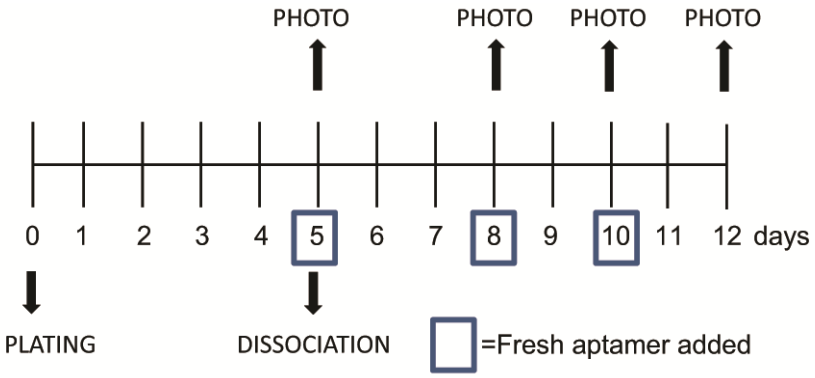

Alternatively, single cells were plated and maintained as above; mammospheres were dissociated at day 5, counted and plated again at the same density, left untreated (controls=ctrl) or treated with 400 nmol/l of axl or axl-148b aptamers. Spheres were analysed as above at day 12. In same cases, cells were labelled with PKH26 (Sigma, 10^{-7}M, 5 min) at day 5 and the percentage (%) of PKH26 positive or negative cells was evaluated at day 12 by FACS analysis following mammosphere dissociation.

FACS procedures

Cells were transfected with pCMV-MCS-GFP vector or with the same vector carrying the sponges and GFP levels were detected 48h post-transfections by flow citometry using a FACSCalibur flow cytometer (Becton Dickinson). Data acquisition and analysis was performed using Cell Quest Software (Becton Dickinson). Results were displayed in histogram as GFP Geo Mean.

For mammosphere, 7 days after the dissociation (day 12), PKH26 labelled mammospheres were collected and disaggregated and FACS analysis performed using a FACSCalibur cell analyzer was performed to evaluate $PKH26^{positive}$ from $PKH26^{negative}$ cells on the total pool (100%).

Histology and immunohistochemistry

5 µm-thick tissue sections were generated from formalin-fixed, paraffin embedded tumor samples and stained with hematoxylin and eosin (H&E) for standard histology observations. Immuno Histo Chemical (I.H.C.) stainings were also performed using an anti-Ki67 or anti-Cleaved caspase 3 antibodies and the avidin-biotin-peroxidase techniques (Anti-Mouse HRP-DAB Cell & Tissue Staining Kit, R&D Systems, Minneapolis, MN). For this purpose, tissue sections were

deparaffinized and rehydrated and 0.3% H_2O_2 was used to ablate the endogenous peroxidase. Next, tissue sections were heated in citrate buffer pH=6 (Bio-Optica, Milano, IT) for antigen retrieval and blocking buffer (3% milk, 5% goat serum in Phosphate Buffered Saline, PBS) was used to suppress nonspecific antibody binding. Tissue sections were incubated at room temperature for 20 minutes and then at 4 °C overnight with the primary antibody+ blocking buffer, or blocking buffer without antibody as negative control. Ki67 antibody was diluted 1:150, Cleaved Caspase3 1:100. Then, the sections were washed and incubated with secondary biotinylated anti-rabbit-IgG at room temperature for 1 h, followed by incubation with avidin-biotin complex at room temperature for 30 minutes. Reactions were developed with diaminobenzidine tetrahydrocloride (DAB). Slides were counterstained with hematoxylin.

ALCAM localization imaging

A total of 2×10^5 HUVEC-GFP were seeded on coverslips coated with fibronectin at 5 $\mu g/cm^2$, and grown till confluency. Then, 5×10^4 ALCAM-overexpressing MA-2 cells (stably transduced with pLVX-ALCAM expressing vector) were seeded on the HUVEC-GFP monolayer. Twenty-four hours later, the cocultures were fixed in cold methanol and immunostained for ALCAM protein. Briefly, samples were blocked with 5% BSA, incubated with anti-CD166/ALCAM mAb MOG/07 (Novocastra Laboratories, 1:100 dilution) for 2 hours, then with anti-mouse IgG Alexa-Fluor-568 for 45 minutes and finally mounted on microscope slides for analyses and photos, performed with Confocal Leica SP5 microscope.

***In vivo* tumor growth and metastasis assays**

All experiments performed with live animals complied with ethical care. For tumor growth, 5×10^6 MC-1 cells (in PBS) were subcutaneously injected into the flanks of 8- to 12-week-old NOD/SCID/IL2R_null (NSG) immunocompromised mice, animals dissected 4 weeks later and proteins extracted from tumors. For experimental metastasis assays, 5×10^5 MA-2 or MC-1 or SK-MEL-28 or 3×10^5 4175-TGL cells were injected into the tail vein of 8- to 12-week-old SCID or NOD/SCID/IL2R_null (NSG) immunocompromised mice and the animals were dissected 7 or 4 weeks later, respectively. Green or red fluorescent lung metastases were evaluated and photographed in fresh lungs *in toto* using a Leica MZ16F fluorescence stereomicroscope. The number of metastases was measured on photographs using the ImageJ software

(http://rsbweb.nih.gov/ij/). Micrometastases were evaluated on paraffin-embedded and haematoxylin and eosin (H&E)-stained slides, scanned with Panoramic Desk (3DHistech, Euroclone).

Alternatively, 5×10^6 4175-TGL or MA-2 cells (in PBS) were subcutaneously injected into the mammary fat pad of 8-12 weeks-old NOD/SCID/IL2R_null (NSG) immunocompromised mice. After 11 or 12 days, tumors were injected with PBS or axl-148b (300 pmol/injection, three injections a week) and tumor growth was monitored every 3 days. Mice were dissected 32 or 33 days after MA-2 or 4175-TGL injection respectively and tumors were weighted. Alternatively, tumors were injected with PBS or axl-148b (300 pmol/injection, three injections a week) from the beginning of the experiment. Red fluorescent lung metastases were evaluated and photographed in fresh lungs *in toto* using a Leica MZ16F fluorescence stereomicroscope. For tumor studies, tumors were formalin fixed, cut in small pieces and paraffin embedded, sectioned and hematoxylin and eosin (H&E) stained.

In vivo extravasation assay

A total of 1.5×10^6 MC-1 or MA-2 or SK-MEL-28 cells, previously labeled with CellTracker Orange CMRA (Molecular Probes, Invitrogen Life Technologies), were injected into the tail vein of 4- to 6-week-old female NSG mice (Charles River Laboratories). Two or 48 hours later, mice were sacrificed, and 4% paraformaldehyde was injected into the trachea. Lungs were dissected and photographed *in toto* using a Leica MZ16F fluorescence stereomicroscope and red fluorescence was quantified 48 hours following injections using the ImageJ software (http://rsbweb.nih.gov/ij/). Lungs were embedded in OCT (Killik, BioOptica), frozen, cryostat-cut in 6-µm-thick sections. Localization of tumor cells, inside/outside the vessels, was evaluated on sections at a Zeiss AxioObserver microscope with the ApoTome Module (78), following blood vessels staining with an anti-CD31 primary antibody in immunofluorescence.

Circulating tumor cells isolation

To isolate circulating tumor cells (CTCs), blood was collected from heart-punctured mice and put in culture plates with normal medium for 3 days; subsequently, attached cells were washed and cultured in fresh medium in presence of puromycin. 7 days later, cells were washed thoroughly to remove non-adherent cells, fixed with 2.5% glutaraldehyde, stained with 0.1% crystal violet and

observed under the microscope. Alternatively, endogenous cell fluorescence was used for visualization at the fluorescent microscope.

Human tumor correlation analyses

Normalized expression values for mRNA and miRNA in breast cancer were downloaded from the European Genome-phenome Archive (EGAS00000000122, EGAD00010000434, and EGAD00010000438; (140,141), and 1302 samples were used. Instead, for melanomas, expression values were downloaded from The Cancer Genome Atlas (TCGA, https://tcga-data.nci.nih.gov/tcga/) and 352 samples were used. All analyses were performed with R using the packages stats (lm) and ggplot2. R: A language and environment for statistical computing. R Foundation for Statistical Computing, Vienna, Austria (URL https://www.R-project.org/).

Statistical analysis

The results are shown as mean ± Standard Deviation (SD) or ± Standard Error of Mean (SEM), as indicated, and two-tailed Student's t test was used for comparison. *=$p<0.05$; ** = $p<0.01$; ***= $p<0.001$ were considered to be statistically significant. ns= indicates a non-statistically significant p-value.

CHAPTER I: miR-214 and miR-148b targeting inhibits dissemination of melanoma and breast cancer

RESULTS

1. miR-214 depletion and miR-148b overexpression inhibit melanoma and breast cancer metastasis formation in mice

High levels of miR-214 are found in malignant melanomas and breast tumors and promote metastatization in mice by regulating a complex network of players, in a negative or positive manner, including the downregulation of the antimetastatic miR-148b. Here, we evaluated the potential therapeutic value of miR-214 depletion and miR-148b overexpression in tumor progression in mice.

Specific miR-214 or miR-148b sponges A or B were bio-informatically designed, cloned at the 3' end of a Green Fluorescent Protein (GFP) expression cassette in lentivirus vectors as in Table 1, Fig. 1A, and ref. (78) and tested in MC-1 or MA-2 melanoma cells. Specifically, cells were transfected with pLenti-214-spongeA/B or pLenti-148bspongeA/ B or pLenti-empty (control) vectors together with precursors for miR-214 or miR-148b or controls (pre-miR-214 or pre-miR-148b or pre-control), and GFP levels were evaluated in cells at the microscope (Fig. 1B and 1C), by Western Blot-WB (Fig. 1D and 1E), or FACS analysis (Fig. 1F and 1G). As shown, all sponges were able to inhibit GFP expression, suggesting miR-214 or miR-148b binding to their complementary sequences.

MC-1 or MA-2 melanoma or 4175-TGL breast cancer cells were then transduced with lentiviruses expressing miR-214-sponges (pLenti-214-spongeA/B) or miR-148b (pLenti4/V5-148b, pLemiR-148b) or with empty controls (pLenti-empty, pLenti4/V5-empty, pLemiR-empty). Alternatively, MA-2 or SK-MEL-28 melanoma or 4175-TGL breast cancer cells were transduced with lentiviruses expressing miR-148b-sponges (pLenti-148b-spongeA/B) or miR-214 (pLemiR-214) or with empty controls (pLenti-empty, pLemiR-empty) to verify the mechanism in the opposite directions. miR-214 and miR-148b levels were evaluated by qRT-PCR analyses as shown in Figs. 3 to 6. Cells with the expected miR-214 or miR-148b modulations were injected in the tail vein of immunocompromised mice, and metastasis dissemination was evaluated 4 to 7 weeks later by measuring the number/area of lung metastasis in H&E-stained lung or liver sections or the fluorescent (green or red) tumor cells present in the whole organs (Fig. 2A–C; Figs. 7A-D and 8A-

D). Single miR-214 downmodulation or miR-148b overexpression significantly blocked metastasis dissemination for MC-1 or MA-2 melanoma or 4175-TGL breast cancer cells compared with controls. Relevantly, simultaneous depletion of miR-214 and increased levels of miR-148b further blocked tumor spreading of melanoma and breast tumor cells compared with single modulations, suggesting a combined action. In parallel, single miR-214 overexpression or miR-148b downmodulation, or simultaneous double targeting, favored melanoma or breast cancer cell dissemination compared with controls.

In conclusion, we can consider miR-214 and miR-148b as promising targets for miRNA-based therapeutic interventions in tumor progression.

Figure 1 – Analysis of miR-214 and miR-148b sponge efficacy. (A) Schematic representation of sponge constructs containing specific sites for miR-214 and miR-148b. (B, C) GFP expression in the indicated melanoma cell lines 48h after transfection of miR-214 (pLenti-214-spongeA/B) or miR-148b (pLenti-148b-spongeA/B) sponges alone or in combination with miR-214 (pre-miR-214) or miR-148b (pre-miR-148b) precursors or negative controls (pre-control). Cells were photographed using a Zeiss Axiovert200M microscope (B, a-i, C, a-i; bar=2 mm;). (D, E) Western Blot analysis of GFP protein expression levels in the indicated melanoma cells transfected as in (B, C). Protein modulations were calculated relative to controls, normalized on loading controls (hsp90) and expressed as percentages (%). (F, G) FACS analyses for GFP levels in the indicated melanoma cells transfected as in (B, C). At least 2 independent experiments were performed and representative results are shown.

Fig. 1

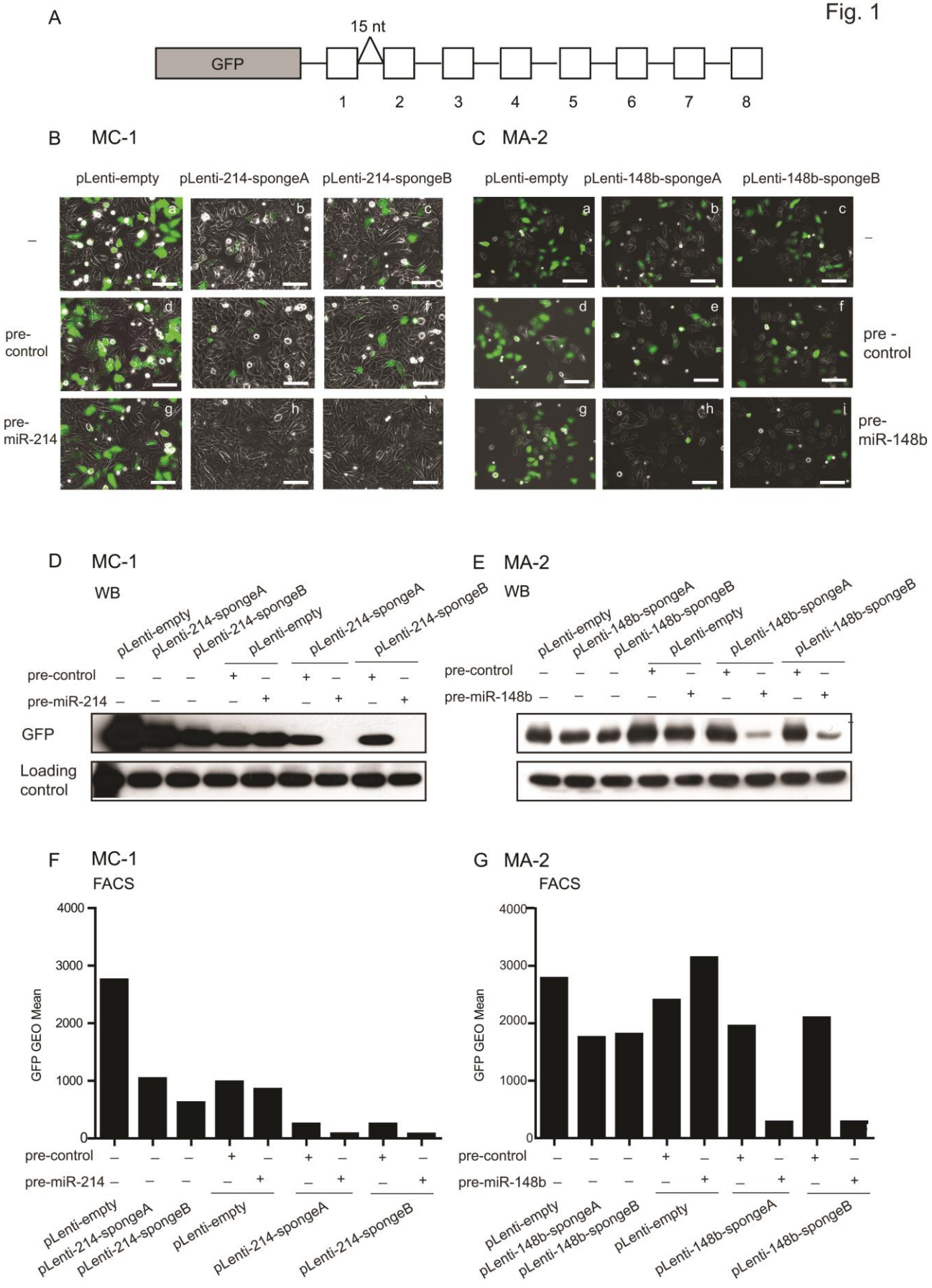
A
15 nt
GFP
1
2
3
4
5
6
7
8
B MC-1
C MA-2
pLenti-empty
pLenti-214-spongeA
pLenti-214-spongeB
pLenti-148b-spongeA
pLenti-148b-spongeB
–
pre-control
pre-miR-214
pre-miR-148b
a
b
c
d
e
f
g
h
i
D MC-1
WB
E MA-2
WB
GFP
Loading control
F MC-1
FACS
G MA-2
FACS
GFP GEO Mean
4000
3000
2000
1000
0

Table 1 – miR-214 and miR-148b sponge sequences

miRNA sponge	Sequence	length	n° of sites
214-spongeA	TTGAAGCTTACTGCCTGTCAATCCTGCTGTCTAAACATAATTCCTACTGCCTGTC CATCCTGCTGTCCTTTCTATTCCCTCACTGCCTGTCCATCCTGCTGTCCCATTGA AATATATACTGCCTGTCTACCCTGCTGTCATTAAAACGCCCCTACTGCCTGTCCC TCCTGCTGTCAAACCTAACTTACAACTGCCTGTCCCCCCTGCTGTCCACTGAAAC TTCCTACTGCCTGTCTCTCCTGCTGTCCTCAAATTTACCTAACTGCCTGTCCCCC CTGCTGTGCAAGCTTGC	292 bp	8
214-spongeB	TTGAAGCTTACTGCCTGTCTATCCTGCTGTCATCTTTATATCTAAACTGCCTGTCA ACCCTGCTGTCACCTCCTAACAAAAACTGCCTGTCTCTCCTGCTGTCACATCACT CCCGCCACTGCCTGTCCCCCCTGCTGTCACCATATCCTACACACTGCCTGTCTC CCCTGCTGTCTTAACTACATATATACTGCCTGTCCCCCCTGCTGTCTACAAATAC CCCCTACTGCCTGTCTCCCCTGCTGTCCAACATTTCCAATCACTGCCTGTCACTC CTGCTGTGCAAGCTTGC	292 bp	8
148b-spongeA	TTGAAGCTTACAAAGTTCTGCCTGCACTGAAACCTAAACCTACCTACAAAGTTCT GACTGCACTGATTTCCACAATAAAAAACAAAGTTCTGCGTGCACTGATTAAAATTT CCATATACAAAGTTCTGCCTGCACTGACATCTCATAACCTGGACAAAGTTCTGCC TGCACTGATAAAAAAGACATAATACAAAGTTCTCCCTGCACTGAGTTCCCCACCA CACCACAAAGTTCTACTTGCACTGAATCCACCACCCAATAACAAAGTTCTATCTG CACTGAGCAAGCTTGC	292 bp	8
148b-spongeB	TTGAAGCTTACAAAGTTCTCTGTGCACTGACATTACCCCCTCTACACAAAGTTCT CCCTGCACTGACCATAAACCTACACCACAAAGTTCTGATTGCACTGATTCCCCTC TCTATTAACAAAGTTCTACCTGCACTGACCATCCACCCAATTTACAAAGTTCTGC CTGCACTGAAAAATATCTATCTCCACAAAGTTCTGCCTGCACTGATCTCATACAA AATATACAAAGTTCTGACTGCACTGATAATAATACCACCCTACAAAGTTCTAACTG CACTGAGCAAGCTTGC	292 bp	8

Figure 2- miR-214 depletion and miR-148b overexpression inhibit melanoma and breast cancer metastasis formation in mice Lung or liver colony formation in immunodeficient mice, 7 (A) or 4 (B and C) weeks after tail-vein injection of MC-1 (A) or 4175-TGL (B and C) cells. Cells were transduced with controls (pLenti-empty, pLenti4/V5-empty) or miR-214-sponge (pLenti-214-spongeB) or miR-148b-overexpressing (pLenti4/V5-148b) vectors, single or in combination, as indicated in the panels. Representative pictures of H&E-stained sections (A, B, a–d, bar, 500 mm; C, a–d, bar, 100 mm) are shown. Graphs (bottom of each figure) represent quantitated results as mea±SEM H&E-stained colonies number (A) or as a percentage of metastatic/total areas (B) in lungs or as mean metastases/field in liver, referring to the indicated number of mice (n). Two independent experiments were performed and representative results are shown.

Fig. 2

A MC-1

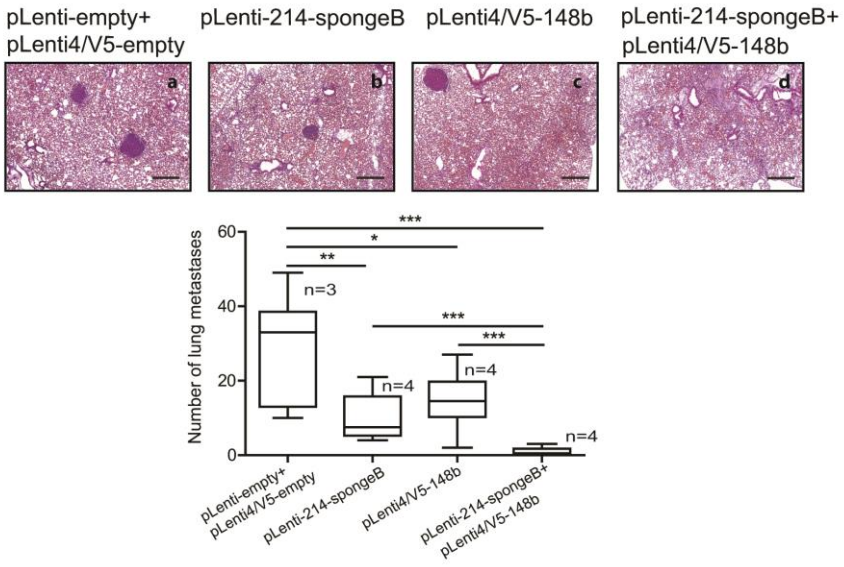

B 4175-TGL

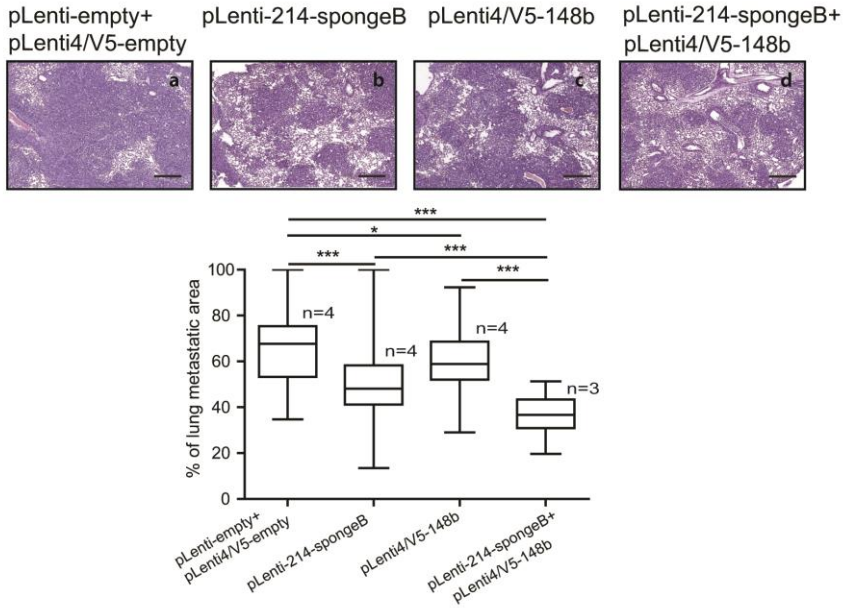

C 4175-TGL

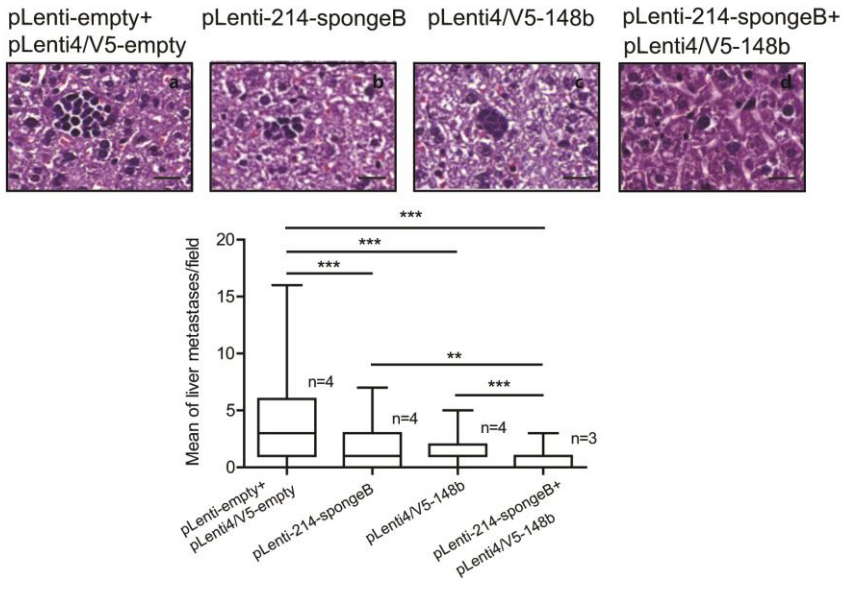

Figure 3- miR-214 expression modulations in melanoma cells. (A-E) miR-214 expression levels were tested by qRT-PCR analyses for the indicated melanoma cell lines stably transduced with control (pLenti-empty, pLenti4/V5-empty) or miR-214 sponges (pLenti-214-spongeA/B) or with miR-148b (pLenti4/V5-148b) overexpression vectors, alone or in combination. (F-J) Alternatively, cells were transiently transfected with miR-148b (anti-miR-148b) or miR-214 (anti-miR-214) inhibitors; miR-214 or miR-148b precursors (pre-miR-214 or pre-miR-148b) or negative controls (anti- or pre-control), alone or in combination, as indicated in the graphs. Results are shown as fold changes (mean±SD of triplicates) relative to controls, normalized on U6 or U44 small nucleolar RNA level.

Fig. 3

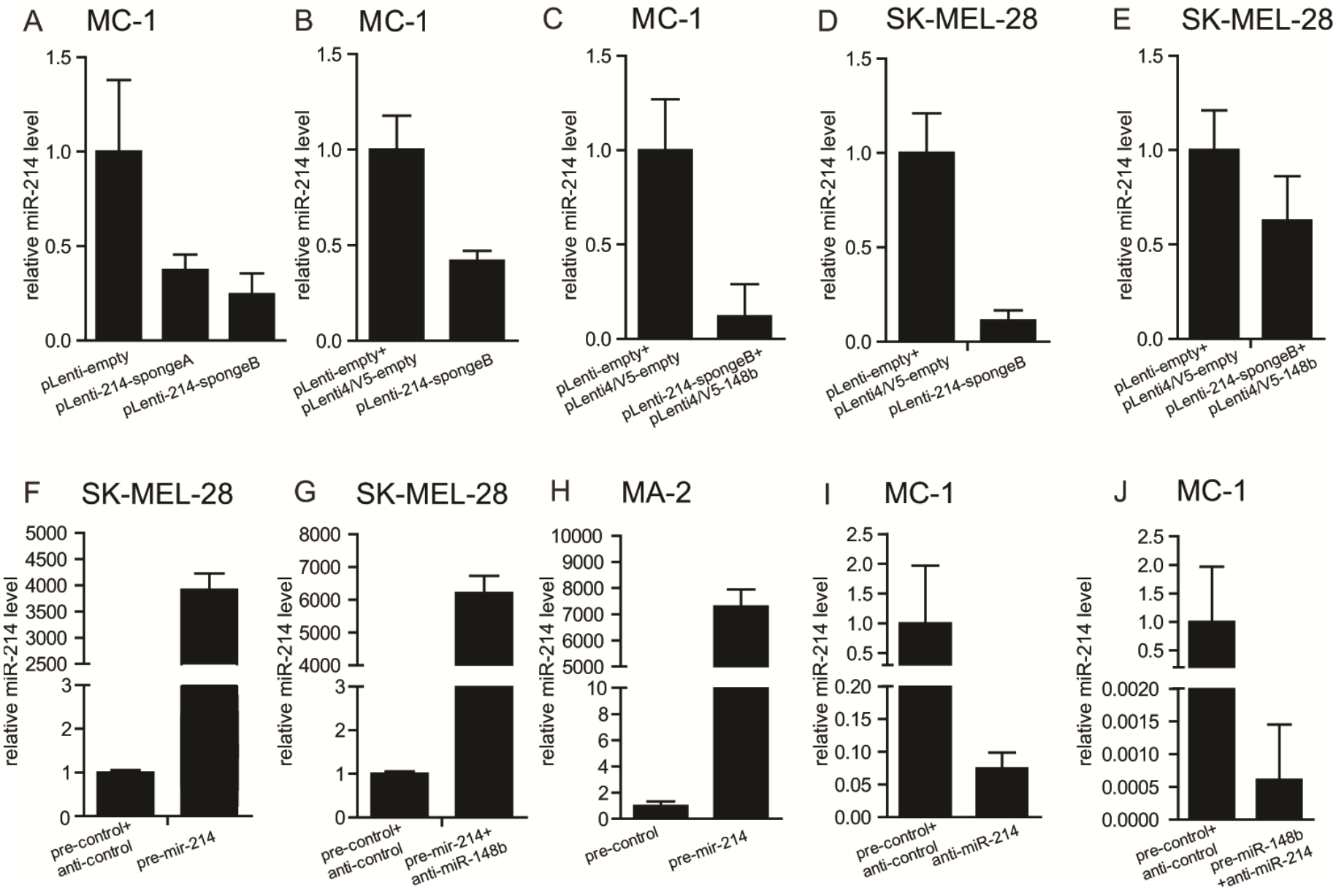
A MC-1
B MC-1
C MC-1
D SK-MEL-28
E SK-MEL-28
relative miR-214 level
1.5
1.0
0.5
0.0
pLenti-empty
pLenti-214-spongeA
pLenti-214-spongeB
pLenti-empty+
pLenti4/V5-empty
pLenti-214-spongeB
pLenti-214-spongeB+
pLenti4/V5-148b
F SK-MEL-28
G SK-MEL-28
H MA-2
I MC-1
J MC-1
5000
4500
4000
3500
3000
2500
3
2
1
0
pre-control+
anti-control
pre-mir-214
8000
7000
6000
5000
4000
pre-mir-214+
anti-miR-148b
10000
9000
8000
7000
6000
5000
10
8
6
4
2
0
pre-control
2.5
2.0
1.5
1.0
0.5
0.20
0.15
0.10
0.05
0.00
anti-miR-214
0.0020
0.0015
0.0010
0.0005
0.0000
pre-miR-148b
+anti-miR-214

Figure 4 - miR-214 expression modulations in normal or tumor breast cells. (A-E) miR-214 expression levels were tested by qRT-PCR analyses for the indicated normal or tumor breast cell lines stably transduced with control (pLenti-empty, pLenti4/V5-empty or pLemiR-empty) or miR-214 (pLenti-214-spongeB) or miR-148b (pLenti-148b-spongeB) sponges or with miR-148b (pLenti4/V5-148b) or miR-214 (pLemiR-214) overexpression vectors, alone or in combination. (F-I) Alternatively, cells were transiently transfected with miR-148b (anti-miR-148b) inhibitors or miR-214 precursors (pre-miR-214) or negative controls (anti- or pre-control), alone or in combination, as indicated in the graphs. Results are shown as fold changes (mean±SD of triplicates) relative to controls, normalized on U6 or U44 small nucleolar RNA level.

Fig. 4

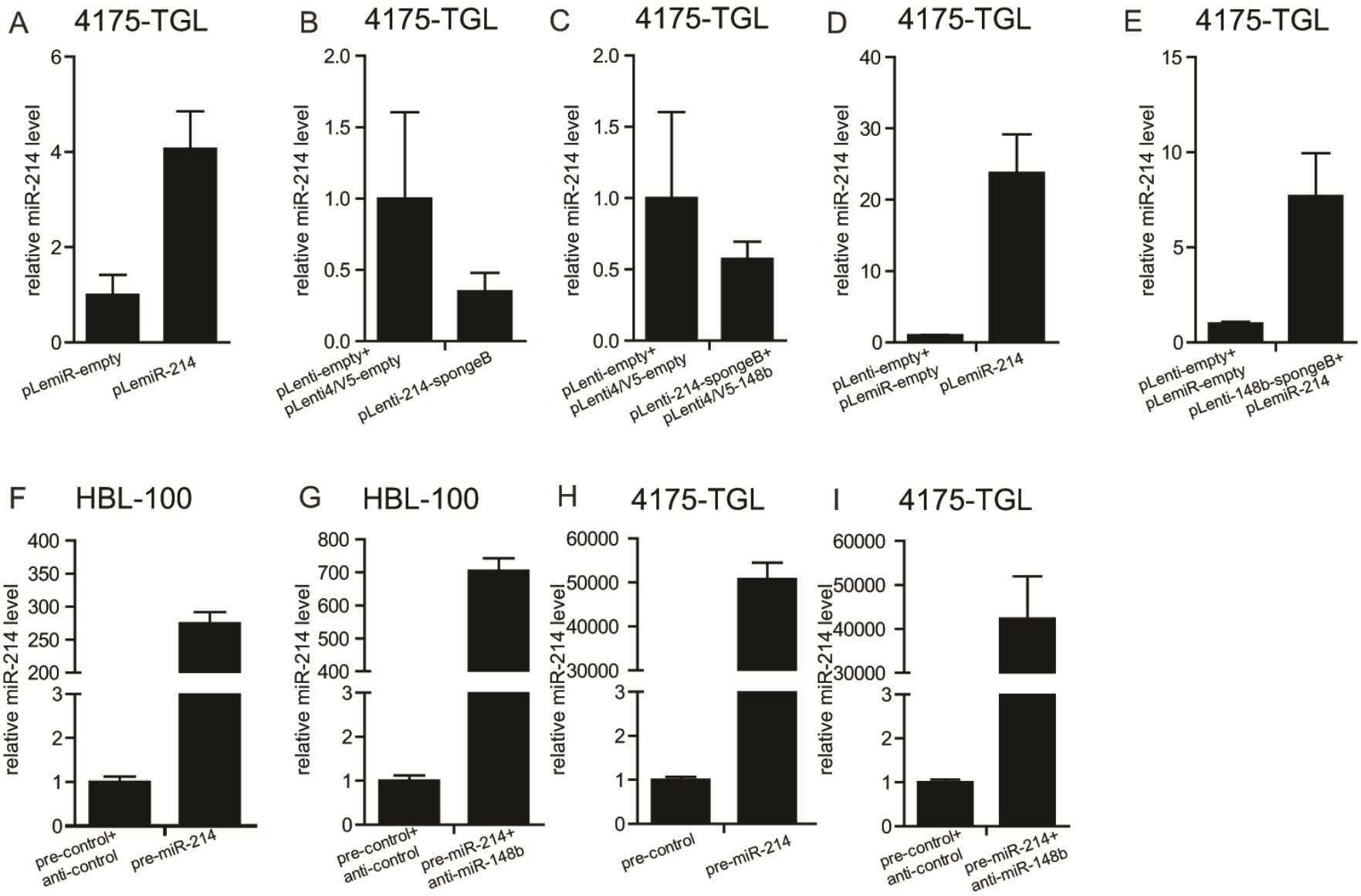
A
4175-TGL
relative miR-214 level
6
4
2
0
pLemiR-empty
pLemiR-214
B
4175-TGL
relative miR-214 level
2.0
1.5
1.0
0.5
0.0
pLenti-empty+ pLenti4/V5-empty
pLenti-214-spongeB
C
4175-TGL
relative miR-214 level
2.0
1.5
1.0
0.5
0.0
pLenti-empty+ pLenti4/V5-empty
pLenti-214-spongeB+ pLenti4/V5-148b
D
4175-TGL
relative miR-214 level
40
30
20
10
0
pLenti-empty+ pLemiR-empty
pLemiR-214
E
4175-TGL
relative miR-214 level
15
10
5
0
pLenti-empty+ pLemiR-empty
pLenti-148b-spongeB+ pLemiR-214
F
HBL-100
relative miR-214 level
400
350
300
250
200
3
2
1
0
pre-control+ anti-control
pre-miR-214
G
HBL-100
relative miR-214 level
800
700
600
500
400
3
2
1
0
pre-control+ anti-control
pre-miR-214+ anti-miR-148b
H
4175-TGL
relative miR-214 level
60000
50000
40000
30000
3
2
1
0
pre-control
pre-miR-214
I
4175-TGL
relative miR-214 level
60000
50000
40000
30000
3
2
1
0
pre-control+ anti-control
pre-miR-214+ anti-miR-148b

Figure 5 - miR-148b expression modulations in melanoma cells. (A-G) miR-148b expression levels were tested by qRT-PCR analyses for the indicated cell lines stably transduced with control (pLenti-empty, pLenti4/V5-empty or pLemiR-empty) or miR-214 (pLenti-214-spongeB) or miR-148b (pLenti-148b-spongeB) sponges or with miR-148b (pLemiR-148b or pLenti4/V5-148b) overexpression vectors, alone or in combination. (H-M) Alternatively, cells were transiently transfected with miR-148b (anti-miR-148b) or miR-214 (anti-miR-214) inhibitors; miR-214 or miR-148b precursors (pre-miR-214 or pre-miR-148b) or negative controls (anti- or pre-control), alone or in combination, as indicated in the graphs. Results are shown as fold changes (mean±SD of triplicates) relative to controls, normalized on U6 or U44 small nucleolar RNA level.

Fig. 5

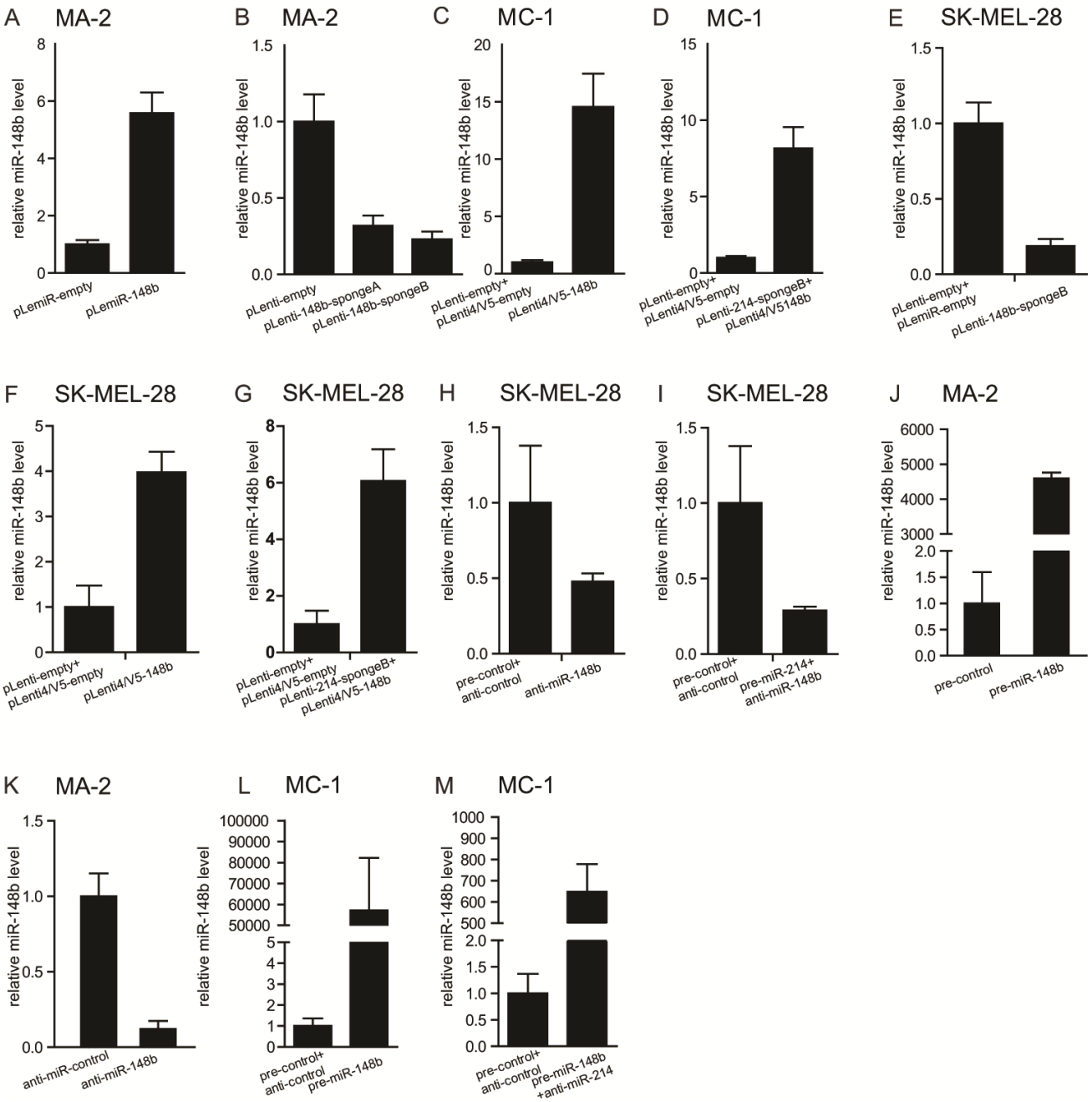
A MA-2
relative miR-148b level
pLemiR-empty
pLemiR-148b
B MA-2
pLenti-empty
pLenti-148b-spongeA
pLenti-148b-spongeB
C MC-1
pLenti-empty+ pLenti4/V5-empty
pLenti4/V5-148b
D MC-1
pLenti-empty+ pLenti4/V5-empty
pLenti-214-spongeB+ pLenti4/V5148b
E SK-MEL-28
pLenti-empty+ pLemiR-empty
pLenti-148b-spongeB
F SK-MEL-28
pLenti-empty+ pLenti4/V5-empty
pLenti4/V5-148b
G SK-MEL-28
pLenti-empty+ pLenti4/V5-empty
pLenti-214-spongeB+ pLenti4/V5-148b
H SK-MEL-28
pre-control+ anti-control
anti-miR-148b
I SK-MEL-28
pre-control+ anti-control
pre-miR-214+ anti-miR-148b
J MA-2
pre-control
pre-miR-148b
K MA-2
anti-miR-control
anti-miR-148b
L MC-1
pre-control+ anti-control
pre-miR-148b
M MC-1
pre-control+ anti-control
pre-miR-148b +anti-miR-214

Figure 6 - miR-148b expression modulations in normal or tumor breast cells. (A-D, I) miR-148b expression levels were tested by qRT-PCR analyses for the indicated cell lines stably transduced with control (pLenti-empty, pLenti4/V5-empty or pLemiR-empty) or miR-214 (pLenti-214-spongeB) or miR-148b (pLenti-148b-spongeA/B) sponges or with miR-148b (pLenti4/V5-148b) or miR-214 (pLemiR-214) overexpression vectors, alone or in combination. (E-H) Alternatively, cells were transiently transfected with miR-148b (anti-miR-148b) inhibitors or miR-214 precursors (pre-miR-214) or negative controls (anti- or pre-control), alone or in combination, as indicated in the graphs. Results are shown as fold changes (mean±SD of triplicates) relative to controls, normalized on U6 or U44 small nucleolar RNA level.

Fig. 6

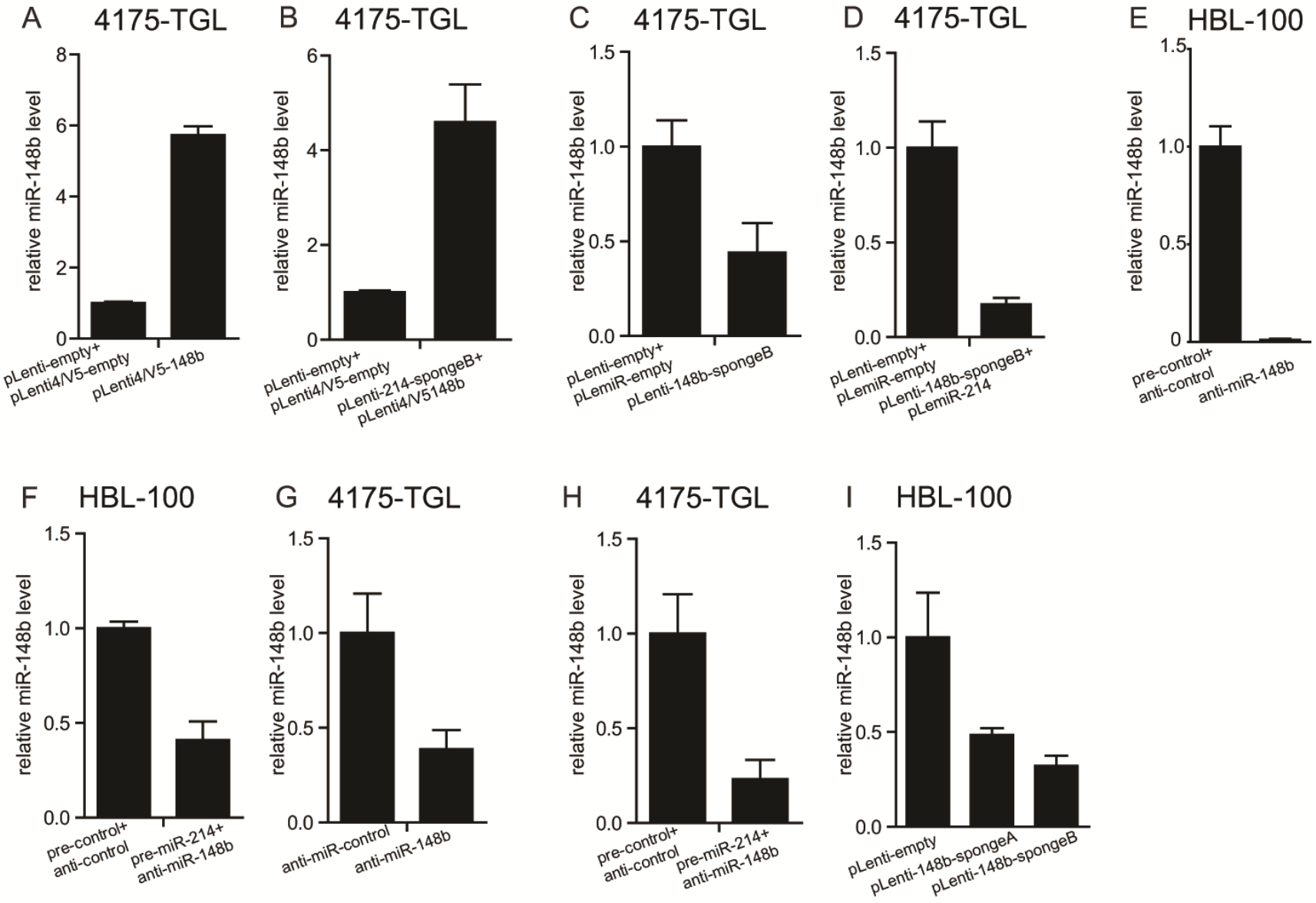
A
4175-TGL
relative miR-148b level
8
6
4
2
0
pLenti-empty+
pLenti4/V5-empty
pLenti4/V5-148b
B
4175-TGL
relative miR-148b level
6
4
2
0
pLenti-empty+
pLenti4/V5-empty
pLenti-214-spongeB+
pLenti4/V5148b
C
4175-TGL
relative miR-148b level
1.5
1.0
0.5
0.0
pLenti-empty+
pLemiR-empty
pLenti-148b-spongeB
D
4175-TGL
relative miR-148b level
1.5
1.0
0.5
0.0
pLenti-empty+
pLemiR-empty
pLenti-148b-spongeB+
pLemiR-214
E
HBL-100
relative miR-148b level
1.5
1.0
0.5
0
pre-control+
anti-control
anti-miR-148b
F
HBL-100
relative miR-148b level
1.5
1.0
0.5
0.0
pre-control+
anti-control
pre-miR-214+
anti-miR-148b
G
4175-TGL
relative miR-148b level
1.5
1.0
0.5
0.0
anti-miR-control
anti-miR-148b
H
4175-TGL
relative miR-148b level
1.5
1.0
0.5
0.0
pre-control+
anti-control
pre-miR-214+
anti-miR-148b
I
HBL-100
relative miR-148b level
1.5
1.0
0.5
0.0
pLenti-empty
pLenti-148b-spongeA
pLenti-148b-spongeB

Figure 7 - miR-214 and miR-148b coordinate lung metastasis formation in an opposite manner. Lung colony formation in immunodeficient mice, 7 (A) or 4 (B-D) weeks after tail vein injection of MC-1 (A), MA-2 (B, C), or 4175-TGL (D) cells. Cells were transduced as indicated in the panels: controls (pLenti-empty or pLemiR-empty) or miR-214-sponge (pLenti-214-spongeA/B) or miR-148b-sponge (pLenti-148b-spongeA/B) or miR-148b-overexpressing (pLemiR-148b) or miR-214-overexpressing (pLemiR-214) vectors, expressing GFP or tRFP. Representative pictures of green or red fluorescent whole lungs (A and C, a-c; B and D, a-b; bar=800 μm) or H&E stained sections (A and C, d-f; B and D, c-d, bar=200 μm) are shown. Graphs (bottom of each figure) represent quantitated results as mean±SEM of the number of fluorescent colonies in lungs, referring to the indicated number of mice (n). 2 independent experiments were performed and representative results are shown. SEM= Standard Error of Mean; H&E=Haematoxylin and Eosin.

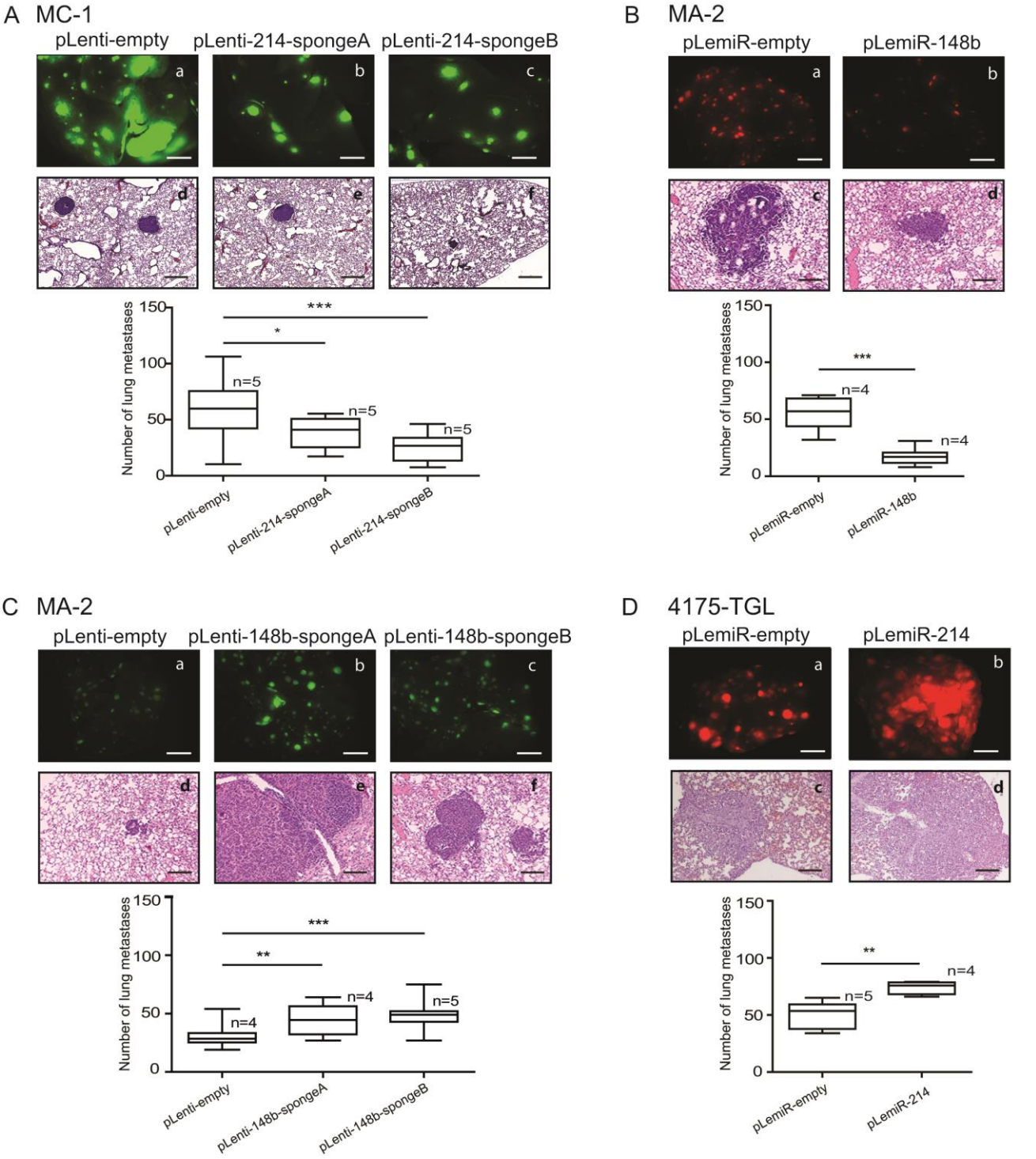
A MC-1
pLenti-empty
pLenti-214-spongeA
pLenti-214-spongeB
a
b
c
d
e
f
Number of lung metastases
150
100
50
0
***
*
n=5
n=5
n=5
pLenti-empty
pLenti-214-spongeA
pLenti-214-spongeB
B MA-2
pLemiR-empty
pLemiR-148b
a
b
c
d
Number of lung metastases
150
100
50
0
***
n=4
n=4
pLemiR-empty
pLemiR-148b
C MA-2
pLenti-empty
pLenti-148b-spongeA
pLenti-148b-spongeB
a
b
c
d
e
f
Number of lung metastases
150
100
50
0
***
**
n=4
n=4
n=5
pLenti-empty
pLenti-148b-spongeA
pLenti-148b-spongeB
D 4175-TGL
pLemiR-empty
pLemiR-214
a
b
c
d
Number of lung metastases
150
100
50
0
**
n=5
n=4
pLemiR-empty
pLemiR-214

Figure 8 - miR-148b reduces liver and lung metastasis formation. Liver (A, B) and lung (C, D) colony formation in immunodeficient mice, 4 (A, B, D) or 7 (C) weeks after tail vein injection of MA-2 or SK-MEL-28 or 4175-TGL cells transduced with the following overexpressing vectors: control (pLenti-empty and/or pLemiR-empty) or miR-148b sponges (pLenti-148b-spongeA/B) or miR-148b (pLemiR-148b) or miR-214 (pLemiR-214), including GFP or tRFP expression or not, single or in combination. Representative pictures of fluorescent whole livers (A, a-b; B, a-c, bar=800 µm) or of H&E-stained lung sections are shown (C, D a-b, bar=40 µm and 500 µm, respectively). Graphs (bottom of each figure) present quantitated results as mean±SEM of the number of fluorescent colonies in livers (A, B) or of the number of H&E colonies (C) or of the percentage of metastatic/total area in lungs (D) referring to the number of mice (n) indicated. 2 independent experiments were performed and representative results are shown. SEM= Standard Error of Mean.

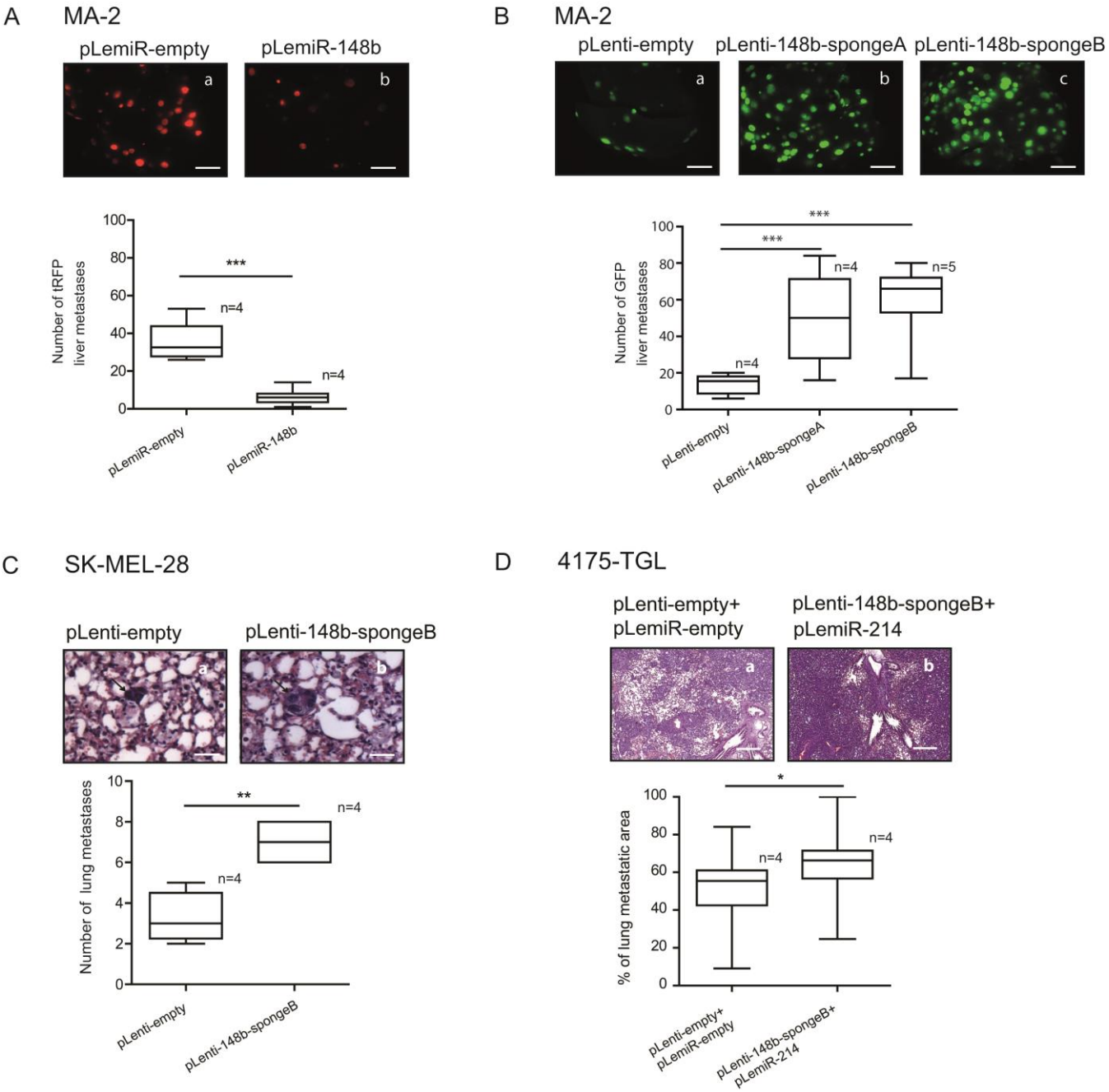
A
MA-2
pLemiR-empty
pLemiR-148b
a
b
Number of tRFP liver metastases
100
80
60
40
20
0
***
n=4
n=4
pLemiR-empty
pLemiR-148b
B
MA-2
pLenti-empty
pLenti-148b-spongeA
pLenti-148b-spongeB
a
b
c
Number of GFP liver metastases
100
80
60
40
20
0
***
***
n=4
n=4
n=5
pLenti-empty
pLenti-148b-spongeA
pLenti-148b-spongeB
C
SK-MEL-28
pLenti-empty
pLenti-148b-spongeB
a
b
Number of lung metastases
10
8
6
4
2
0
**
n=4
n=4
pLenti-empty
pLenti-148b-spongeB
D
4175-TGL
pLenti-empty+
pLemiR-empty
pLenti-148b-spongeB+
pLemiR-214
a
b
% of lung metastatic area
100
80
60
40
20
0
*
n=4
n=4
pLenti-empty+
pLemiR-empty
pLenti-148b-spongeB+
pLemiR-214

2. miR-214 inhibition and miR-148b overexpression control specific tumor cell metastatic traits

To understand which metastatic traits of melanoma (MA-2, MC-1, and SK-MEL-28) and normal or tumor breast (HBL-100 and 4175-TGL) cells were affected by miR-214 and miR-148b modulations, we evaluated proliferation, migration, invasion through matrigel and transendothelial migration on a HUVEC monolayer *in vitro*. Cells were either transduced with lentiviruses for the depletion (pLenti-214-spongeB, pLenti-148b-spongeB) or overexpression (pLemiR-214, pLenti4/V5-148b) of miR-214 or miR-148b or with empty controls (pLemiR-empty, pLenti-empty, pLenti4/V5-empty) or transiently transfected with miRNA precursors or inhibitors (pre-miR-214, anti-miR-148b, pre/anti-control). miR-214 and miR-148b modulations were evaluated by qRT-PCR assays as shown in Figs. 3 to 6. Single or double alterations of miR-214 and miR-148b did not significantly affect proliferation compared with controls in any tested cell line (Fig. 9A and B; and Fig. 10). Instead, modulations of miR-214 or miR-148b significantly affected migration, cell movement across a HUVEC monolayer (transendothelial migration) and invasion in matrigel compared with controls (Fig. 11A–F; Fig. 12A–F). Precisely, in all assays, cell movement was impaired in miR-214-depleted and miR-148b-overexpressing cells. Opposite results were observed when miR-214 was highly expressed in cells while miR-148b expression was reduced. Relevantly, in transendothelial migration assays, but generally not in migration or invasion analyses, simultaneous miR-214 inhibition and miR-148b overexpression almost always led to combined effects, like for *in vivo* metastasis (Fig. 2), suggesting a combinatorial, specific effect of miR-214 and miR-148b at the level of tumor–endothelial cell interactions.

Fig. 9

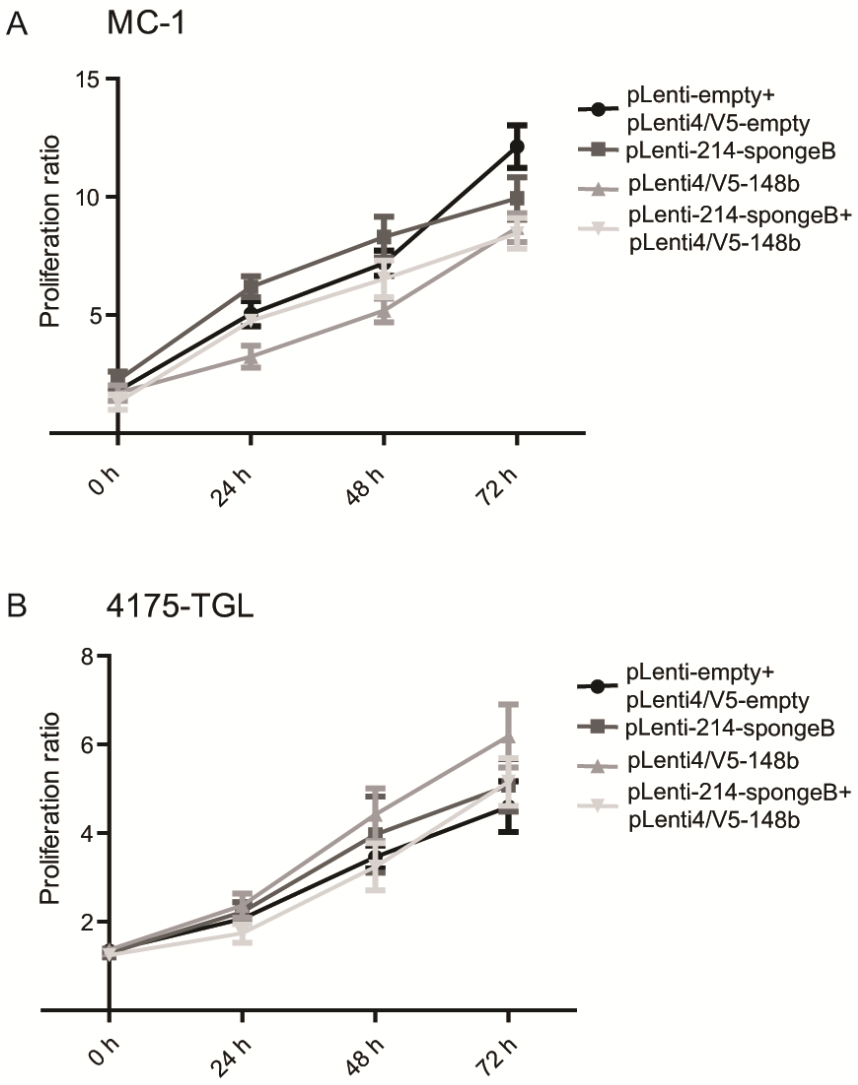

Figure 9 - miR-214 depletion and miR-148b overexpression do not affect proliferation. A and B, proliferation of MC-1 (A) or 4175-TGL (B) cells stably transduced with control (pLenti-empty, pLenti4/V5-empty) or miR-214-sponge (pLenti-214- spongeB) or miR-148b-overexpressing (pLenti4/V5-148b) vectors, single or in combination, as indicated in the graphs. Results are indicated as mean±SD of the proliferation ratio versus plated cells, measured by optical density at 0–72 hours. At least two independent experiments (with triplicates) were performed, and representative results are shown.

Fig. 10

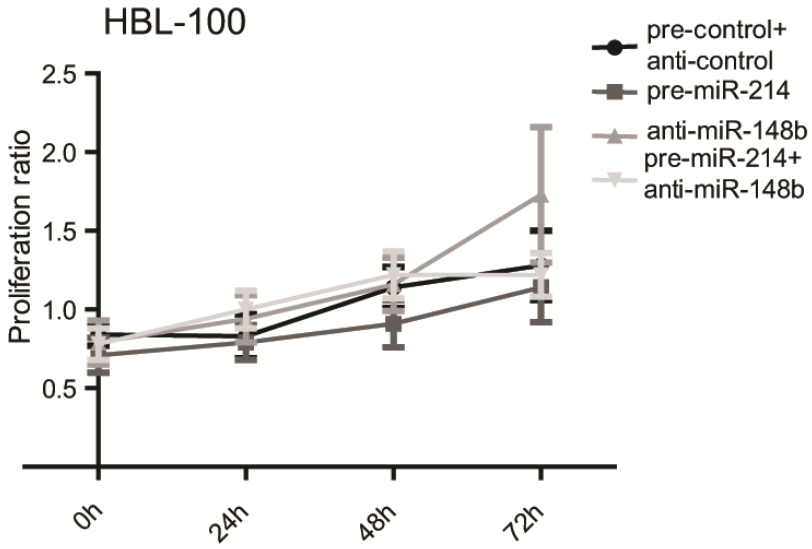

Figure 10 - miR-214 and miR-148b do not significantly affect proliferation. Proliferation of HBL-100 cells transiently transfected with miR-214 precursors (pre-miR-214) or miR-148b (anti-miR-148b) inhibitors or negative controls (pre- or anti-control) in single or in combination as indicated in the graphs. Results are indicated as mean±SD of the proliferation ratio versus plated cells, measured by optical density at 0-72h. At least 2 independent experiments (with triplicates) were performed and representative results are shown. SD=Standard Deviation.

Figure 11 - miR-214 depletion and miR-148b overexpression inhibit transendothelial migration. Transwell migration assays were used to evaluate migration (through a porous membrane) or transendothelial migration (through an HUVEC monolayer on top of a porous membrane) for MC-1 (A, B) or 4175-TGL (C and D) or SK-MEL-28 (E and F) cells stably transduced with control (pLenti-empty, pLenti4/V5-empty) or miR-214-sponge (pLenti-214-spongeB) or miR-148b-overexpressing (pLenti4/V5-148b) vectors, single or in combination, as indicated in the panels. For migration, results are indicated as a ratio of mean±SEM of the area covered by migrated versus plated tumor cells; for transendothelial migration, results are shown as mean±SEM of the area covered by tumor migrated cells. At least two independent experiments (with triplicates) were performed, and representative results are shown.

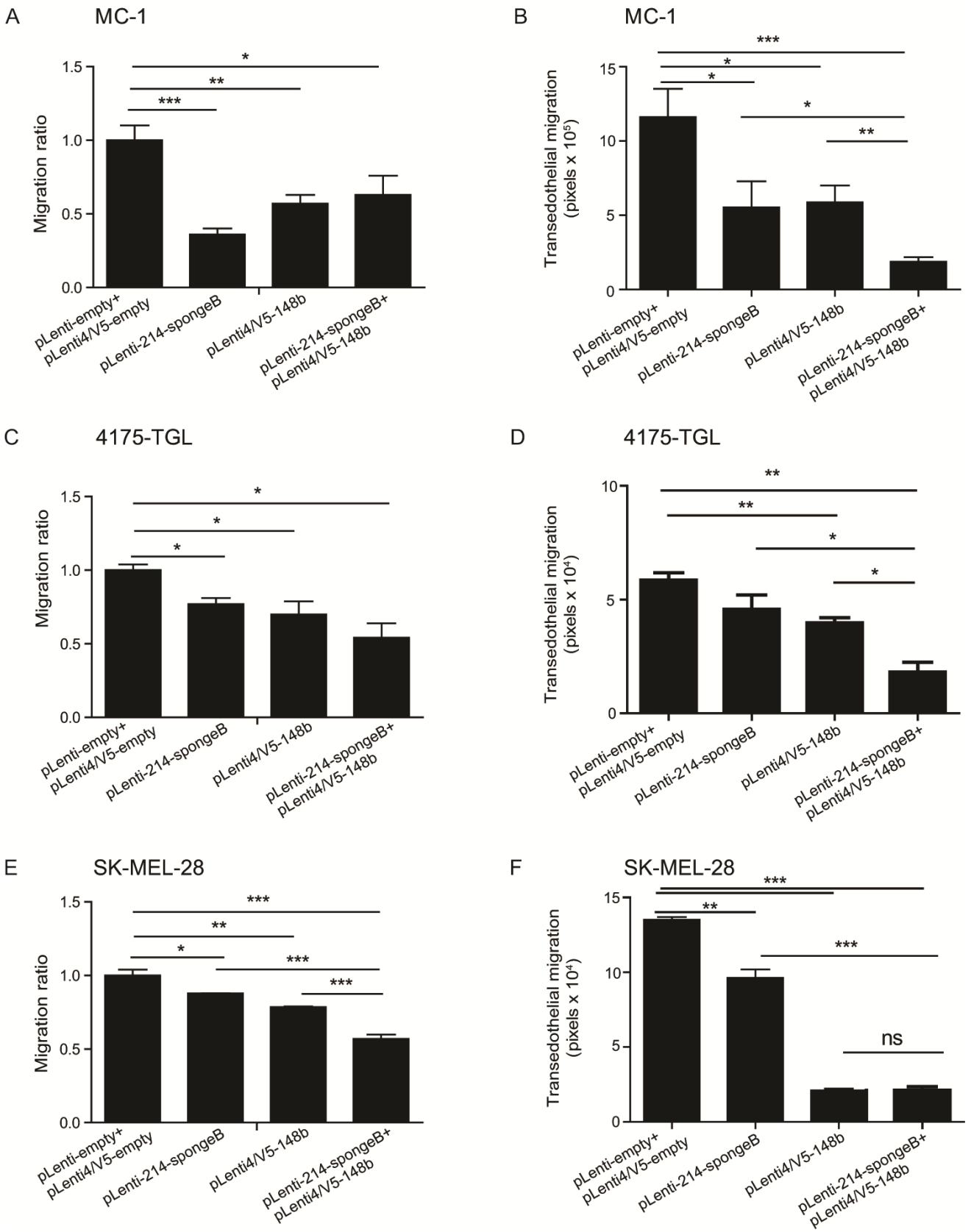
A
MC-1
Migration ratio
1.5
1.0
0.5
0.0
*
**
***
pLenti-empty+ pLenti4/V5-empty
pLenti-214-spongeB
pLenti4/V5-148b
pLenti-214-spongeB+ pLenti4/V5-148b
B
MC-1
Transedothelial migration (pixels x 10⁵)
15
10
5
0
***
*
*
*
**
pLenti-empty+ pLenti4/V5-empty
pLenti-214-spongeB
pLenti4/V5-148b
pLenti-214-spongeB+ pLenti4/V5-148b
C
4175-TGL
Migration ratio
1.5
1.0
0.5
0.0
*
*
*
pLenti-empty+ pLenti4/V5-empty
pLenti-214-spongeB
pLenti4/V5-148b
pLenti-214-spongeB+ pLenti4/V5-148b
D
4175-TGL
Transedothelial migration (pixels x 10⁴)
10
5
0
**
**
*
*
pLenti-empty+ pLenti4/V5-empty
pLenti-214-spongeB
pLenti4/V5-148b
pLenti-214-spongeB+ pLenti4/V5-148b
E
SK-MEL-28
Migration ratio
1.5
1.0
0.5
0.0
***
**
*
***
***
pLenti-empty+ pLenti4/V5-empty
pLenti-214-spongeB
pLenti4/V5-148b
pLenti-214-spongeB+ pLenti4/V5-148b
F
SK-MEL-28
Transedothelial migration (pixels x 10⁴)
15
10
5
0
***
**
***
ns
pLenti-empty+ pLenti4/V5-empty
pLenti-214-spongeB
pLenti4/V5-148b
pLenti-214-spongeB+ pLenti4/V5-148b

Figure 12 - miR-214 and miR-148b affect migration and invasion ability. Transwell migration (A-C) or invasion on matrigel (D-F) assays for HBL-100 (A), 4175-TGL (B), SK-MEL-28 (C, D), MC-1 (E) or MA-2 (F) cells transiently transfected with miR-214 precursors (pre-miR-214) or miR-148b inhibitors (anti-miR-148b) or negative controls (pre-control or anti-control), alone or in combination, or stably transduced with controls (pLenti-empty and/or pLenti4/V5-empty) or miR-214 (pLenti-214-spongeB) or miR-148b (pLenti-148b-spongeB) sponges or miR-148b-overexpressing (pLenti4/V5-148b) vectors, single or in combination, as indicated in the panels. Results are indicated as ratio mean±SEM of the area covered by migrated versus plated cells. At least 2 independent experiments (with triplicates) were performed and representative results are shown. SEM= Standard Error of Mean.

Fig. 12

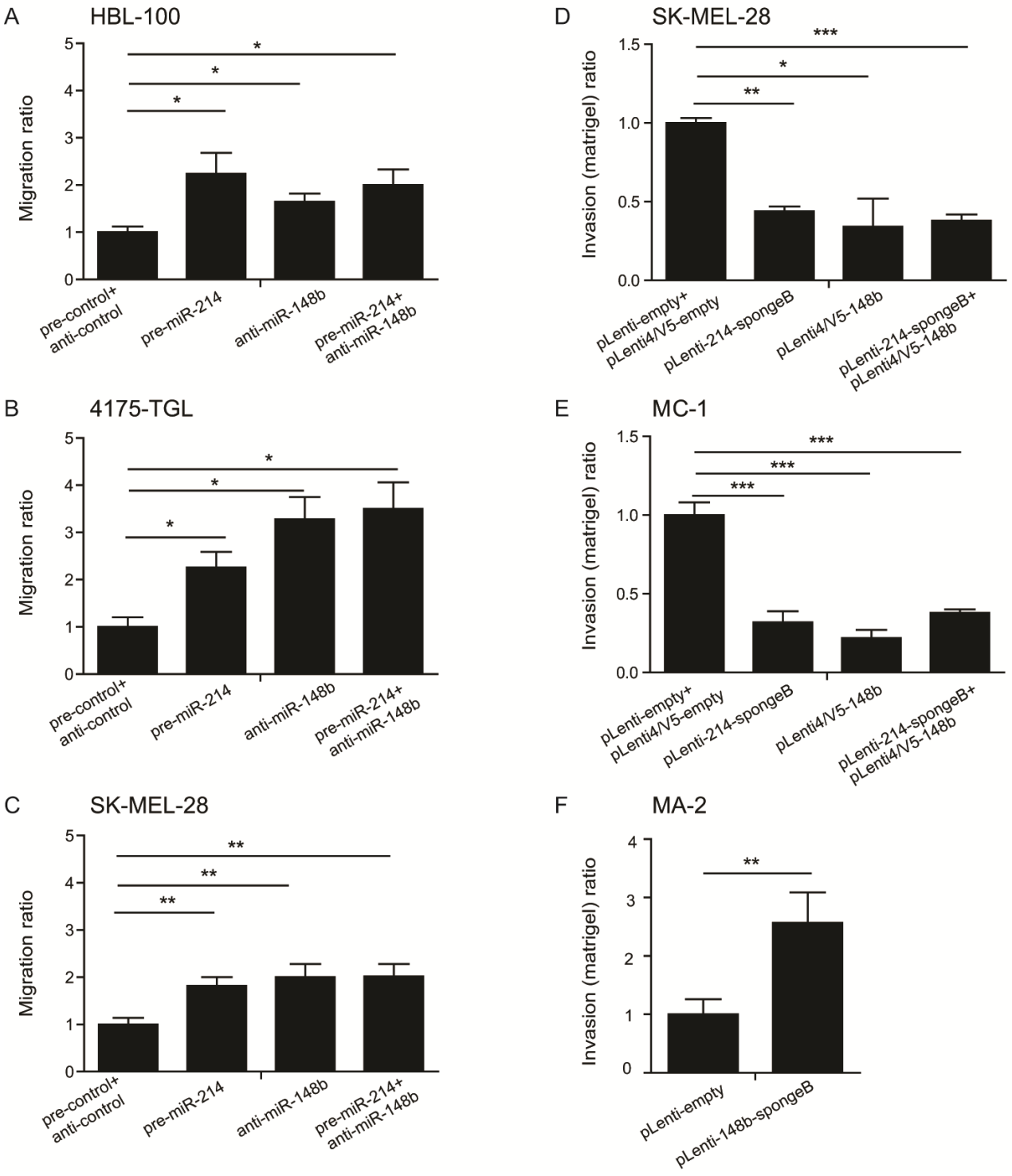
A
HBL-100
Migration ratio
pre-control+ anti-control
pre-miR-214
anti-miR-148b
pre-miR-214+ anti-miR-148b
B
4175-TGL
Migration ratio
C
SK-MEL-28
Migration ratio
D
SK-MEL-28
Invasion (matrigel) ratio
pLenti-empty+ pLenti4/V5-empty
pLenti-214-spongeB
pLenti4/V5-148b
pLenti-214-spongeB+ pLenti4/V5-148b
E
MC-1
Invasion (matrigel) ratio
F
MA-2
Invasion (matrigel) ratio
pLenti-empty
pLenti-148b-spongeB

3. miR-214 depletion and miR-148b overexpression impair tumor cell extravasation in mice

The effect of single or combined sponge-induced miR-214 depletion and miR-148b overexpression was investigated on *in vivo* cell extravasation of tumor cells. CMRA-labeled MC-1 or SK-MEL-28 cells stably expressing miR-214-sponge (pLenti-214-spongeB) or miR-148b (pLenti4/V5-148b) or control vectors (pLenti-empty or pLenti4/V5-empty) were injected in the tail vein of immunocompromised mice (Fig. 13a–l and graph, Figs. 14a–h and graph). Lodging to the lung vasculature was evaluated 2 hours after injection (Fig. 13a–d; Fig. 14a–b), and no difference was observed among modified cells. Instead, a strong decrease in early (48 hours after injection) lung colonization was observed following single or combined sponge-driven miR-214 downmodulation and miR-148b overexpression compared with controls in MC-1 (Fig. 13e–h) or SK-MEL-28 (Fig. 14c–d) cells. Note that cells were localized inside blood vessels or associated with them at 2 hours, as shown in Fig. 14e–f. Instead, cells were found in the lung parenchyma at 48 hours (Fig. 13i–l; Fig. 14g–h). As for metastasis dissemination (Fig. 2) and transendothelial migration (Fig. 11), simultaneous miR-214 inhibition and miR-148b overexpression led to combined effects, suggesting, once more, a combinatorial, specific effect of miR-214 and miR-148b at the level of tumor– endothelial cell interactions.

Fig. 13

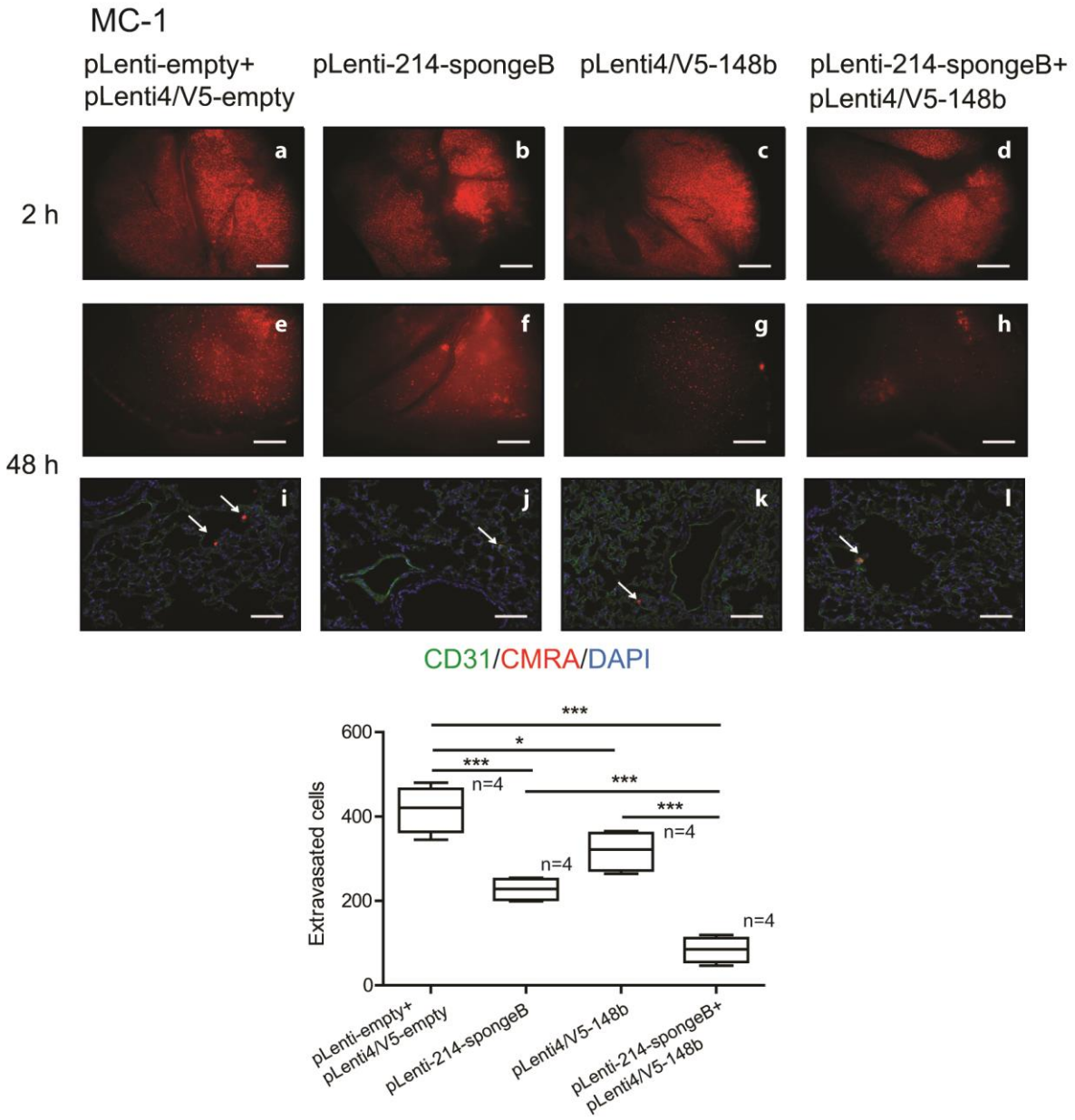

Figure 13 - miR-214 depletion and miR-148b overexpression inhibit extravasation in mice. In vivo extravasation 2 hours (A–D) or 48 hours (E–H) following tail-vein injections in immunodeficient mice of CMRA-labeled MC-1 cells transduced with control (pLentiempty, pLenti4/V5-empty) or miR-214- sponge (pLenti-214-spongeB) or miR-148boverexpressing (pLenti4/V5-148b) vectors, single or in combination, as indicated in the panels. Representative pictures of whole red fluorescent lungs at 2 hours or 48 hours after injection (A–H) and representative fields of murine lung sections, 48 hours after injection (I–L), stained for CD31 and counterstained with DAPI are shown; bar, 800 mm. Results are indicated in the graphs (bottom) as mean±SEM of the number of extravasated cells at 48 hours for n ¼ 4 mice per group. White arrows, extravasated cells. Two independent experiments were performed, and representative results are shown.

Figure 14 - miR-214 inhibition and miR-148b overexpression impair melanoma cell extravasation. *In vivo* extravasation 2h (a, b) or 48h (c, d) following tail vein injections in immunosuppressed mice of CMRA-labeled SK-MEL-28 cells transduced with a combination of control (pLenti-empty, pLenti4/V5-empty) or miR-214-sponge (pLenti-214-spongeB) and miR-148b-overexpressing (pLenti4/V5-148b) vectors as indicated in the panels. Representative pictures of whole red fluorescent lungs are shown (a-d); bar=800 µm. Representative fields of murine lung sections 2h (e, f) or 48h (g, h) post-injections, stained for CD31 (red) and counterstained with DAPI (blue). Arrows indicate metastatic cells. Results are indicated in the graph (bottom) as mean±SEM of the fluorescence intensity at 48h for n=4 mice per group. 2 independent experiments were performed and representative results are shown. SEM= Standard Error of Mean.

Fig. 14

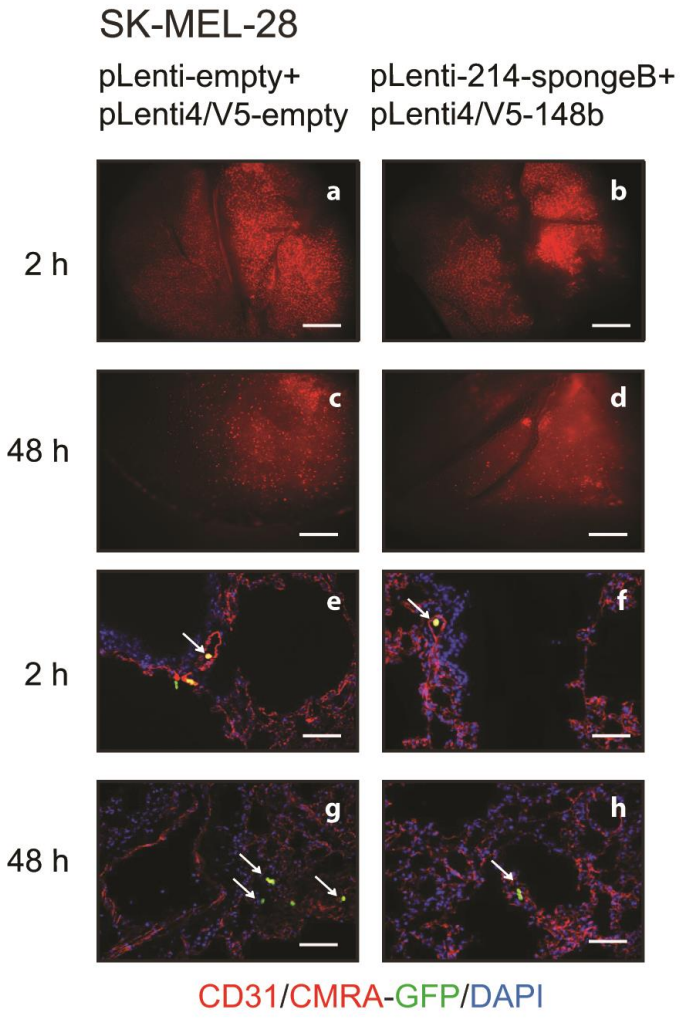
SK-MEL-28
pLenti-empty+
pLenti4/V5-empty
pLenti-214-spongeB+
pLenti4/V5-148b
2 h
48 h
2 h
48 h
a
b
c
d
e
f
g
h
CD31/CMRA-GFP/DAPI

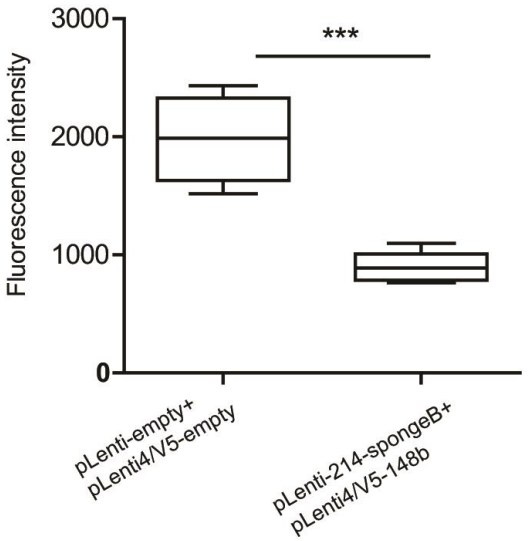
3000
2000
1000
0
Fluorescence intensity
***
pLenti-empty+
pLenti4/V5-empty
pLenti-214-spongeB+
pLenti4/V5-148b

4. Depletion of miR-214 and overexpression of miR-148b affect the adhesion molecules ITGA5 and ALCAM

To identify the molecular players involved in reduced cancer dissemination/extravasation by miR-214 depletion and miR-148b overexpression in tumor cells, expression of ITGA5 and ALCAM, two validated miR-148b direct targets, known to be highly relevant for cancer cell dissemination, was analyzed in cell cultures or in mouse subcutaneous tumors. Single or combined miR-214 depletion and miR-148b overexpression in melanoma (MA-2, MC-1, SK-MEL-28) and breast cancer (4175-TGL) cells were obtained following stable transduction of lentivirus vectors for the expression of miR-214 sponges (pLenti-214-spongeB) or miR-148b (pLenti4/V5-148b) or empty controls (pLenti-empty, pLenti4/V5-empty). miR-214 and miR-148b alterations were evaluated by qRT-PCR analyses as in Figs. 3 to 6. Important reduction of ITGA5 or ALCAM expression was observed for single or combined miRNA-modulations. Combined inhibitions of ITGA5 and ALCAM by dual miR-214/miR-148b interventions were rarely observed compared with single alterations (Fig. 15A–D; and Fig. 16A–E). Considering the relevance of ITGA5 and ALCAM expression impairment for the inhibition of transendothelial migration following simultaneous miR-214/miR148b alterations, as presented below (see the next paragraph), we can speculate that the effects of combined miR-214/miR-148b changes occur specifically when tumor cells get in contact with endothelial cells. Alternatively, supplementary alterations of gene expression could be involved in the passage of tumor cells through the blood vessels.

Opposite stable or transient modulations were obtained in some of the cells (MA-2, 4175-TGL) listed above and in HBL-100 normal breast cells to further evaluate this mechanism. Cells were transduced with pLenti-148b-spongeA/B or pLemiR-214 or the relative empty controls (pLenti-empty, pLemiR-empty) or transiently transfected with anti-miR-148b or pre-miR-214 or anti/pre-control and modulations evaluated by qRT-PCR assays as in Figs. 3 to 6. Here, increased levels of ITGA5 and ALCAM and their downstream players ROCK1 and PIK3CA were observed (Fig. 16A–E), thus reinforcing the importance of this pathway in miR-214/miR-148b-driven tumor dissemination.

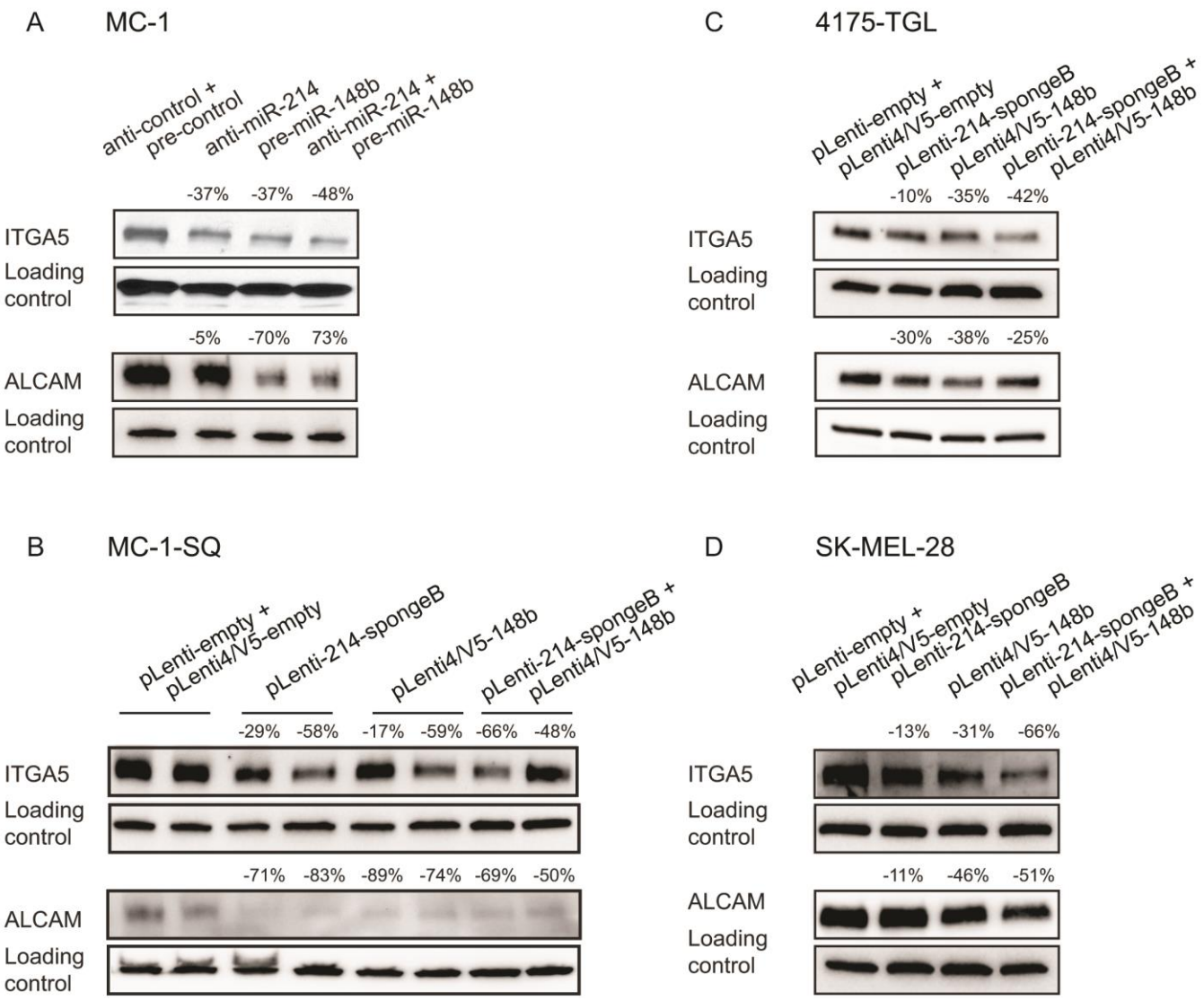

Figure 15 - miR-214 depletion and miR-148b overexpression affect ITGA5 and ALCAM expression. A–D, Western blot analysis of ITGA5 or ALCAM protein expression levels in MC-1 (A), MC-1-SQ (B), 4175-TGL (C), SK-MEL-28 (D), transiently transfected with precursors for miR-148b (pre-miR-148b) or inhibitors for miR-214 (anti-miR-214) or negative controls (pre-control or anti-control), single or in combination, or stably transduced with controls (pLenti-empty, pLenti4/V5-empty) or miR-214-sponge (pLenti-214-spongeB) or miR-148b-overexpressing (pLenti4/V5-148b) vectors, single or in combination, as indicated. Protein modulations were calculated relative to empty controls, normalized on loading controls (GAPDH or actin or hsp90 or tubulin) and expressed as percentages (%). Three independent experiments were performed, and representative ones are shown. SQ, subcutaneous tumors.

Figure 16 - miR-148b target genes analysis.(A-E) Western blot analysis of ALCAM, ITGA5, ROCK1 and PIK3CA protein expression levels in MA-2 or 4175-TGL or HBL-100 cells transiently transfected with miR-214 (pre-miR-214) or miR-148b (pre-miR-148b) precursors or miR-148b inhibitors (anti-miR-148b) or negative controls (anti- or pre-control), alone or in combination, or stably transduced with control (pLemiR-empty and/or pLenti-empty) or miR-214-overexpressing (pLemiR-214) or miR-148b-sponges (pLenti-148b-spongeA/B) vectors as indicated. Protein modulations were calculated relative to controls, normalized on loading controls (GAPDH or Actin or hsp90 or Tubulin) and expressed as percentages (%). 3 independent experiments were performed and representative ones are shown.

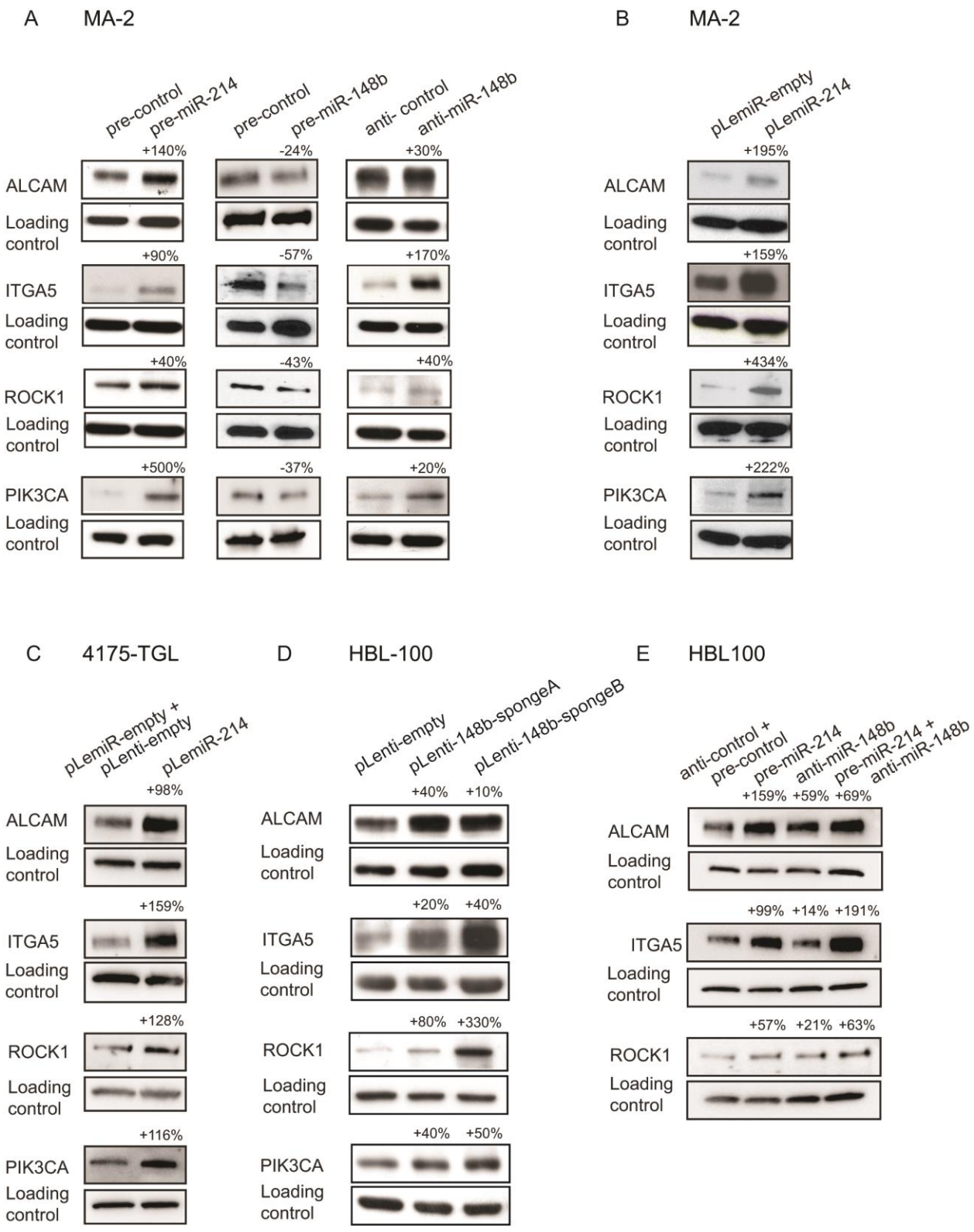
A
MA-2
pre-control
pre-miR-214
pre-control
pre-miR-148b
anti- control
anti-miR-148b
+140%
-24%
+30%
ALCAM
Loading control
+90%
-57%
+170%
ITGA5
Loading control
+40%
-43%
+40%
ROCK1
Loading control
+500%
-37%
+20%
PIK3CA
Loading control
B
MA-2
pLemiR-empty
pLemiR-214
+195%
ALCAM
Loading control
+159%
ITGA5
Loading control
+434%
ROCK1
Loading control
+222%
PIK3CA
Loading control
C
4175-TGL
pLemiR-empty + pLenti-empty
pLemiR-214
+98%
ALCAM
Loading control
+159%
ITGA5
Loading control
+128%
ROCK1
Loading control
+116%
PIK3CA
Loading control
D
HBL-100
pLenti-empty
pLenti-148b-spongeA
pLenti-148b-spongeB
+40%
+10%
ALCAM
Loading control
+20%
+40%
ITGA5
Loading control
+80%
+330%
ROCK1
Loading control
+40%
+50%
PIK3CA
Loading control
E
HBL100
anti-control + pre-control
pre-miR-214
anti-miR-148b
pre-miR-214 + anti-miR-148b
+159%
+59%
+69%
ALCAM
Loading control
+99%
+14%
+191%
ITGA5
Loading control
+57%
+21%
+63%
ROCK1
Loading control

5. Impairment of tumor dissemination by miR-214 depletion and miR-148b overexpression depends on ITGA5 and ALCAM expression inhibition

In order to understand if reduction of ITGA5 or ALCAM was essential for miR-214/miR-148b-driven extravasation inhibition, we modulated ITGA5 or ALCAM levels in the presence of miR-214 depletion and miR-148b overexpression.

First, ITGA5 or ALCAM expression was inhibited by RNA interference in a transient (si-ITGA5 or si-ALCAM) or stable (sh-ALCAM) manner in MA-2 melanoma or 4175-TGL breast cancer cells and transendothelial migration or extravasation evaluated by comparison with empty (si-control, sh-control) cells. As shown in Fig. 17, reduced levels of ITGA5 or ALCAM significantly impaired transendothelial migration (Fig. 17A-B) or lung extravasation, 48 hours after injection (tail vein) in immunocompromised mice (Fig. 17C-D) compared with controls. Modulations of ITGA5 or ALCAM were evaluated by Western blot analysis (Fig. 17). Tumor–endothelial cell contacts are shown in a confocal microscope image (Fig. 17E) in which red (ALCAM staining) MA-2 tumor cells were in contact with green (GFP expression) HUVECs. All these results suggest the relevance of ITGA5 and ALCAM in the control of tumor cell transendothelial migration or extravasation during tumor progression. At this point, ITGA5 or ALCAM were overexpressed in MC-1 or 4175-TGL cells previously transduced with pLenti-214-spongeB or pLenti4/V5-148b or pLenti-empty/pLenti4/V5-empty lentivirus vectors, in single or dual combinations, and cells used to evaluate transendothelial migration. Modulations of ITGA5 or ALCAM were evaluated by Western blot analysis (Fig. 18A–F). In all conditions, we observed increased transendothelial migration, compared with controls, when ITGA5 or ALCAM was overexpressed in cells. Thus, suggesting that repression of transendothelial migration, driven by miR-214-depletion and miR-148b-upregulation, depends on the reduction of these adhesion molecules in tumor cells. In fact, transendothelial migration inhibition was rescued when ITGA5 or ALCAM levels were increased.

Taken together, our results prove that the negative targeting of miR-214 and/or the positive modulation of miR-148b impairs dissemination by acting on ITGA5 or ALCAM, two main players for tumor cell extravasation.

Fig. 17

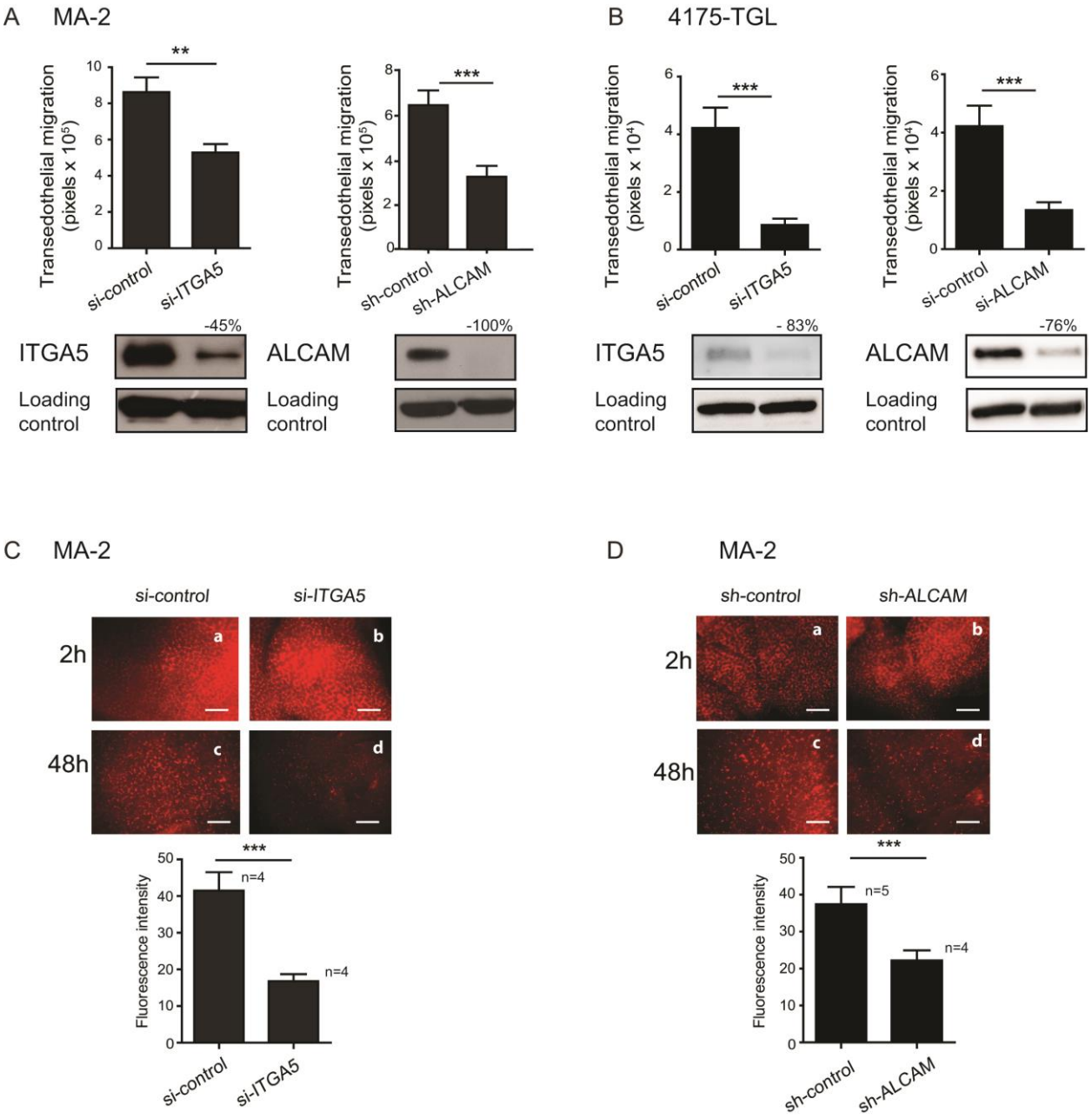
A MA-2
Transedothelial migration (pixels x 10^5)
si-control
si-ITGA5
sh-control
sh-ALCAM
ITGA5
ALCAM
Loading control
-45%
-100%
B 4175-TGL
Transedothelial migration (pixels x 10^4)
si-control
si-ITGA5
si-ALCAM
- 83%
-76%
C MA-2
si-control
si-ITGA5
2h
48h
Fluorescence intensity
n=4
D MA-2
sh-control
sh-ALCAM
n=5
E MA-2
pLVX-ALCAM + HUVEC-GFP / ALCAM

Figure 17 –ITGA5 and ALCAM control transendothelial migration *in vitro* and extravasation in mice.(A-B) Transendothelial migration was evaluated in MA-2 (A) or 4175-TGL (B) cells transiently transfected with si-ITGA5 or si-ALCAM or control siRNAs (si-control) or transduced for sh-ALCAM or sh-control, as indicated in the panels (A, B). ITGA5 and ALCAM levels were evaluated by Western Blot analysis, 48h following transfections or in stably transduced cells. Protein modulations were calculated relative to negative controls, normalized on loading controls (GAPDH or Actin) and expressed as percentages (%). Transmigration results are indicated as mean±SEM of the area covered by tumor migrated cells. At least 2 independent experiments (with triplicates) were performed and representative results are shown. SEM= Standard Error of Mean. (C-D) *In vivo* extravasation 2h or 48h following tail vein injections in immunocompromised mice of CMRA-labeled MA-2 cells transfected with si-control or si-ITGA5 or transduced for sh-ALCAM or sh-control, as indicated. Representative pictures of whole red fluorescent lungs are shown (a-b=2h; c-d=48h); bar=800 µm. Results are presented as mean±SEM of the number of extravasated cells at 48 h for the indicated number of mice (n). 2 independent experiments were carried out (with triplicates) and representative ones are shown. SEM= Standard Error of Mean. (E) Confocal microscopy image for HUVECs-MA-2 co-cultures: HUVECs are green for GFP expression, MA-2 are red for ALCAM staining. Nuclei are blue for DAPI staining.

Figure 18 - Transendothelial migration depends on ITGA5 and ALCAM expression in miR-214-depleted and/or miR-148b-overexpressing tumor cells. A–F, transendothelial migration was evaluated in MC-1 (A, C, E) or 4175-TGL (B, D, F) cells stably transduced with miR-214-sponge (pLenti-214-spongeB) or miR-148b-overexpressing (pLenti4/V5-148b) vectors, single or in combination, and, in addition, transiently transfected with recombinant vectors for the overexpression of ITGA5 or ALCAM or empty controls, as indicated in the panels. ITGA5 and ALCAM levels were evaluated by Western blot analysis, 24 hours or 48 hours following transfections. Protein modulations were calculated relative to negative controls, normalized on loading controls (GAPDH or actin) and expressed as percentages (%). Transmigration results are indicated as mean±SEM of the area covered by tumor-migrated cells. At least two independent experiments (with triplicates) were performed, and representative results are shown.

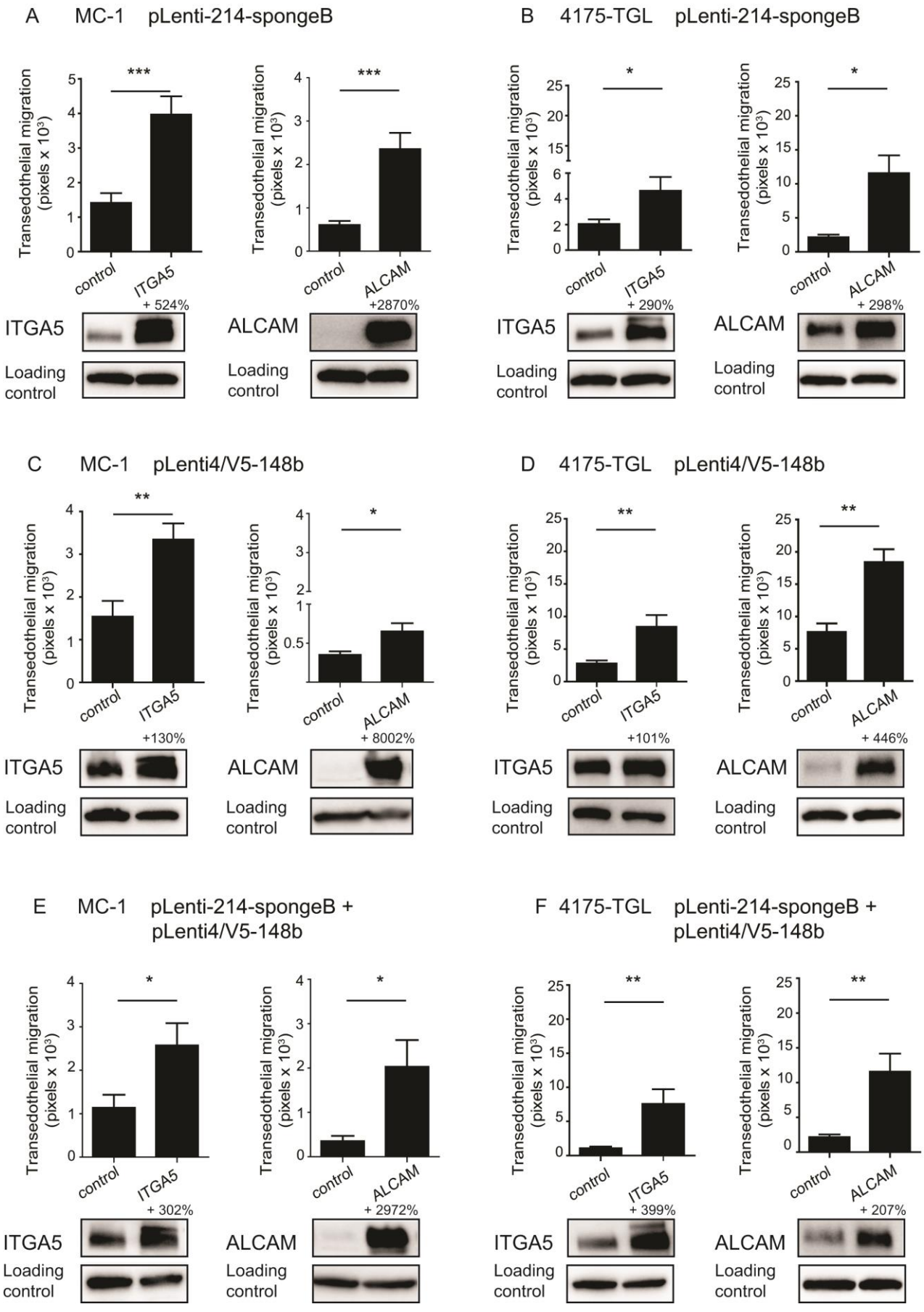
A MC-1 pLenti-214-spongeB
B 4175-TGL pLenti-214-spongeB
C MC-1 pLenti4/V5-148b
D 4175-TGL pLenti4/V5-148b
E MC-1 pLenti-214-spongeB + pLenti4/V5-148b
F 4175-TGL pLenti-214-spongeB + pLenti4/V5-148b
Transedothelial migration (pixels x 10³)
control
ITGA5
ALCAM
+ 524%
+2870%
+ 290%
+ 298%
+130%
+ 8002%
+101%
+ 446%
+ 302%
+ 2972%
+ 399%
+ 207%
ITGA5
ALCAM
Loading control

6. miR-214 expression correlates with ITGA5 and ALCAM levels, while it anticorrelates with miR-148b, in melanoma metastases and in primary breast tumors

Breast cancer (n = 1302; refs. 10, 11) and melanoma metastasis (TCGA, https://tcga-data.nci.nih.gov/tcga/; n =352) datasets were used to evaluate miR-214, miR-148b, ITGA5, and ALCAM expression and to look for possible correlations or anticorrelations with one another (Fig. 19A and B). Relevantly, we found that miR-214 and miR-148b anticorrelate in melanoma metastases (P = 7.91e-05) and in primary breast tumors (P = 5.43e-08), while miR-214 significantly correlates with ITGA5 and ALCAM in both datasets. P values were the following: for melanoma metastases: ITGA5 (P = 3.09e-24) and ALCAM (P = 2.69e-09); for primary breast tumors: ITGA5 (P = 1.68e-23) and ALCAM (P = 9.27e-07). These results are therefore in line with our above-presented investigations, thus strengthening the link between miR-214, miR-148b, ITGA5, and ALCAM and its relevance in human tumor progression.

Figure 19 - miR-214 anticorrelates with miR-148b, while it correlates with miR-148b targets ITGA5 and ALCAM, in melanoma metastases or human primary breast tumors. The indicated datasets were used to evaluate miR-214, miR-148b, ITGA5, and ALCAM expression in melanoma metastases (A) and in primary breast tumors (B). Statistically significant negative or positive correlations are shown for miR-214 and miR-148b (anticorrelations) and for miR214 and ITGA5 or ALCAM (correlations). Correlations of normalized expression are represented with a dot plot superimposing the regression line. The shaded area represents the 0.95 standard error confidence interval of the modl predictions. Statistically significant R2 and P values and number of samples (n) are indicated.

A

Melanoma Dataset
(TGCA)
Metastases

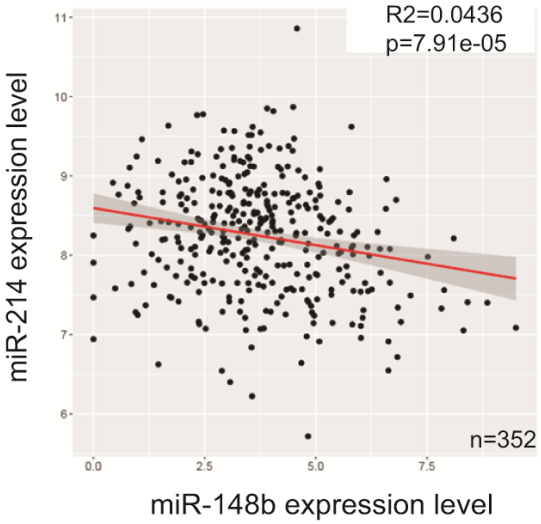

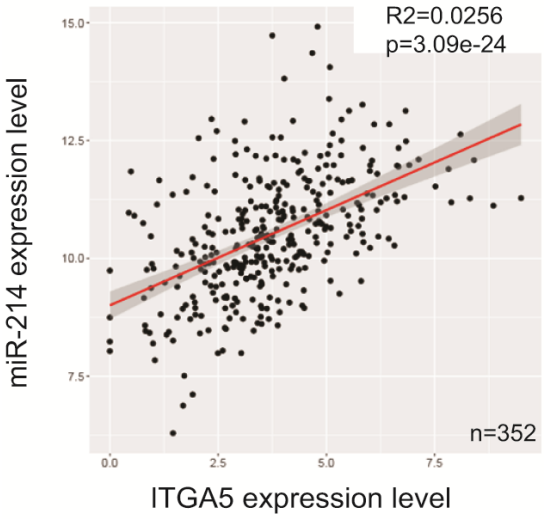

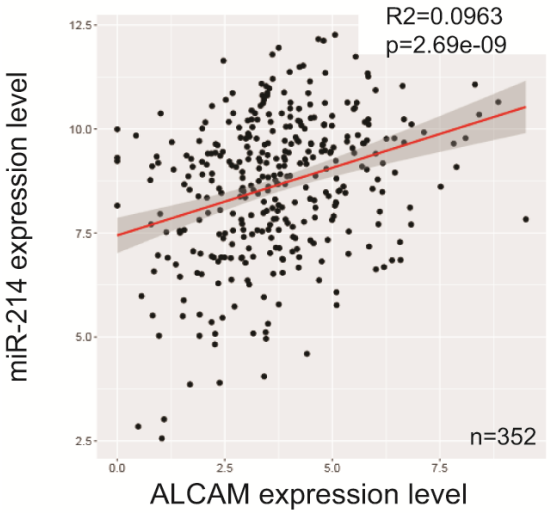

B

Breast Cancer Dataset
(Dvinge et al., 2013; Curtis et al., 2012)
Primary

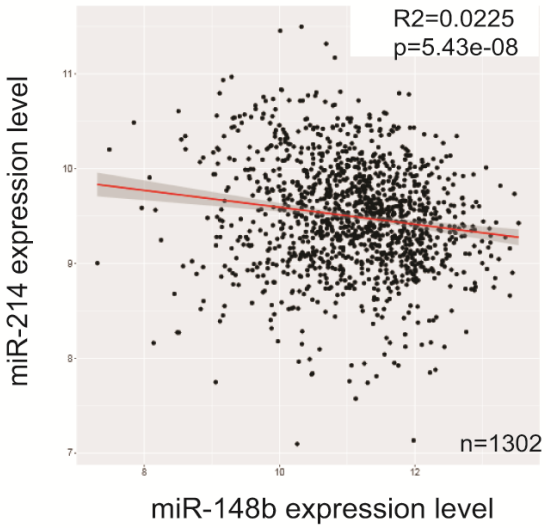

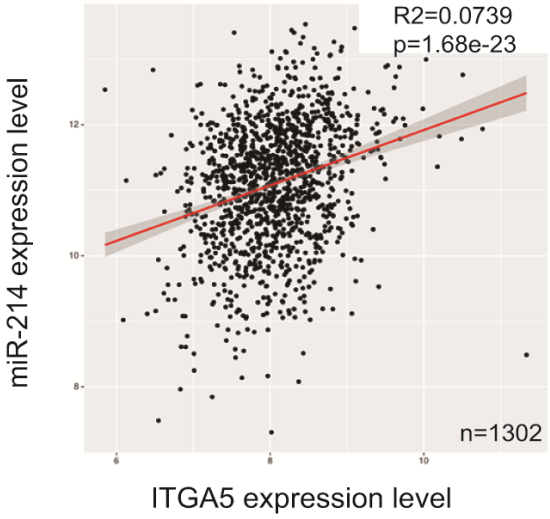

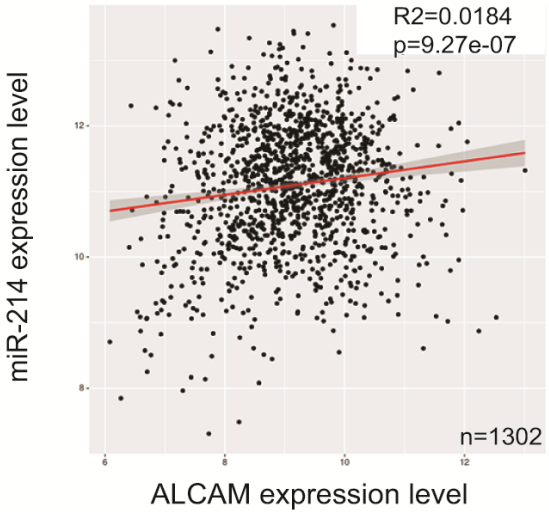

DISCUSSION

We previously demonstrated the prometastatic role of miR-214 (78) and its link with the antimetastatic miR-148b (137). Here, we show that single or combined miR-214 inhibition and miR-148b overexpression in tumor cells strongly modulate metastasis formation by acting mainly during the passage across the vessel endothelium (transendothelial migration/extravasation), a metastatic trait that involves two direct miR-148b targets, the adhesion receptors ITGA5 and ALCAM, in a cell–fibronectin and cell–cell dependent manner. Our data suggest that miR-214 and miR-148b are valuable candidates for miRNA-based targeted therapy.

miR-214 is highly expressed in malignant cutaneous and ocular melanomas (137,142,143) as well as in breast, osteosarcoma, ovary, pancreas, prostate, and gastric cancers (144–149). In line with these findings, upregulation of miR-214 in various tumor cells increases metastasis formation (78,137,150–152). On the other hand, miR-148b is poorly expressed in melanomas and in breast, pancreatic, and hepatocellular carcinomas (83,153–155) and its modulation in tumor cell lines reveals its antimetastatic function (83,156–158). Here, by modulating miR-214 and miR-148b, respectively, in a negative and positive manner, we show that miR-214 and miR-148b are part of a miR-ON-miR regulatory axis where miR-214 favors tumor dissemination following the downregulation of miR-148b and the consequent upregulation of miR-148b direct targets, ITGA5 and ALCAM as well as some of their downstream players (136). Similarly, recent investigations underline the relevance of multiple miR connections (miR-ON-miR) or of miRs and transcription factors (TF) reciprocal regulations (miR-ON-TF-ONmiR). Examples are Lin28-let-7-miR-181 in megakaryocyte differentiation (159), miR-181b-FOS-miR-21 in glioma progression (160), miR-103/107-miR-200 in epithelial-to-mesenchymal transition (161), miR-199a/miR-214-let-7b-miR-34a-miR-762-miR-1915 in breast cancer metastasis (162). All these lines of evidence open up the possibility to target multiple players of the same pathway and give hope for combined therapeutic interventions. In line with this hypothesis, it has recently been shown that the simultaneous systemic delivery of two small non-coding RNAs acting as tumor suppressors, miR-34 and let-7, leads to reduced non–small lung cancer growth (163).

We propose that the presented miR-214-ON-miR-148b regulatory axis controls tumor dissemination acting, in particular, when tumor cells cross the blood vessels endothelium, via the modulation of ITGA5 and ALCAM (136,164–168). In fact, the silencing of ALCAM or ITGA5 inhibits transendothelial migration *in vitro* and extravasation *in vivo*. More relevantly, when miR-214 is depleted and/or miR-148b overexpressed, transendothelial migration suppression can be

overcome by ITGA5 or ALCAM upregulation, thus suggesting that these two adhesion molecules are essential modulators of tumor–endothelial cell interactions. These results are in line with the fact that ALCAM is a cell-to-cell adhesion receptor known to play a major role in mediating the interactions between endothelial and tumor or immune cells during transendothelial migration (164,169,170). Moreover, ALCAM was found to be involved in cell movement (171) and in the conversion of the prometastatic pro-MMP-2 to its active form in malignancy (164). On the other hand, modulations of integrin levels were associated with various metastatic phenotypes (165,172–174). In particular, increased ITGA5 expression has been observed in metastatic melanoma cell lines compared with primary ones (175), and survivin-dependent ITGA5 upregulation was shown to enhance motility of melanoma cells (176). In MDA-MB-231 breast cancer cells, ITGA5 promoted lung metastasis in both spontaneous and experimental lung metastasis models (165). In breast and ovarian cancer patients, ITGA5 expression was shown to be predictive of metastasis and poor prognosis (83,174,177). ITGA5 has also been linked to extravasation; in fact, it has been shown that Cav1–Rho-GTPase-dependent control of cell extravasation depends on ITGA5 levels and inhibition of this regulatory axis impairs extravasation and survival of metastatic cells (178). The fact that high levels of ITGA5 and ALCAM correlate with miR-214 and that miR-214 expression anticorrelates with miR-148b in human breast and melanoma, tumors, or metastases, further strengthens the importance of these players and their direct functional connections in tumorigenesis.

With particular relevance for targeted therapy, the evidence that single or combined miR-214 downregulation and miR-148b upregulation in tumor cells inhibit metastasis formation in mice, gives hope for an miRNA-based therapy. Due to the relevance of ALCAM and ITGA5 in the pathway presented here, one could even speculate to target these two adhesion molecules with specific antibodies, in addition to miRNA targeting, to further affect metastasis formation. Considering that the main issue of the miRNA-based targeted therapy is the *in vivo* delivery, it is essential to identify safe, selective, and efficient compound systemic deliveries. For this purpose, we are currently developing new tools to administer miR-214 inhibitors and miR-148b precursors to animals and test their efficacy on metastasis formation.

In conclusion, our data demonstrate that the cascade of events, including miR-214, miR-148b, ALCAM, and ITGA5, is controlling melanoma and breast cancer progression and it can be exploited for combinatorial therapeutic interventions.

CHAPTER II: Axl-148b aptamer inhibits melanoma and breast cancer tumor progression

RESULTS

1. **Axl-mediated delivery of miR-148b using axl-148b aptamers**.

In the first chapter of this work, we demonstrated the therapeutic potential of imposed miR-148b overexpression in tumor cells. With the intent to specifically deliver miR-148b to cancer cells, we used an aptamer as a carrier of miR-148b. Precisely, we used GL21.T aptamer, an antagonist of the axl tyrosine kinase receptor, previously well characterized (133) and shown to work successfully for miRNAs delivery (130,132,179,180). Relevantly, axl is highly expressed in tumor cells (melanoma, breast cancer), but not in normal cells: it is, in fact, a well-known oncogene. A multifunctional conjugate (axl-148b) composed by the axl aptamer and the human miR-148b was generated (Fig. 20A): miR-148b was attached to a 34-mer truncated version of the 92-mer original axl aptamer (133) able to specifically bind to and antagonize axl. The passenger strand of miR-148b was elongated at the 3' end with a sticky sequence that could bind the aptamer sticky sequence. Then, the complementary miR-148b guide strand was annealed to the passenger strand. 2'-fluoro pyrimidines (2'F-Py) were included in the sequence in order to protect from degradation by nucleases. miR-148b guide strand also held two overhanging bases (UU) at 3' end to favor Dicer processing (181). To obtain the selection of the correct strand and, consequently, target specificity, we used the distal stem portion of the human mir-148b pre-miRNA sequence. Specifically, the first 5' end 27 bases and the first 3' end 26 bases of miR-148 precursor (pre-miR-148b) were employed instead of the mature miR-148b. The resulting miRNA duplex should correspond to the native mature miR-148b in terms of stability and thermodynamic properties.

First of all, axl levels were evaluated by qRT-PCR analysis in lung adenocarcinoma (A549), melanoma (MA-2 and MC-1) and breast cancer (MDAMB231, 4175-TGL and SKBR3) cell lines. All cells, apart from the SKBR3 line, showed detectable axl mRNAs (Fig. 20B). However, the triple negative cancer cell lines MDAMB231 and 4175-TGL expressed substantially higher axl mRNA levels than lung cancer and melanoma lines. Precisely, a 17 or 7 fold increase was evidenced for axl mRNA levels respectively in MDAMB231 and 4175-TGL cells compared to the A549 counterparts.

To assess whether axl aptamer could function as a selective delivery carrier for the conjugated miR-148b, we treated A549, MA-2, MDAMB231, 4175-TGL and SKBR3 cells for 48 hours with 400 nmol/l of axl-148b and determined miR-148b extent by qRT-PCR analysis. Compared to cells left untreated (control=ctrl) or treated with the axl aptamer only, A549 (Fig. 20C), MA-2 (Fig. 20D), MDAMB231 (Fig. 20E) and 4175-TGL (Fig. 20F) cells treated with the chimeric axl-148b aptamer showed an important overexpression of miR-148b levels, however lower than cells transfected with pre-miR-148b (pre-148b). Here, a negative miRNA control (pre-control) was used. For all cell lines, treatments with axl aptamer alone did not alter miR-148b levels. Importantly, the administration of axl-148b conjugates to SKBR3 axl negative (-) cells did not affect miR-148b levels. However, miR-148b levels in pre-148b transfected SKBR3 cells was comparable to what obtained for A549, MA-2, MDAMB231 and 4175-TGL transfected cells (Fig. 20G). In line, the expression of miR-148b paralleled axl levels on cell surfaces. In fact, higher miR-148b levels were found in cells expressing more axl (MDAMB231 and 4175-TGL) compared to lower expressing cells (A549 and MA-2). Similarly, the conjugation of let-7g to axl aptamer, resulted specific for let-7g. No alteration of miR-148b was found. These results suggest that only axl-driven internalization of miR-148b occurred (Fig. 21A-B). Moreover, treating A549 and MA-2 cells with axl-148b chimeras increased miR-148b levels in a time and dose dependent way (Fig. 21C and D, respectively). Specifically, when A549 were treated for 1 or 5 hours (5h) or over/night (O/N) expression of miR-148b resulted 5 or 16 or 200 fold increased, respectively compared to untreated (ctrl) or axl-treated A549 cells (Fig. 21C). When we evaluated the effect of different axl-148b aptamer concentrations on miR-148b levels in MA-2 cells: 400 (1x), 800 (2x) or 1600 (4x) nmol/l (Fig. 21D), we observed a 120, 450 or 1800-2000 fold increase of miR-148b respectively, compared to no treatment or axl aptamer only.

Taken together, all these results indicate that axl aptamer works in a selective manner to convey miR-148b inside the cells. In fact, only axl-expressing cells show increased levels of miR-148b in an aptamer concentration and time dependent manner. Instead, in absence of axl on the cells surface, no increased levels of miR-148b can be seen.

Fig. 20

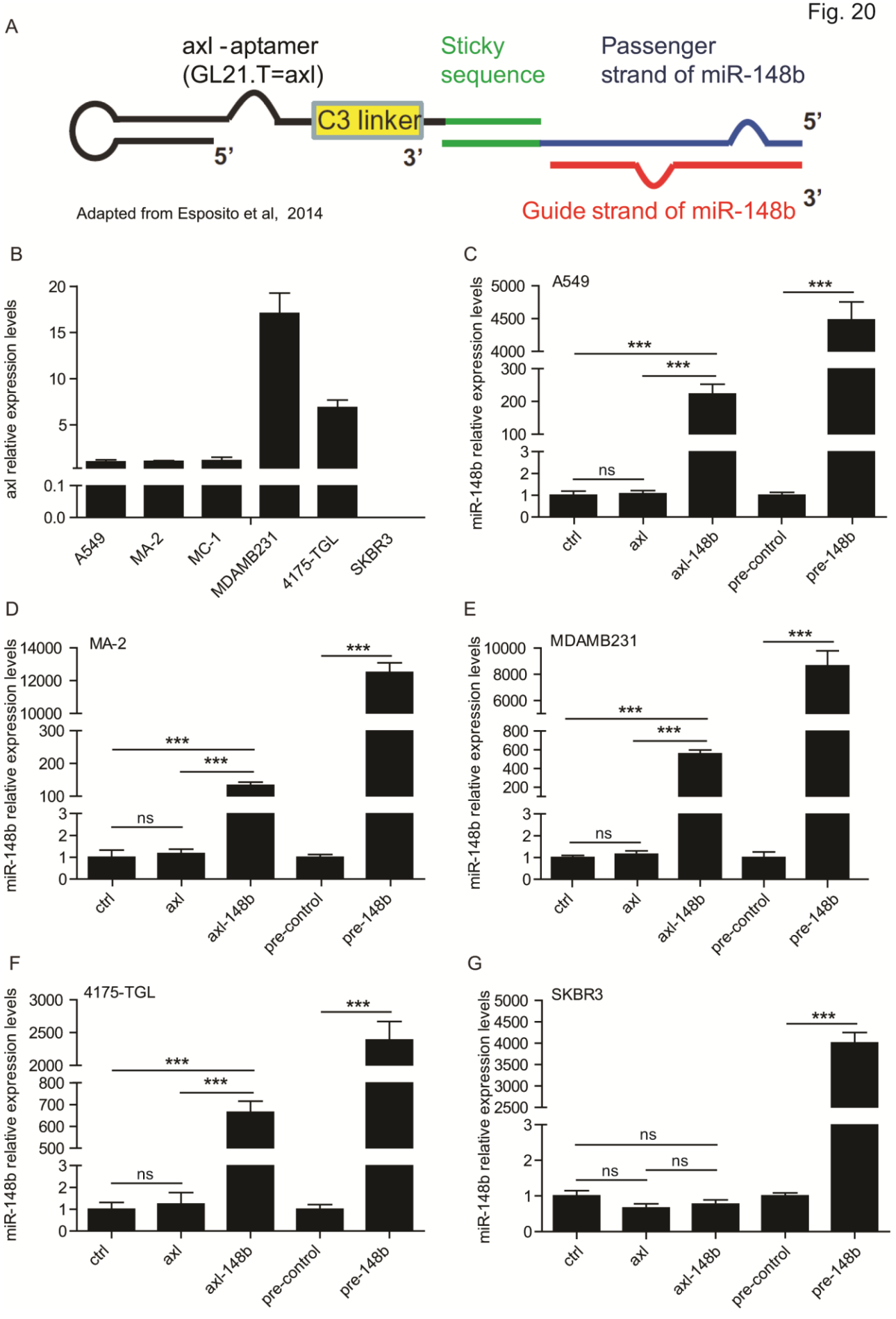
A
axl -aptamer
(GL21.T=axl)
Sticky
sequence
Passenger
strand of miR-148b
C3 linker
5'
3'
5'
3'
Guide strand of miR-148b
Adapted from Esposito et al, 2014
B
axl relative expression levels
A549
MA-2
MC-1
MDAMB231
4175-TGL
SKBR3
C
A549
miR-148b relative expression levels
ns
***
ctrl
axl
axl-148b
pre-control
pre-148b
D
MA-2
E
MDAMB231
F
4175-TGL
G
SKBR3

Figure 20 – Preparation of axl-148b and miR-148b delivery in tumor cells. (A) Schematic representation of the axl-148b aptamer conjugate adapted from (129). (B) Axl mRNA levels were analysed by qRT-PCR in melanoma MA-2, MC-1 and breast cancer MDAMB231, 4175-TGL cells. The axl^+ A549 lung cancer and axl^- SKBR3 cell lines were used respectively as positive and negative controls of expression. Results are shown as fold changes (mean±SD) relative to A549 cells, normalized on GAPDH mRNA levels. Two experiments with independent RNA preparations were performed and a representative one is shown. (C-G) miR-148b expression levels were tested by qRT-PCR analysis for the indicated cell lines left untreated (controls=ctrl) or treated with 400 nmol/l of axl or axl-148b aptamers. Alternatively, cells were transfected with 75 nmol/l of miR-148b precursor (pre-148b) or its negative control (pre-control). Results are shown as fold changes (mean±SD) relative to controls (ctrl or pre-control), normalized on U6 or U44 small nucleolar RNA levels. 2 experiments with triplicates were performed and a representative one is shown. ns = not significant; * $p < 0.05$, ** $p < 0.01$, *** $p < 0.001$. SD=standard deviation.

Figure 21 – miR-148b or let-7g expression modulation in tumor cells or mammospheres treated with axl-148b or axl-let-7g aptamers. miR-148b (A, C, D) or let-7g (B) expression levels were evaluated by qRT-PCR analysis in A549 (A-C) or MA-2 (D) cells. (A) miR-148b levels in A549 cells left untreated (controls=ctrl) or treated with 400 nmol/l of axl, axl-148b or axl-let-7g aptamers or transfected with 75 nmol/l of miR-148b precursor (pre-148b) or its control (pre-control). (B) let-7g levels in A549 cells treated with 400 nmol/l of axl or axl-let-7g aptamers. (C) miR-148b levels in A549 cells treated with 400 nmol/l of axl or axl-148b aptamers at the indicated time points. (D) MA-2 cells treated with 400 (1x), 800 (2x) or 1600 (4x) nmol/l of axl or axl-148b aptamers or transfected with 75 nmol/l of miR-148b precursor (pre-148b) or its negative control (pre-control). (E) miR-148b expression levels were tested by qRT-PCR analysis for 4175-TGL mammospheres left untreated (controls=ctrl) or treated with 400-200 nmol/l of axl or axl-148b aptamers. All results are shown as fold changes (mean±SD of triplicates) relative to controls (ctrl or pre-control), normalized on U6 or U44 small nucleolar RNA levels. 2 independent experiments were performed and representative results are shown. ns = not significant; * $p < 0.05$, ** $p < 0.01$, *** $p < 0.001$. SD=standard deviation. O/N= overnight.

Fig. 21

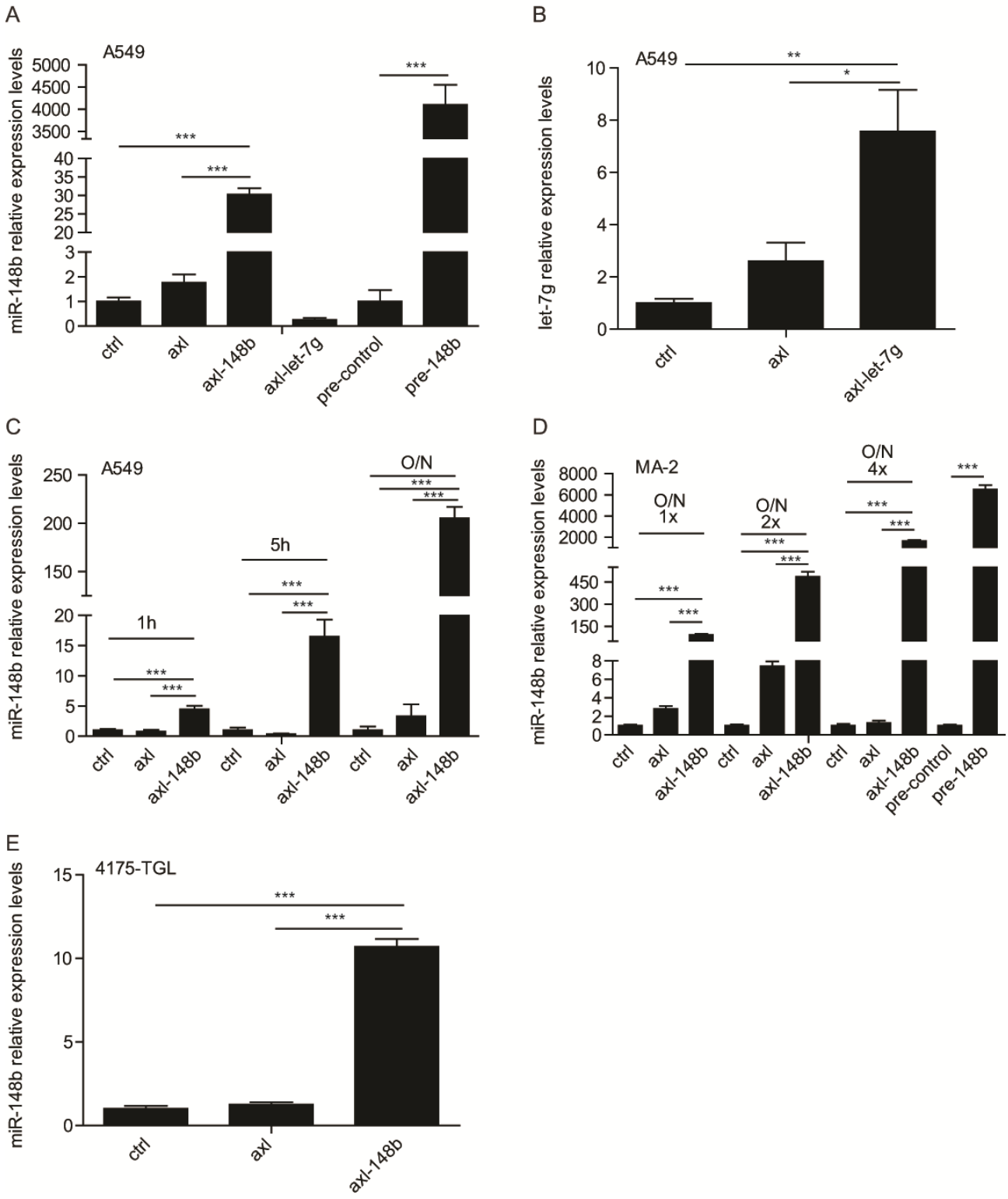
A
A549
miR-148b relative expression levels
5000
4500
4000
3500
40
35
30
25
20
3
2
1
0
***
***
***
ctrl
axl
axl-148b
axl-let-7g
pre-control
pre-148b
B
A549
let-7g relative expression levels
10
8
6
4
2
0
**
*
ctrl
axl
axl-let-7g
C
A549
miR-148b relative expression levels
250
200
150
20
15
10
5
0
1h
5h
O/N
***
ctrl
axl
axl-148b
D
MA-2
miR-148b relative expression levels
8000
6000
4000
2000
450
300
150
8
6
4
2
0
O/N 1x
O/N 2x
O/N 4x
pre-control
pre-148b
E
4175-TGL
miR-148b relative expression levels
15
10
5
0

2. Axl-148b conjugates inhibit tumor cell movement and favor *anoikis*, but they do not affect proliferation.

We previously demonstrated that miR-148b is an antimetastatic small non-coding RNA able to coordinate metastatic traits such as migration, invasion and metastasis formation (83,182). Here, we investigated the ability of axl-148b conjugates to affect tumor cell dissemination, also considering synergistic effects of miR-148b with axl aptamer only. In fact, an effect on cell motility by axl aptamer has already been demonstrated (133). Specifically, we analysed migration, invasion through matrigel, transendothelial invasion on a HUVECs monolayer, *anoikis* and proliferation *in vitro*. Lung cancer (A549), melanoma (MA-2) or breast cancer (MDAMB231, 4175-TGL and SKBR3) cells were left untreated (ctrl), treated with axl aptamers only (axl) or with miR-148b (axl-148b) or, alternatively, transfected with miR-148b precursor (pre-148b) or its control (pre-control). miR-148b modulations were evaluated by qRT-PCR analysis as shown in Fig. 20C-G. Axl aptamers could reduce cell migration/invasion compared to untreated cells (29-45% inhibition) in A549, MA-2, 4175-TGL and MDAMB231 (Fig. 22A-E). In the same cell lines, cell movement/invasion was further decreased by axl-148b conjugates compared to untreated controls (45-76% inhibition) as in Fig. 22A-E, suggesting a specific miR-148b contribution. In fact, for all cells, migration/invasion was significantly inhibited by axl-148b conjugate treatments compared to axl aptamer administration only (33-55%) as in Fig. 22A-E. miR-148b ability to affect cell movement was also assessed for pre-148b transfected cells cells. Here, 33 to 89% reduction of motility was observed in cells transfected with pre-148b compared to controls (pre-control). Relevantly, axl negative cells (SKBR3) did not show any effect on transwell migration when treated with axl aptamers only or in combination with miR-148b (Axl-148b) (Fig, 22F). On the other hand, when miR-148b overexpression was forced by SKBR3 transfection, cell movement was impaired compared to control miRNA (57% inhibition).

To further investigate axl-148b involvement in later steps of tumor cells invasion, such as extravasation, we simulated transendothelial migration *in vitro*. For this purpose, we seeded CMRA-labelled (red) untreated, axl- or axl-148b treated MA-2 or 4175-TGL cells in the upper chambers of gelatin-coated transwells, covered by a confluent human umbilical vein endothelial cells (HUVECs) monolayer and evaluated tumor cell migration in the lower chambers (Fig. 23A-B). Reduced trasendothelial migration was observed for axl-aptamer treated (axl) or axl-148b conjugate treated cells compared to untreated controls (ctrl). A specific decrease of transendothelial migration was observed for axl-148b treated cells compared to axl aptamer administrations only

(58-72% inhibition). miR-148b transfected cells showed a strong inhibition of transendothelial migration compared to pre-controls (pre-control versus pre-148b).

miR-148b is not only involved in cell motility, but also in another metastatic trait: in the control of *anoikis* (83), a form of apoptosis induced by the lack of a correct attachment between the cell and the Extracellular Matrix (ECM). To investigate this metastatic feature, we evaluated apoptosis in 4175-TGL cells treated or not with axl-148b aptamer, kept without serum and without (*anoikis*) adhesion for 48 h by cytofluorimetric analyses. Reduced survival (20% inhibition) was observed for 4175-TGL cells following axl-148b aptamer treatments compared con controls (ctrl) as in Fig. 24, suggesting a potential intervention of axl-148b aptamers on cell survival without attachment.

Instead, axl-148b treatments did not significantly modify cell proliferation compared to untreated (ctrl) or axl aptamer (axl) treated cells as in Fig. 25A-C. Similar data were obtained for cells transfected with pre-148b versus controls (pre-control) (Fig. 25A-C).

Taken together, these results show that axl-148b aptamers affect cell migration, invasion, transendothelial migration and *anoikis* and that miR-148b work synergistically with axl aptamer. Our results prove axl-148b specificity, since miR-148b levels increase only in axl positive cells.

Figure 22 – Axl-148b aptamers inhibit migration and invasion of tumor cells. (A-F) Transwell migration assays were used to evaluate migration (A-C, E-F) or invasion through matrigel (D) for axl^+ A549 (A), MA-2 (B), 4175-TGL (C,D), MDAMB231 (E) and axl^- SKBR3 (F) cells left untreated (controls=ctrl) or treated with 400 nmol/l of axl or axl-148b aptamers. Alternatively, cells were transfected with 75 nmol/l of miR-148 precursor (pre-148b) or its negative control (pre-control). Results are expressed as ratio of mean±SEM of the area covered by migrated/invaded versus plated tumor cells. At least 2 independent experiments (with triplicates) were performed and representative results are shown. SEM= Standard Error of Mean, ns = not significant; * $p < 0.05$, ** $p < 0.01$, *** $p < 0.001$.

Fig. 22

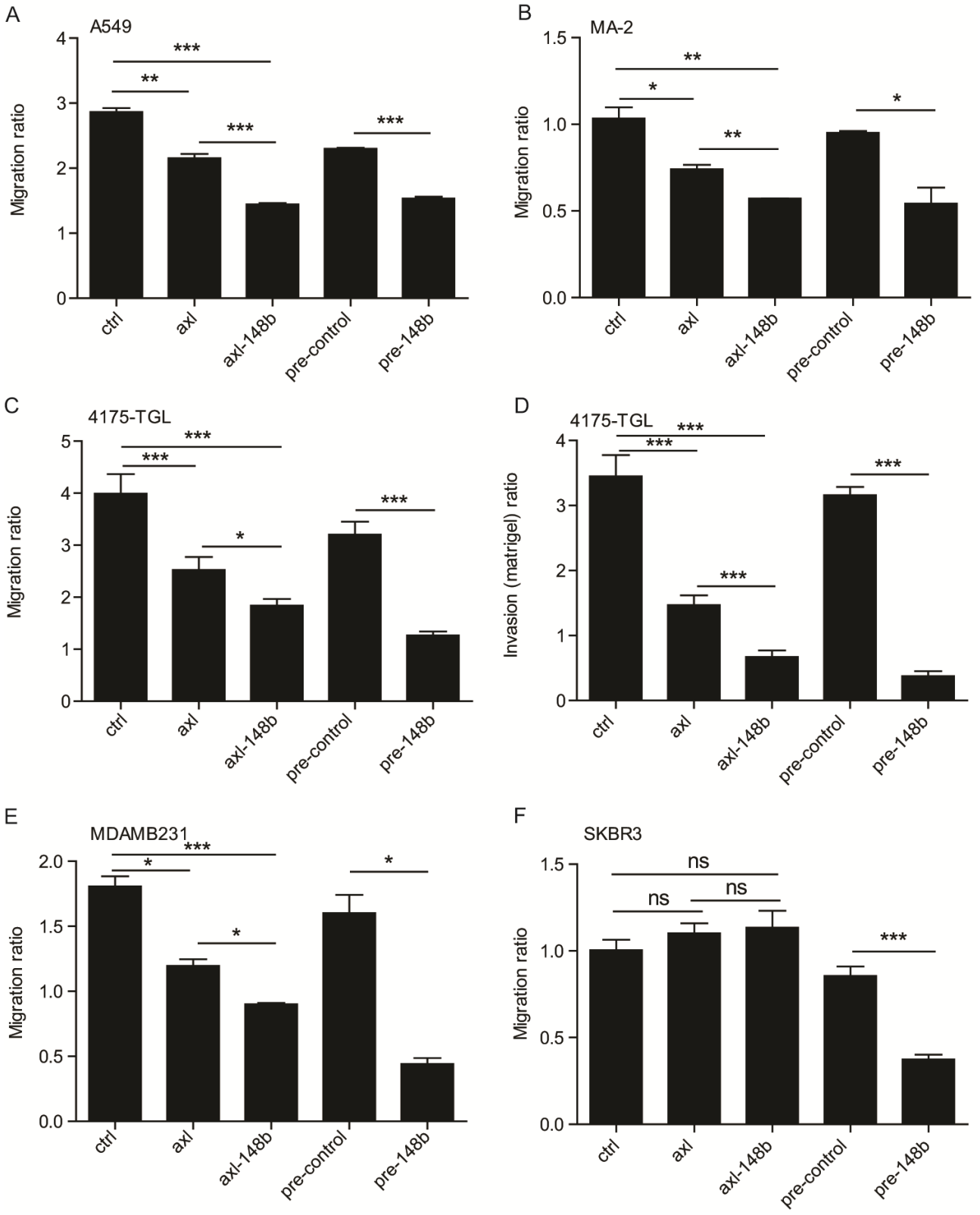
A
A549
Migration ratio
B
MA-2
Migration ratio
C
4175-TGL
Migration ratio
D
4175-TGL
Invasion (matrigel) ratio
E
MDAMB231
Migration ratio
F
SKBR3
Migration ratio
ns
ctrl
axl
axl-148b
pre-control
pre-148b

Fig. 23

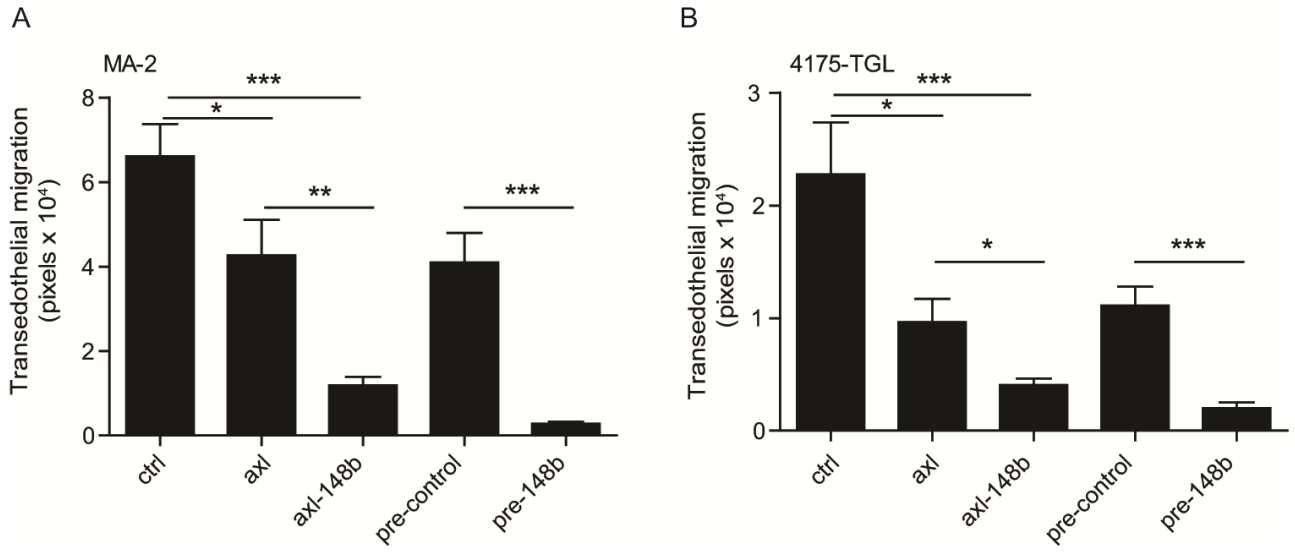

Figure 23 - Axl-148b aptamers inhibit transendothelial migration of tumor cells. (A-B) Transendothelial migration through a HUVECs monolayer on top of a porous membrane for MA-2 (A) or 4175-TGL (B) cells left untreated (controls=ctrl) or treated with 400 nmol/l of axl or axl-148b aptamers. Alternatively, cells were transfected with 75 nmol/l of miR-148b precursor (pre-148b) or its negative control (pre-control). Results are shown as mean±SEM of the area (pixels) covered by migrated cells. At least 2 independent experiments (with triplicates) were performed and representative results are shown. SEM= Standard Error of Mean, ns = not significant; * $p<0.05$, ** $p<0.01$, *** $p< 0.001$.

Fig. 24

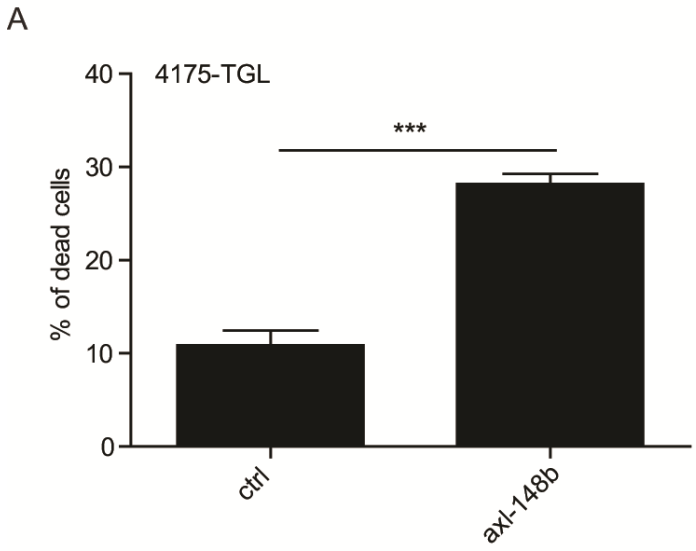

Figure 24 – Axl-148b aptamers induce cell dead of tumor cells in anoikis conditions. 4175-TGL cells were left untreated (controls=ctrl) or treated with 400 nmol/l of axl or axl-148b and grown in absence (anoikis) of attachment and without serum for 48h. Percentage (%) of dead cells was evaluated by annexinV-FITC staining in a FACS analysis. 2 independent experiments were performed in triplicate and representative results are shown. SEM= Standard Error of Mean.

Figure 25 – Axl-148b aptamers do not significantly affect tumor cell growth (A-F) Proliferation of MA-2 (A,B), MDAMB231 (C,D) and 4175-TGL (E-F) cells left untreated (controls=ctrl) or treated with 400 nmol/l of axl or axl-148b aptamers. Allternatively, cells were transfected with 75 nmol/l of miR-148b precursor (pre-148b) or its negative control (pre-control). Results are indicated as mean±SD of the proliferation ratio versus plated cells, measured by optical density at 0-72h. At least 2 independent experiments (with triplicates) were performed and representative results are shown. SD= Standard Deviation.

Fig. 25

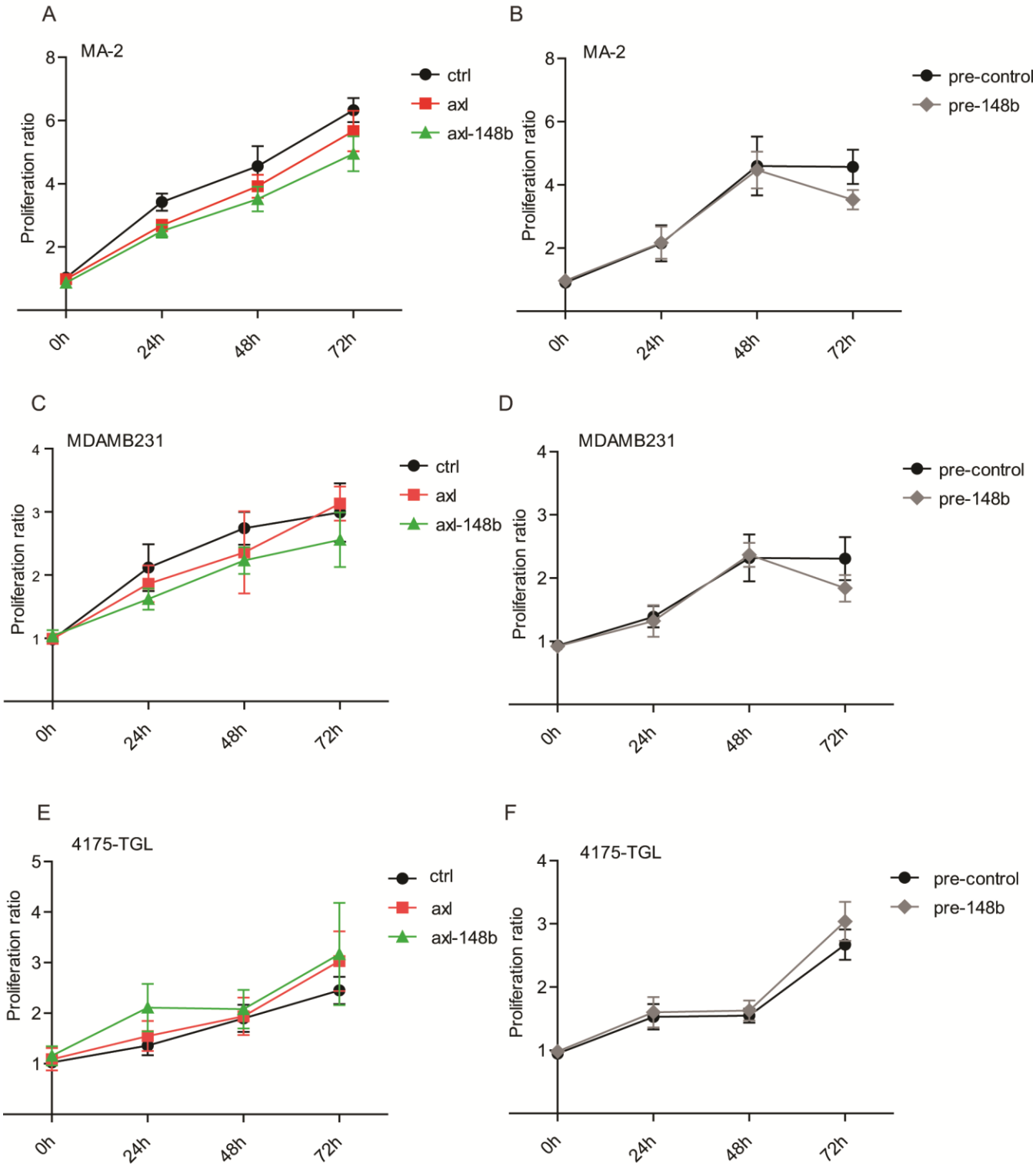
A
MA-2
Proliferation ratio
8
6
4
2
0h
24h
48h
72h
ctrl
axl
axl-148b
B
MA-2
Proliferation ratio
pre-control
pre-148b
C
MDAMB231
Proliferation ratio
4
3
2
1
ctrl
axl
axl-148b
D
MDAMB231
Proliferation ratio
pre-control
pre-148b
E
4175-TGL
Proliferation ratio
5
4
3
2
1
ctrl
axl
axl-148b
F
4175-TGL
Proliferation ratio
pre-control
pre-148b

3. Axl-148b aptamers affect miR-148b direct targets in tumor cells.

Since miRNA functions are exerted by negative regulations on their target genes, we analysed ALCAM and ITGA5, two validated miR-148b direct targets involved in cell extravasation (83,182). We therefore determined whether miR-148b preserved its ability to act on these two molecules when cells were treated with axl-148b conjugates. Lung cancer (A549), melanoma (MA-2) or breast cancer (4175-TGL and SKBR3) cells were left untreated or treated with 400 nmol/l of axl or axl-148b aptamers and protein levels were evaluated by Western Blot (WB) analyses. miR-148b alterations were evaluated by qRT-PCR analysis as in Fig. 20C-G. As shown, axl-148b aptamer treatments led to decreased ALCAM (38 -51%) and ITGA5 (21%-70%) protein expression compared to controls (ctrl or axl) cells (Fig. 26A-C, axl^+ cells). Similarly, transfections with pre-148b inhibited ALCAM and ITGA5 endogenous protein levels of about 30-57% and 25-95% compared to controls (pre-control) as visible 48h post-transfection. Notably, axl negative SKBR3 cells did not show any effect on ALCAM expression when cells were treated with axl or axl-148b aptamers, however reduced ALCAM expression was seen following transfection of these cells with pre-148b compared to controls (pre-control) as in Fig. 26D.

These results suggest that when axl expressing cells are treated with axl-148b conjugates, miR-148b levels increase and its two direct targets, ALCAM and ITGA5 decrease. Moreover, they show axl-148b aptamer specificity because no effect is observed on axl^- cells.

Figure 26 – Axl-148b aptamers affect ALCAM and ITGA5 expression in tumor cells. (A-D) Western blot analysis of ALCAM and ITGA5 protein expression levels in axl^+ A549 (A), MA-2 (B), 4175-TGL (C) and axl^- SKBR3 (D) cells left untreated (controls=ctrl) or treated with 400 nmol/l of axl or axl-148b aptamers. Alternatively, cells were transfected with 75 nmol/l of miR-148b precursors (pre-148b) or its negative control (pre-control). Protein modulations were calculated relative to controls (ctrl or pre-control), normalized on loading controls (α-tubulin or GAPDH) and expressed as percentages (%). At least 2 independent experiments were performed and representative results are shown.

Fig. 26

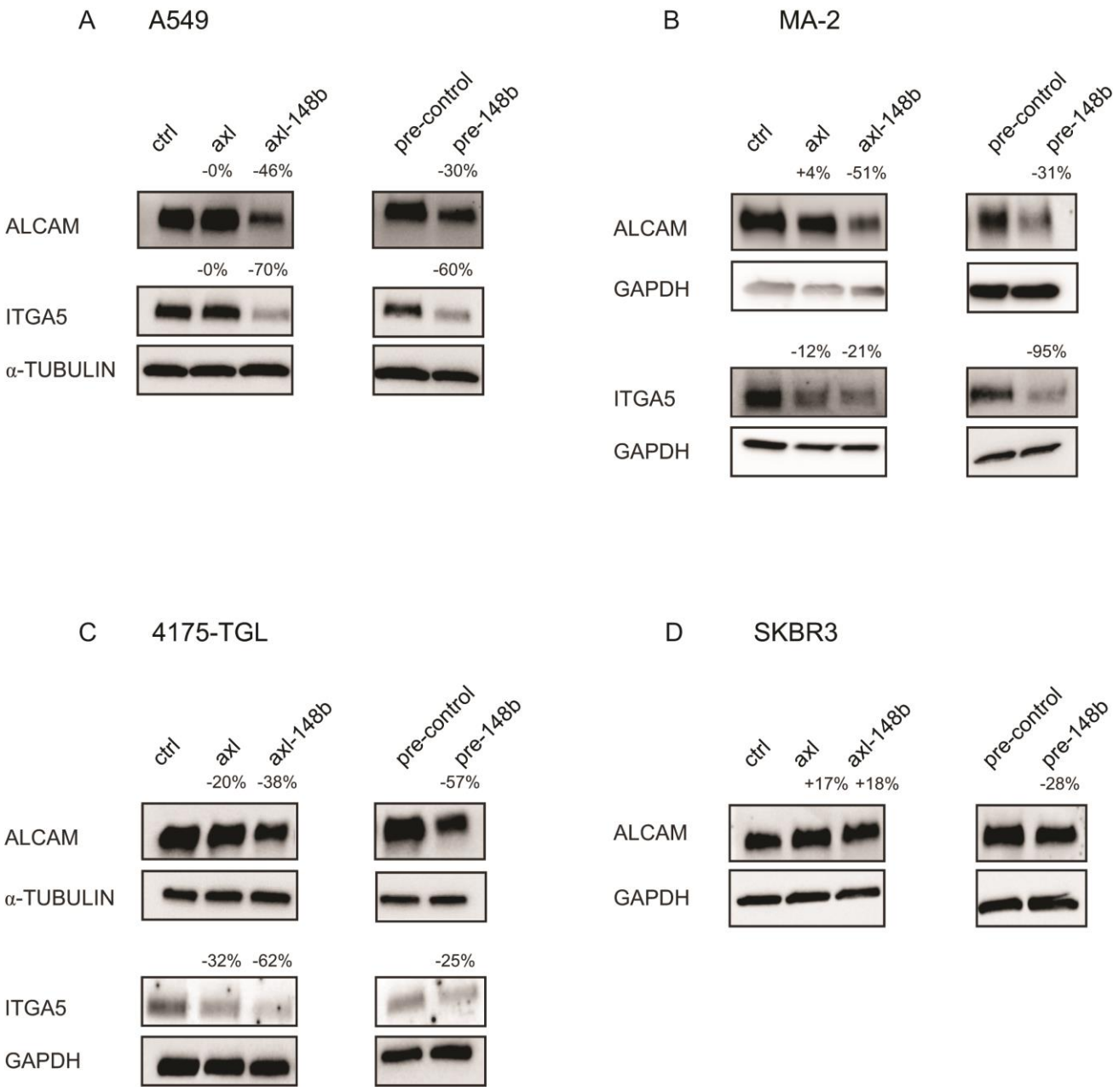
A
A549
ctrl
axl
axl-148b
pre-control
pre-148b
-0%
-46%
-30%
ALCAM
-0%
-70%
-60%
ITGA5
α-TUBULIN
B
MA-2
ctrl
axl
axl-148b
pre-control
pre-148b
+4%
-51%
-31%
ALCAM
GAPDH
-12%
-21%
-95%
ITGA5
GAPDH
C
4175-TGL
ctrl
axl
axl-148b
pre-control
pre-148b
-20%
-38%
-57%
ALCAM
α-TUBULIN
-32%
-62%
-25%
ITGA5
GAPDH
D
SKBR3
ctrl
axl
axl-148b
pre-control
pre-148b
+17%
+18%
-28%
ALCAM
GAPDH

4. Axl-148b aptamers affect mammosphere number and growth.

We used mammospheres originated from 4175-TGL and SKBR3 breast cancer cells to evaluate how axl-148b aptamers could function in a 3D model. As shown in in Fig. 27A, single cells were left untreated (controls=ctrl) or treated with 400 nmol/l of axl or axl-148b aptamers, treatments were then renewed at day 3 and 5 by adding fresh aptamer/conjugates (200 nmol/l) and spheres analysed at day 5. Alternatively, we plated single cells and waited 5 days for mammosphere formation, then we dissociated them and replated the single cells without treating them (controls=ctrl) or by treating the units with 400 nmol/l of axl or axl-148b conjugates. Treatments were renewed by adding aptamer/conjugates (200 nmol/l) for a total of tree treatments/week as shown in Fig. 27B. miR-148b levels were evaluated by qRT-PCR analysis at day 5 and increased miR-148b levels were observed following axl-148b aptamer treatments, suggesting that our conjugates could enter in the mammospheres and be processed (Fig. 21E).

Then we investigate the effect of axl-148b aptamers on mammosphere formation by measured their size (µm) at day 5 (Fig. 27C) or 12 (Fig. 27D) and observed a significant reduction of mean lenght comparing to controls (ctrl) or to axl-treated cells, thus suggesting that the multifunctional conjugates work and synergize together (Fig. 27C-D). Importantly, when axl-148b aptamers were used to treat SKBR3 mammospheres (axl^-), no effect on size was detected (Fig. 28A).

We also analysed axl-148b aptamers ability to act on mammosphere stemness. To do so, we counted the mammospheres at day 5 or 12 (Fig. 27E-F). No significative difference in mammospheres number was detected for axl-aptamer treated mammospheres compared to controls (ctrl). However, a significant decrease was observed for axl-148b aptamer treated cells compared to controls (ctrl) and to axl aptamers only. This effect on stemness was further evaluated on the same cells used in Fig. 27B, previously labelled, at day 5, with PKH26, a membrane dye that dilutes every time cells divide. At day 12, mammospheres were harvested, trypsinized and single cells analysed by FACS for their retention of epifluorescence ($PKH26^{positive}$ and $PKH26^{negative}$ cells). Here, we observed that following axl-148b aptamer treatments, the number of positive cells was higher than for axl aptamers treated cells or for control (ctrl) cells (85% versus 79% versus 75%). On the contrary, there were more negative cells in control (ctrl) or axl aptamer treated cells (Fig. 27G). Importantly, axl-148b aptamer was not able to interfere with mammospheres forming ability in SKBR3 axl^- cells (Fig. 28B).

Together, these data indicates that axl-148b aptamers reduce mammosphere size and number in axl^+ cells compared to untreated or axl-aptamer alone treated ones, but they do not affect mammospheres derived from axl^- SKBR3 cells.

Figure 27 –Axl-148b aptamers affect mammospheres derived from axl^{+} tumor cells. (A-B) Time-course of the experiment for 4175-TGL breast cancer cells plated and grown in suspension for 5 days as mammospheres, left untreated (controls=ctrl) or treated with 400 nmol/l of axl or axl-148b or untreated and dissociated again at day 5, replated and treated (B). (C-D) Top: representative images of 4175-TGL derived-mammospheres. Bottom: box-and-whisker plots of sphere dimentions shown as mean±SEM of sphere lenght (µm) at day 5 (C) or 12 (D). (E-F). Box-and-whisker plots of mammosphere quantitations referring to 50 µl volume at day 5 (E) or 12 (F). (G) 4175-TGL cells stained with PKH26 at day 5 and positive or negative units evaluated at day 12 as mean±SE percentage (%) of total based on FACS analysis. 2 or 3 independent experiments (with triplicates) were performed and representative results are shown. Black lines in (C) and (D) corresponds to measurements for size. ns = not significant; * $p < 0.05$, ** $p < 0.01$, *** $p < 0.001$. SEM= Standard Error of Mean.

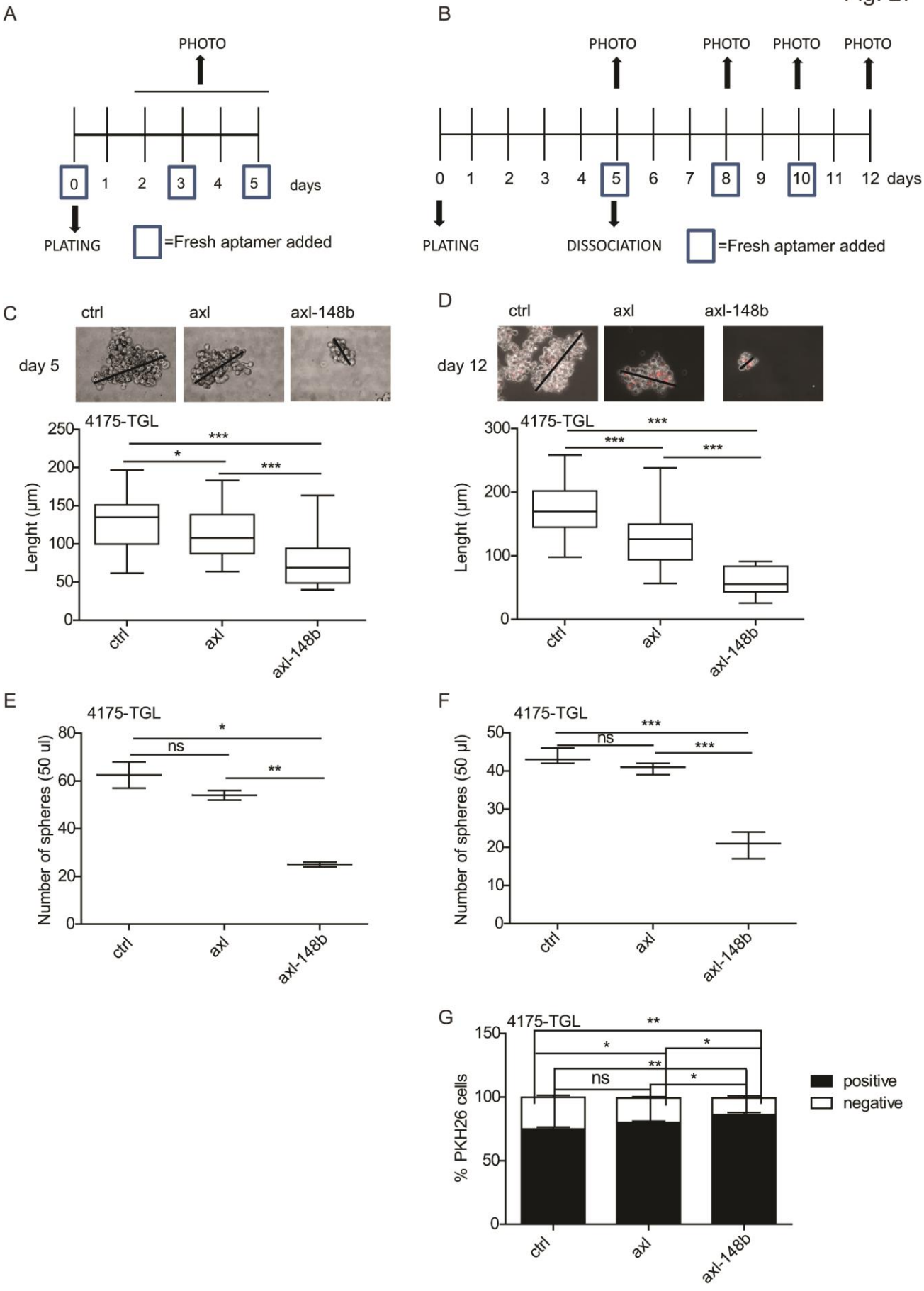
A
PHOTO
0 1 2 3 4 5 days
PLATING
=Fresh aptamer added
B
PHOTO
PHOTO
PHOTO
PHOTO
0 1 2 3 4 5 6 7 8 9 10 11 12 days
PLATING
DISSOCIATION
=Fresh aptamer added
C
ctrl
axl
axl-148b
day 5
4175-TGL
Lenght (µm)
ctrl
axl
axl-148b
D
ctrl
axl
axl-148b
day 12
4175-TGL
Lenght (µm)
ctrl
axl
axl-148b
E
4175-TGL
Number of spheres (50 ul)
ns
ctrl
axl
axl-148b
F
4175-TGL
Number of spheres (50 µl)
ns
ctrl
axl
axl-148b
G
4175-TGL
% PKH26 cells
ns
positive
negative
ctrl
axl
axl-148b

Fig. 28

A

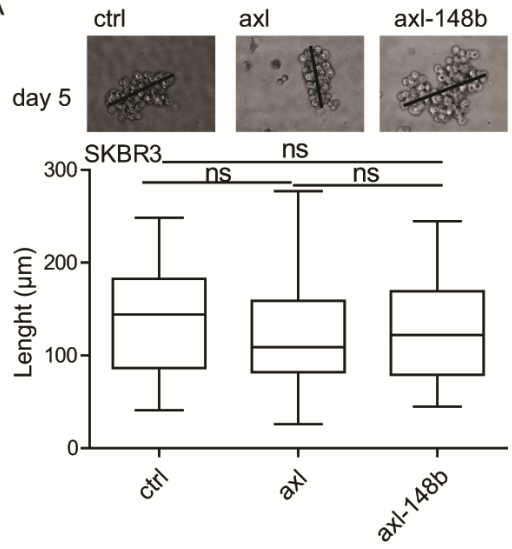

B

SKBR3 Number of spheres (50 µl)

ctrl	axl	axl-148b
45	39	42

Figure 28– Axl-148b aptamers do not affect mammospheres derived from axl$^-$ tumor cells. (A) Top: representative images of SKBR3 derived-mammospheres. Bottom: box-and-whisker plots of sphere lenght shown as mean±SEM of sphere diameters (µm) at day 5. (B) Table showing SKBR3 mammosphere quantitations referring to 50 µl volume at day 5 of treatments as in Figure 5A. Black lines in (A) corresponds to measurements for size 2 experiments with triplicates were performed and representative results are shown. SD=standard deviation. ns = not significant

5. Axl-148b aptamers promote necrosis and apoptosis in primary tumors and block tumor cells dissemination.

In order to evaluate the therapeutic potential of axl-148b based treatments on primary tumors and metastatic dissemination, 4175-TGL breast cancer or MA-2 melanoma cells were injected into the mammary gland fat pad or in the flank (subcutaneously) of NOD/SCID/IL2R_null (NSG) immunocompromised mice. Tumor growth and dissemination of Circulating Tumor Cells (CTCs) were evaluated 32-33 days later in mice treated with PBS only or axl-148b conjugates, 100 µl intratumor, 3 times/week starting from day 11 (4175-TGL) or 12 (MA-2), as in Fig. 29A and 30A. The evaluation of the primary tumor mass, showed a weight reduction for 4175-TGL-derived tumors following axl-148b aptamer injections versus controls (Fig. 29B). However, no difference was revealed for MA-2-derived tumors (Fig. 30B).

When H&E staining were performed on these tumors, we observed increased tumor necrotic areas for breast cancer and melanoma tumors following axl-148b conjugate treatments (Fig. 29C and 30C). ImmunoHistoChemistry (IHC) analysis for Cleavaed Caspase-3 nuclear apoptotic marker revealed that axl-148b aptamers also induced an increase in apoptosis compared to PBS treated mice (Fig. 29D). However, when we measured miR-148b levels in the tumors, at the experiment end point, by qRT-PCR, no differences was found between the two groups of tumors (Fig. 31). Considering the importance of miR-148b in cell dissemination and metastases at distant organs (83,182), we collected Circulating Tumor Cells (CTCs) at the experiment end point. We observed a significant reduction in number of plated CTCs for mice treated with axl-148b aptamers compared to PBS-injected animals both from 4175-TGL (Fig. 29F) and MA-2 (Fig. 30D) originating tumors. However, strangely enough, no difference in macroscopic lung colonies were observed for axl-148b aptamer treated tumors compared to controls (Fig. 29G and 30E).

Before transferring any therapeutics compound to the clinic, safety needs to be evaluated. On this side, the levels of miR-148b were measured in liver (Fig. 32B), spleen (Fig. 32C) and kidney (Fig. 32D) by qRT-PCR analysis and no differences were found between axl-148b aptamer or PBS treated mice. At the same time, no alteration in weight were detected for the liver (Fig. 32E), spleen (Fig. 32F) and kidney (Fig. 32G) at the end point of the experiment. No changes in organs weight were observed, meaning that the chimera is not dangerous.

Together, these results suggests that axl-148b conjugates are powerful therapeutic tools able to affect primary tumors by inducing apoptosis and necrosis of the primary mass and to block cancer cell dissemination and offer the foundations for the translation to the clinic.

Figure 29 - Axl-148b aptamers promote necrosis and apoptosis in tumors breast cancer and prevent dissemination in mice. (A) Scheme of the experiment. Red fluorescent (RFP-expressing) 4175-TGL cells were injected into the mammary gland fat pad of NOD/SCID/IL2R null mice. PBS or axl-148b aptamers were administered into the tumor starting from day 11 post-injection (3 treatments/week, 300 pmol in 100 µl, 10 injections in total) and primary tumor weight as well as circulating tumor cells (CTCs) were evaluated as number 33 days post-tumor-cell injections. (B) Tumor pictures and box-and-whisker plots of tumor weight are shown. Boxes indicate upper, lower and median values. (C-E) Top: representative images of formaline fixed, paraffin embedded sections of primary tumors of H&E (C) or I.H.C (D, E) stainings. Antibodies for Cleaved Caspase-3 (D) or Ki-67 (E) were used in I.H.C. Nuclei were counterstained with hematoxylin (blue). Scale bar=100 µm (C) or 25 µm (D, E). Bottom: graphs show the percentage (%) of necrotic versus total areas (C), Cleaved Caspase-3 (D) or Ki67 (E) positive nuclei versus total number of nuclei; 10 fields/each mouse. (F) Representative pictures (top) and quantitations (bottom) of CTCs at day 33 post-tumor cell injections, evaluated as number of red-fluorescent cells obtained from blood and kept in culture for 7 days. (G) Representative images (top) and quantitations (bottom) of whole lungs with fluorescent micrometastases at day 33 post-tumor cell injections shown as fluorescence intensity (mean±SEM). For all analyses, n=4 or n=5 mice per group were evaluated. mg=milligram. I.H.C.=immunohistochemistry, H&E= hematoxilin & eosin. ns= not significant; * $p< 0.05$, ** $p< 0.01$, *** $p < 0.001$.

Fig. 29

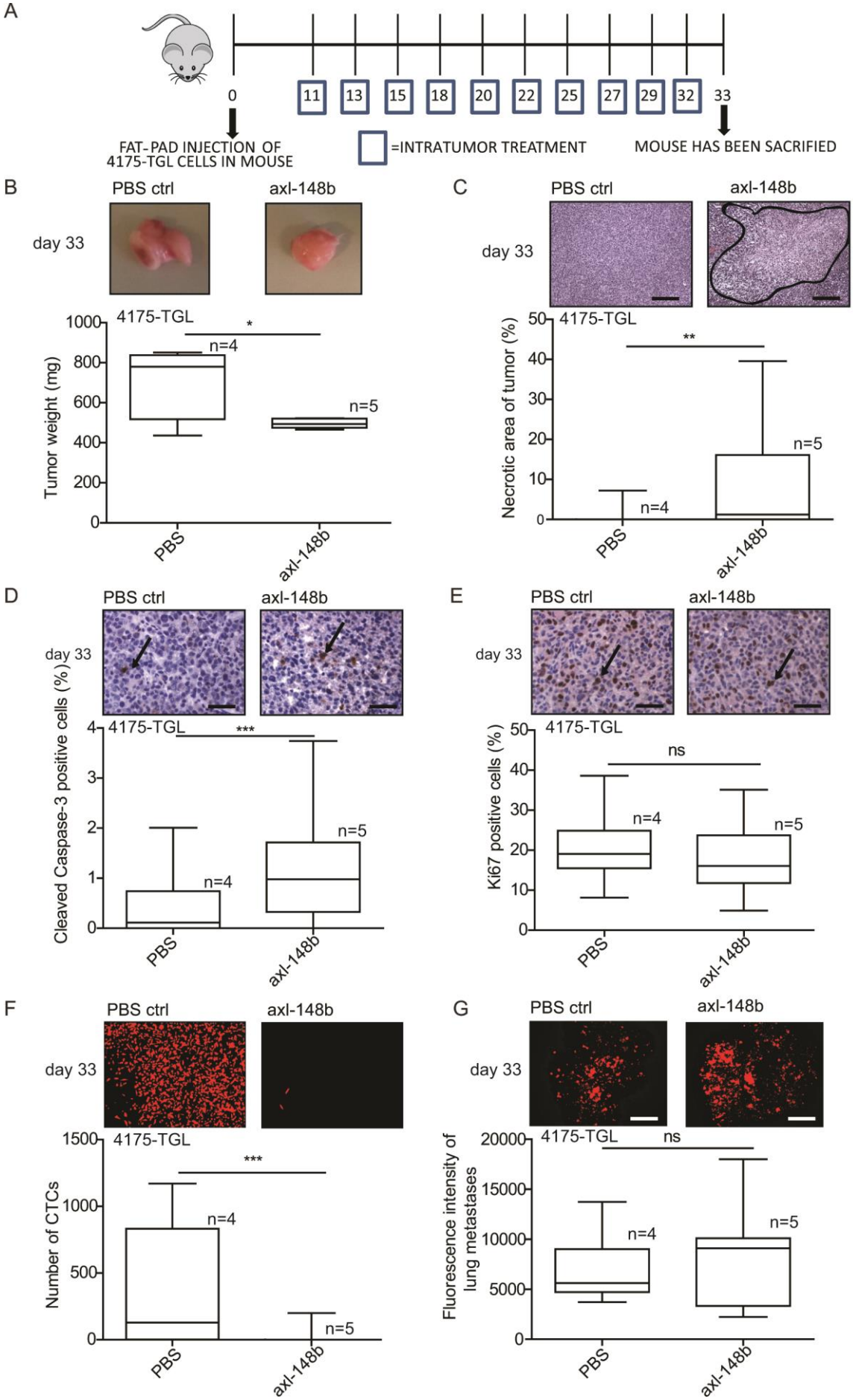
A
0
11
13
15
18
20
22
25
27
29
32
33
FAT-PAD INJECTION OF 4175-TGL CELLS IN MOUSE
=INTRATUMOR TREATMENT
MOUSE HAS BEEN SACRIFIED
B
PBS ctrl
axl-148b
day 33
4175-TGL
Tumor weight (mg)
n=4
n=5
*
PBS
axl-148b
C
PBS ctrl
axl-148b
day 33
4175-TGL
Necrotic area of tumor (%)
**
n=4
n=5
PBS
axl-148b
D
PBS ctrl
axl-148b
day 33
4175-TGL
Cleaved Caspase-3 positive cells (%)
***
n=4
n=5
PBS
axl-148b
E
PBS ctrl
axl-148b
day 33
4175-TGL
Ki67 positive cells (%)
ns
n=4
n=5
PBS
axl-148b
F
PBS ctrl
axl-148b
day 33
4175-TGL
Number of CTCs
***
n=4
n=5
PBS
axl-148b
G
PBS ctrl
axl-148b
day 33
4175-TGL
Fluorescence intensity of lung metastases
ns
n=4
n=5
PBS
axl-148b

Figure 30 - Axl-148b aptamers promote necrosis in primary melanomas and prevent dissemination in mice. (A) Scheme of the experiment. Red fluorescent (RFP-expressing) MA-2 cells were injected into the flank of NOD/SCID/IL2R null mice. PBS or axl-148b aptamers were administered into the tumor starting from day 12 post-injection (3 treatments/week, 300 pmol in 100 µl, 9 injections in total) and primary tumor as well as circulating tumor cells (CTCs) were quantitated respectively as weight and number 32 days post-tumor-cells injections. (B) Tumor pictures and box-and-whisker plots of tumor weight are shown. Boxes indicate upper, lower and median values. (C) Top: representative images of formaline fixed, paraffin embedded sections of primary tumors of H&E stainings. Scale bar=100 µm. Bottom: graphs showing the percentage (%) of necrotic versus total areas; 10 fields/each mouse. (D) Representative pictures (top) and quantitations (bottom) of CTCs at day 32 post-tumor cell injections, evaluated as number of red-fluorescent cells obtained from blood and kept culture for 7 days. (E) Representative images (top) and quantitations (bottom) of whole lungs with fluorescent micrometastases at day 33 post-tumor cell injections shown as fluorescence intensity (mean±SEM). For all analyses, n=5 mice per group were evaluated. mg=milligram. H&E= hematoxilin & eosin. ns= not significant; * $p< 0.05$, ** $p< 0.01$, *** $p < 0.001$.

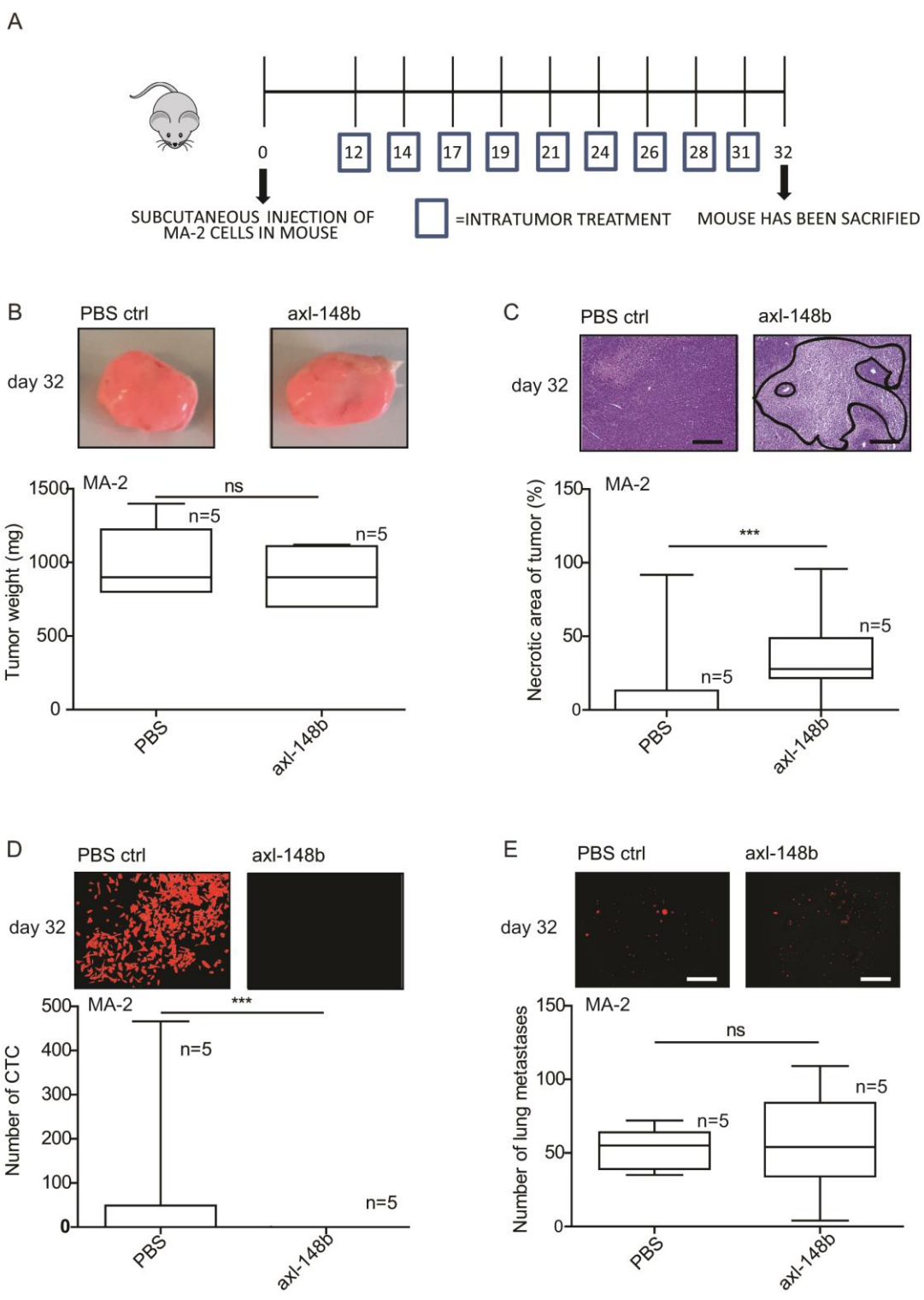
A
0
12
14
17
19
21
24
26
28
31
32
SUBCUTANEOUS INJECTION OF MA-2 CELLS IN MOUSE
=INTRATUMOR TREATMENT
MOUSE HAS BEEN SACRIFIED
B
PBS ctrl
axl-148b
day 32
MA-2
ns
n=5
n=5
Tumor weight (mg)
1500
1000
500
0
PBS
axl-148b
C
PBS ctrl
axl-148b
day 32
MA-2
***
n=5
n=5
Necrotic area of tumor (%)
150
100
50
0
PBS
axl-148b
D
PBS ctrl
axl-148b
day 32
MA-2
***
n=5
n=5
Number of CTC
500
400
300
200
100
0
PBS
axl-148b
E
PBS ctrl
axl-148b
day 32
MA-2
ns
n=5
n=5
Number of lung metastases
150
100
50
0
PBS
axl-148b

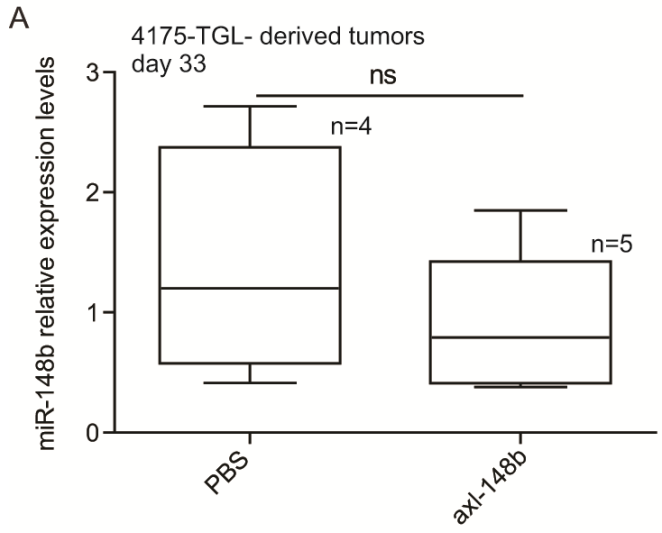

Figure 31 – miR-148b expression in tumors treated with axl-148b aptamers. (A) Red fluorescent (RFP-expressing) 4175-TGL cells were injected into the mammary gland fat pad of NOD/SCID/IL2R null mice. PBS or axl-148b aptamers were injected in the tumor starting from day 11 post-injection (3 treatments/week, 300 pmol in 100 µl, 10 injections in total) and miR-148b levels in tumor were evaluated 33 days post-tumor cell injections. mir-148b expression levels were tested by qRT-PCR analysis in tumor. Results are shown as box-and-whisker plots of the fold changes (mean±SD) relative to PBS, normalized on U6 small nucleolar RNA levels. For all analyses, n=4 or n=5 mice per group were evaluated ns = not significant.

Figure 32 – Axl-148b aptamers are not toxic for mice. (A) Scheme of the experiment. Red fluorescent (RFP-expressing) 4175-TGL cells were injected into the mammary gland fat pad of NOD/SCID/IL2R null mice. PBS or axl-148b aptamers were administered into the tumor starting from day 11 post-injection (3 treatments/week, 300 pmol in 100 µl, 10 injections in total) and miR-148b levels and organs weight were evaluated 33 days post-tumor cell injections. (B-D) mir-148b expression levels were tested by qRT-PCR analysis in liver (B), spleen (C) and kidney (D). Results are shown as box-and-whisker plots of the fold changes (mean±SD) relative to PBS, normalized on U6 small nucleolar RNA levels. (E-G) Box-and-whisker plots of liver (E), spleen (F) and kidney (G) weight. Boxes indicate upper, lower and median values. For all analyses, n=4 or n=5 mice per group were evaluated ns = not significant.

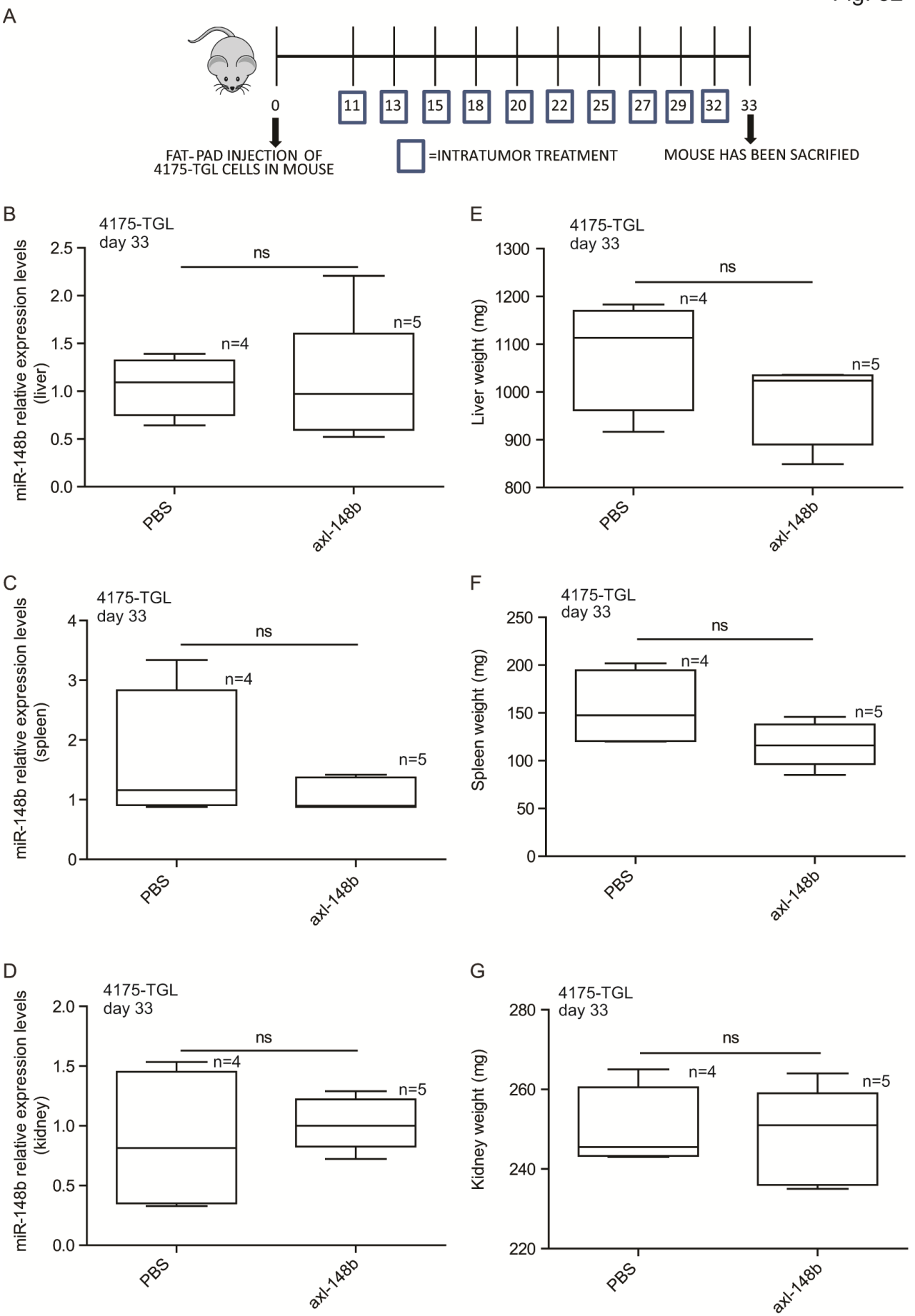
A
0
11
13
15
18
20
22
25
27
29
32
33
FAT-PAD INJECTION OF 4175-TGL CELLS IN MOUSE
=INTRATUMOR TREATMENT
MOUSE HAS BEEN SACRIFIED
B
4175-TGL day 33
miR-148b relative expression levels (liver)
ns
n=4
n=5
PBS
axl-148b
E
4175-TGL day 33
Liver weight (mg)
C
4175-TGL day 33
miR-148b relative expression levels (spleen)
F
4175-TGL day 33
Spleen weight (mg)
D
4175-TGL day 33
miR-148b relative expression levels (kidney)
G
4175-TGL day 33
Kidney weight (mg)

DISCUSSION

We previously reported that miR-214 inhibition and miR-148b overexpression strongly affect metastasis formation by reducing various metastatic traits, in particular tumor cells extravasation in which ITGA5 and ALCAM, two miR-148b known targets, are involved (182). Here, we used an anti-axl aptamer as a moiety to generate an axl-148b conjugate and specifically deliver miR-148b to cancer cells. When tumor cells were treated with axl-148b chimeric aptamers increased expression of the anti-metastatic miR-148b was found as well as inhibition of miR-148b target expression. In parallel, the uptake of the multifunctional conjugates correlated with reduced cell motility and mammosphere formation. More relevantly, following systemic administration of axl-148b aptamers, we observed increased necrosis and apoptosis in primary tumors and reduced number of circulating tumor cells (CTCs).

To date, the Food and Drug Administration (FDA) has approved one RNA aptamer, Macugen (pegatinib sodium, an aptamer against the vascular endothelial growth factor (VEGF), as the world's first therapeutic aptamer and first RNA drug for the treatment of macular degeneration (183). It is administered by ophthalmic intravitreous injection every 6 weeks. Other ten aptamers have undergone clinical trials for the treatment of various conditions, including macular degeneration, coagulation, inflammation and cancer. In particular, AS1411, a DNA anti-nucleolin aptamer, is a promising anticancer agent able to inhibit breast, renal and lung cancer (184,185). Instead, NOX-A12 is an RNA aptamer against CXCL12 that, by modulating tumor microenviroment, act on multiple myeloma, lung, colorectal and renal cancer (120,186).

Here, we took advantage of an anti-axl aptamer, known as GL21.T., generated by Cerchia et al., able to bind the extracellular domain of the Tyrosine Kinase Receptor axl at high affinity and to inhibit its catalytic activity and its downstream signaling (133). In 2014, it was used as a carrier to deliver the anti-tumor let-7g miRNAs to specific cell types *in vitro* and *in vivo* (179). Since that, it became a moiety to target oncosuppressor miRNAs in the form of pre-miRNAs such as miR-212 (131) and miR-137 (132) to cancer cells. Interestingly, GL21.T was also conjugated to anti-miR-222 to target the oncomiR-222 (130). To note, even when linked to different miRNAs, the predicted secondary structure of axl-aptamer, as well as the binding to axl expressing cells and internalization, and action in blocking axl-dependent signaling pathway, were preserved. Importantly, the miRNA cargo was still recognized as a Dicer substrate and efficiently processed once inside the cells to produce a mature miRNA (130,131,187). These results were in agreement with John Rossi's group previous studies about processing of aptamer-siRNA conjugates in cells (188), thus suggesting the possibility to bind different oligonucleotides to aptamers and maintain their function intact.

The natural uptake of aptamers is a major advantage since aptamer-drug conjugates depend on cell internalization for efficacy. We demonstrated that cells expressing higher levels of axl mRNAs, could internalize the aptamer better than cells expressing lower amounts as demonstrated by miR-148b levels. In fact, triple negative breast cancer cells, such as MDAMB231 and 4175-TGL, that showed 7 to 17 fold increase of axl mRNAs compared to A549 and MA-2 cancer cells, expressed almost twice as much miR-148b when treated with axl-148b aptamers. This is in line with other studies demonstrating that the efficacy of drugs, such as immunotoxins and antibody-drug conjugates (ADCs), depends on the efficiency of target-mediated internalization to deliver the cargo to cells (189,190). Relevantly, the ability of MDAMB231 and 4175-TGL cells to express high levels of miR148b following axl-148b aptamer treatments is particularly appealing since these cells derive from poor prognosis triple negative breast tumors and no effective specific targeted therapy is readily available (191). Thus, better characterization of axl-148b aptamers may be of particular interest for the treatment of such a killer. Interestingly, SKBR3 breast cancer cells that do not express axl receptors on their surface, did not show miR-148b overexpression following axl-148b aptamer treatments. This further confirmed aptamer specificity. Similarly, it was previously shown that axl aptamers did not bind to MCF7 cells, negative for axl expression (130,133,179,180). We also showed that axl-148b aptamer increased miR-148b levels in a time and dose dependent manner in A549 and MA-2 cells. Axl aptamer alone was also proved to have biological dose-dependent effects: in fact, when A549 cells were incubated with increasing concentrations of aptamers (from 0 to 1000 nmol/l), inhibitory effects on transwell-migration were observed. Time and dose-response of aptamers was also demonstrated for RLA01, RLA02 and RLA03 Caov-3-specific aptamers (192).

We analyzed if miR-148b binding to axl aptamer, still retained its ability to act on its direct targets ALCAM and ITGA5 (83,182). We showed that miR-148b conjugation to axl didn't alter the inhibition of ALCAM and ITGA5. This was in agreement with the papers in which axl aptamer was bound to other miRNAs (187,180).

We proved that axl-148b aptamer was able to act on cell movement *in vitro.* miR-148b involvement in decreasing cell motility was demonstrated in melanoma (78,182), breast (83,182) and non-small cell lung (158) cancer and hepatocellular carcinoma (193). Also axl aptamer was known as a migration inhibitor (133). We interestingly demonstrated that miR-148b conjugation to axl aptamer allows both molecules to decrease cell movement and migration is synergistically blocked. On the other hand, in our experiments mir-148b had no effect on cell proliferation. This was not surprising,

in fact we previously showed that miR-148b didn't affect proliferation in breast cancer and melanoma models (83,182). Similarly, *in vivo* proliferation of primary tumors was not affected by axl-148b injections. Conversely, overexpression of miR-148b inhibited hepatocellular carcinoma (HCC) HepG2 cells proliferation (194). On the other hand, functional studies demonstrated that plasmid-mediated overexpression of miR-148b promoted cell proliferation in the 786-O and OS-RC-2 renal cancer cell lines (195). These opposite results suggests that miR-148b role on cell proliferation strongly depends on the type of cancer analysed.

To test axl-148b aptamer ability to work in a 3D model, we used the multifunctional conjugate on mammospheres. Xiang et al., demonstrated that EpCAM aptamer could effectively penetrate into the tumorsphere cores and remains in tumorspheres for at least 24 h (196). Importantly, axl aptamer was able to reduce tumorsphere size generated from a glioblastoma cell line or from samples derived from patients (132). We analysed the compound's ability to act on mammospheres size and stemness. Cancer Stem Cells (CSCs) are cancer cells able to give rise to all cell types of a cancer sample. CSCs show great tumorigenic potential: in fact they may generate tumors through self-renewal and differentiation into multiple cell types (197). We observed a reduction in mammosphere size and number when treated with axl-148b aptamer. Esposito et al., demonstrated that axl-137, together with PDGFRβ-anti-10b aptamer, selectively targeted Glioblastoma-Stem-like Cells (GSCs) (132). Interestingly, miR-148b was proved to suppress hepatic cancer stem cell by targeting neuropilin-1 (198). In 4175-TGL mammosphere PKH26 labelled cells, the percentage of dye positive cells was higher for axl-148b aptamer treatment compared to untreated or axl-aptamer treated cells. This could possibly be related to the interference of miR-148b with stemness or cell death. In HCC, miR-148b induced cell apoptosis by activating caspase-3 and caspase-9 (194). miR-148b involvement in enhancing apoptosis was also confirmed in cervical cancer (199) and pituary adenoma (200). All these studies confirm the role of miR-148b in inducing cell death and could possibly explain what observed in xenotraplants (necrosis and apoptosis).

Another important result obtained with axl-148b aptamer treated mice, was the strong reduction in cancer circulating cell number. For the first time a chimeric aptamer has been reported to act on CTCs and this gives hope for the treatment of metastatic tumors. A backbone-modified DNA aptamer against E-selectin (ESTA) was also proven to act on circulating tumor cells. Particularly, ESTA blocked the shear-resistant adhesion of CTCs within the premetastatic niche by blocking the binding of CD44 to E-selectin (201). Our results, let us hypothesize that the reduction of tumor mass in treated mice, lead to the reduction of the number of the escaping cells. So, treatments of primary tumors with axl-148b should lead to decreased tumor progression. On this side we still do

not have positive results. In fact, no reduction on lung metastatization was detected. This could be due to our treatment protocols, therefore we need to plan different experiments with, for instance, earlier treatments.

Aptamers can be administered by either intravenous, subcutaneous or retro-orbital injection. With good solubility (>150 mg/mL) and comparatively low molecular weight (aptamer: 10–50 kD;), a weekly dose of aptamer may be delivered by injection in a volume of less than 0.5 mL. Aptamer bioavailability via subcutaneous administration was >80% in monkey studies (202). Axl aptamers in combination or not with miRNAs were previously delivered in mice by caudal vein (133,203) or retro-orbital (187) injections with successful functional effects. In our experiments, we opted for a local intra-tumor delivery obtaining a reduction of tumor weight in some cases, increased necrosis and apoptosis and a block of tumor cell dissemination. *In vitro* studies on axl-222 aptamer stability were performed (203). The conjugate was incubated in human serum for increasing times up to one week and it was stable up to approximately 8 hours, then gradually degraded suggesting a trial with tail vein injections (203). Alternatively, we are considering pulmonary administrations *via* aerosol.

The major hurdle to *in vivo* delivery of therapeutics is represented by toxicity. Although aptamer caused adverse events are rare in clinical evaluations till now, potential toxicity may come from unexpected tissue accumulation, intensive chemical modifications and nonspecific immune activation (183,204,205). Negatively charged molecules (e.g. nucleic acids) may bind to blood proteins in a non-specific way, resulting in an uptake by non-target tissues and causing side-effects (206). Unnatural oligonucleotides may cause chemical toxic effects or be immunogenic: in fact, LNA-modified nucleic acids may give hepatotoxicity (207). To increase axl-148b stability, we substituted the pyrimidines with 2'-F-Py. This modification was reported to be tolerated with low toxicity (208) as it was also present in Macugen. Axl aptamer *in vivo* experiments demonstrated no toxicity since inflammatory cytokines were nor increased in liver and spleen of treated animals (130,187). In our experiments, no increase in liver, kidney and spleen weight was detected. To note, we showed that the amount of miR-148b and targets downmodulation depend on the level of axl expression on the cell surface, suggesting that non-target cell effects due to aptamer internalization into low-axl cells should be negligible.

In the first chapter of this thesis, we demonstrated that miR-148b, together with miR-214 takes part on a miR-ON-miR regulatory axes. In particular, we proved that simultaneous miR-214 inhibition and miR-148b overexpression in cells successfully reduced metastasis dissemination. Here, we demonstrated that aptamers are important tools to deliver miR-148b. At the moment, we did not developed an aptamer to target miR-214 expression, but it is feasible since, axl aptamer was already

linked to anti-miR-222 (130). However, delivering miR-148b and miR-214 in cancer cells using the same aptamer may lead to competition between axl-148b and axl-anti-miR-214 for axl receptors binding. A possibility is represented by the use of two different aptamers as carriers to deliver the two miRNAs as in (132). We could even speculate to target ITGA5 with a specific aptamer conjugated with miR-214 or bind a sponge sequence for miR-214 to an aptamer. Alternatively, we can act on miR-214 and miR-148b with two different strategies: an axl-148b aptamer and an anti-miR-214. In our lab we already tested a chemically modified anti-miR-214 by Regulus Therapeutics. We injected this compound in mice carrying miR-214 overexpressing melanomas or breast cancers and observed a strong impairment of lung/local lymph node metastatization and number of circulating tumor cells (Mol Therapy, Dettori et al., under revision). Coupling these two strategies (axl-148b+anti-214) may be of particular interest for a combined therapy.

In summary, in this work we provided the characterization of an aptamer-based conjugate and showed that it can act as a multifunctional molecule for a selective *in vivo* target delivery of miR-148b. This chimeric aptamer was able to specifically act on primary tumors by inducing apoptosis and necrosis and to reduce the number of circulating tumor cells. Better characterization of axl-148b are still needed, but the data obtained till now give hope for target therapy in cancer medicine.

CONCLUSIONS

We started from previous observation that demonstrated the capability of:

-miR-214 to promote melanoma and breast cancer metastasis dissemination by increasing migration, invasion, extravasation/survival of melanoma cells via a pathway involving transcriptions factors and adhesion molecules (78);

-miR148b to oppose tumor progression, acting directly on the integrin signaling players ITGA5, ROCK1, and PIK3CA/p110a (83);

-miR-214 to downregulate miR-148b in tumor cells with the consequent upregulation of specific miR-148b direct targets such as ALCAM and ITGA5 (137).

In order to explore the relevance of miR-214 and miR-148b for miRNA-based therapeutic interventions in melanoma and breast cancer, we analysed the dissemination of miR-214-depleted and miR148b-overexpressing cells in mice by specifically investigating various metastatic traits and molecular players. We proved that the simultaneous downregulation of miR-214 and upregulation of miR-148b in tumor cells inhibited metastasis formation in mice in a more effective manner than single modulations. Furthermore, we evidenced that dual miR-214/miR-148b targeting reduced extravasation of tumor cells *in vivo*, by impairing the expression of the adhesion receptors ITGA5 and ALCAM, two miR-148b direct target respectively involved in tumor-ExtraCellular Matrix (ECM) and cell–cell interactions. These results gave hope for the efficacy of combined miRNA therapeutic interventions and proved the relevance of interfering on miR-214-miR-148b axis to target cancer progression. Starting from these results we aimed at developing tools to attack cells from the outside and eventually with specific delivery to target miR-214 miR-148b with a possible transfer to the clinics. Based on the success observed with the systemic injection of anti-122 (Regulus Therapeutics) in HCV patients (90), our lab set up a collaboration with Regulus Therapeutics and demonstrated the inhibition of metastasis dissemination in mice carrying miR-214 overexpressing melanomas and breast cancers (Mol Therapy, under revision). In parallel, I tried to develop a conjugated axl-148b aptamer (in collaboration with de Franciscis lab) to administer to mice bearing axl-expressing tumors. Relevantly, aptamers have already been proven effective to treat different pathological conditions (184,209). We showed that axl-148b are, in fact, specific for axl-expressing cells since increased miR-148b levels can be seen only in cells expressing axl on their surface. Moreover, we proved that axl-148b modulates tumor cell metastatic traits in a manner similar to pre-148b (following transfections or lentivirus transduction). More importantly, axl-148b

injected into the primary tumors led to tumor regression (necrosis, apoptosis) and block of tumor cell dissemination measured as circulating tumor cells (CTCs) in the circulation. Taken together, all these results, indicate that axl aptamer works in a selective manner to convey miR-148b inside the cells. In fact, only axl-expressing cells show increased levels of miR-148b in an aptamer concentration and time dependent manner.

This study opens the possibility to act on miR-214 miR-148b axis using aptamers to overexpress miR-148b. We plant to develop a new conjugated aptamer carrying anti-miR-214 or a sponge against miR-214.

In Summary, from our work, we believe miR-214 miR-148b axis is a relevant target for therapy and that chimeric aptamers are promising tools that can help to inhibit metastatic traits on their own or in combination with traditional anti-cancer therapies (Fig. 33).

Figure 33 – (A) Scheme of cancer progression: in tumor condition, cancer cells may intravasate, survive in blood circulation, extravasate and give rise to metastases at distant organs. (B) Scheme of Chapter I. We injected modified tumor cells (miR-214 depleted and miR-148b overexpressing) in the tail vein of mice and observed impaired tumor cell extravasation and metastatization. (C) Scheme of Chapter II. We injected axl-148b aptamer in the tumor of mice and showed tumor regression and a decrease of Circulating Tumor Cells.

Fig. 33

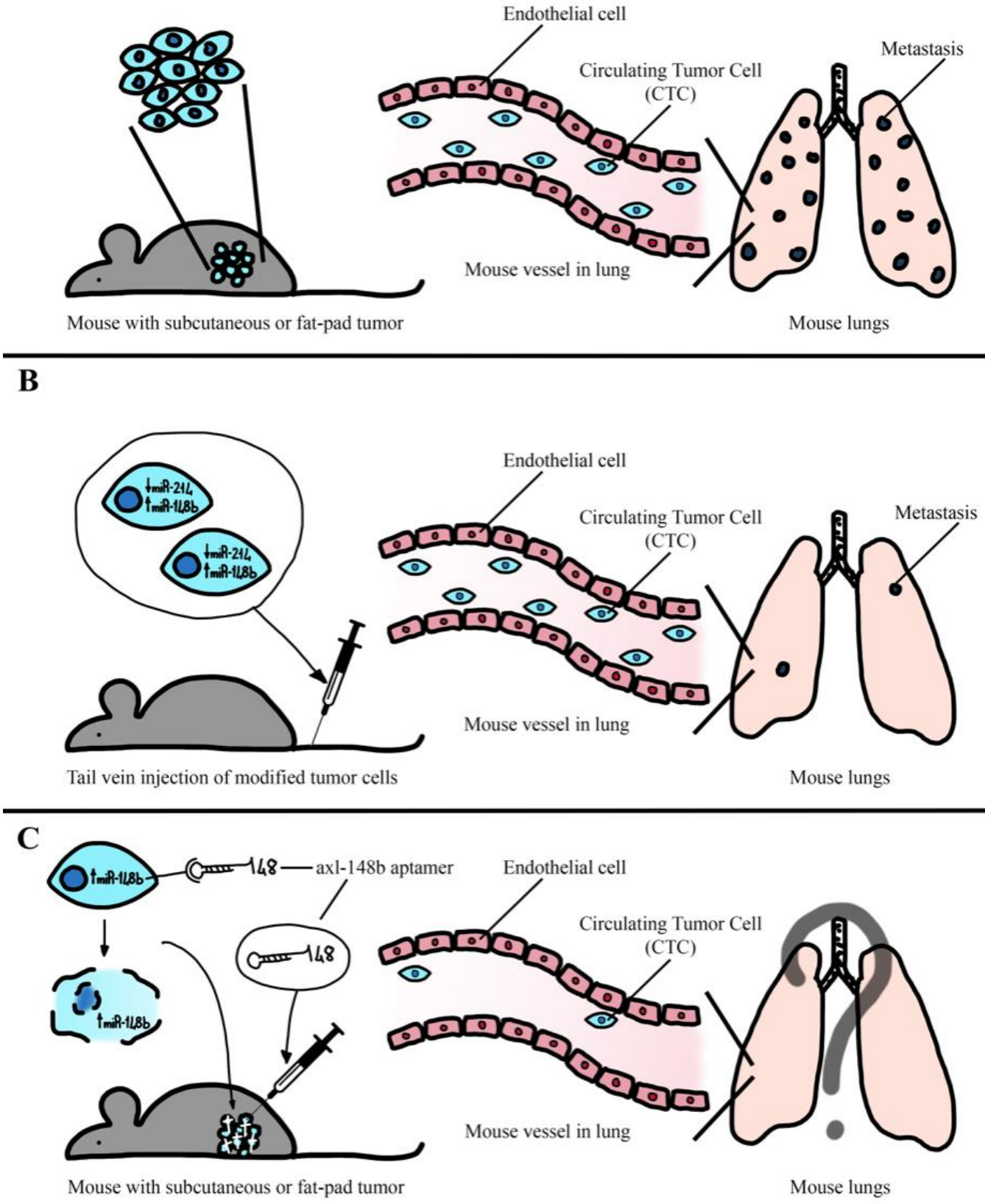
A
Endothelial cell
Circulating Tumor Cell
(CTC)
Metastasis
Mouse vessel in lung
Mouse with subcutaneous or fat-pad tumor
Mouse lungs
B
↓miR-214
↑miR-148b
↓miR-214
↑miR-148b
Endothelial cell
Circulating Tumor Cell
(CTC)
Metastasis
Mouse vessel in lung
Tail vein injection of modified tumor cells
Mouse lungs
C
↑miR-148b
148
axl-148b aptamer
148
↑miR-148b
Endothelial cell
Circulating Tumor Cell
(CTC)
Mouse vessel in lung
Mouse with subcutaneous or fat-pad tumor
Mouse lungs

APPENDIX

Papers published by the candidate during the Ph. D.

"miR-214 and miR-148b targeting inhibits dissemination of melanoma and breast cancer" F. Orso*, **L. Quirico***, F. Virga, E. Penna, D. Dettori, D. Cimino, , R. Coppo, E. Grassi, AR Elia, D. Brusa, S. Deaglio, M.F. Brizzi M. Stadler, P. Provero, M. Caselle and D. Taverna; Cancer Res September 1 2016 (76) (17) 5151-5162; DOI: 10.1158/0008-5472.CAN-15-1322.

*: equal contribution

Papers in preparation

"Axl-148b aptamer inhibits melanoma and breast cancer tumor" L. Quirico, F. Orso, C. L. Esposito, L. Conti, F. Cavallo, V. de Franciscis, D. Taverna. In preparation

"miRNAs in tumor-endothelial cell interactions", F. Orso, D. Dettori, **L. Quirico**, R. Coppo, F. Virga, L. C. Ferreira, C. Paoletti, D. Baruffaldi, E. Penna and D. Taverna. Review **in preparation for CMLS (invited).**

"miR-214 promotes loss of polarity, multiacinar formation, EMT and malignancy of breast cells via the miR-148b-regulated TGF-beta pathway" I. Vercellino**,** F. Orso, **L. Quirico**, M. Sciortino, M. Caselle, S. Cabodi and D. Taverna. In preparation

"ESDN/DCBLD2/CLCP1 protects from melanoma progression by inhibiting E-selectin expression in endothelial cells" R. Coppo, F. Orso, D. Dettori, F. Virga, E. Grassi, **L. Quirico,** L. Nie, P. Provero, M. Mazzone , M.M. Sadeghi and D. Taverna. In preparation

BIBLIOGRAFY

1. Lee RC, Feinbaum RL, Ambros V. The C. elegans heterochronic gene lin-4 encodes small RNAs with antisense complementarity to lin-14. Cell [Internet]. 1993 [cited 2017 Dec 12];75:843–54. Available from: http://www.ncbi.nlm.nih.gov/pubmed/8252621

2. Reinhart BJ, Slack FJ, Basson M, Pasquinelli AE, Bettinger JC, Rougvie AE, et al. The 21-nucleotide let-7 RNA regulates developmental timing in Caenorhabditis elegans. Nature [Internet]. 2000 [cited 2017 Dec 12];403:901–6. Available from: http://www.ncbi.nlm.nih.gov/pubmed/10706289

3. Fabian MR, Sonenberg N, Filipowicz W. Regulation of mRNA translation and stability by microRNAs. Annu Rev Biochem [Internet]. 2010 [cited 2017 Dec 12];79:351–79. Available from: http://www.annualreviews.org/doi/10.1146/annurev-biochem-060308-103103

4. Hamilton AJ, Baulcombe DC. A species of small antisense RNA in posttranscriptional gene silencing in plants. Science [Internet]. 1999 [cited 2017 Dec 12];286:950–2. Available from: http://www.ncbi.nlm.nih.gov/pubmed/10542148

5. Pillai RS, Bhattacharyya SN, Filipowicz W. Repression of protein synthesis by miRNAs: how many mechanisms? Trends Cell Biol [Internet]. 2007 [cited 2017 Dec 12];17:118–26. Available from: http://linkinghub.elsevier.com/retrieve/pii/S096289240600359X

6. Chiang HR, Schoenfeld LW, Ruby JG, Auyeung VC, Spies N, Baek D, et al. Mammalian microRNAs: experimental evaluation of novel and previously annotated genes. Genes Dev [Internet]. 2010 [cited 2017 Dec 12];24:992–1009. Available from: http://genesdev.cshlp.org/cgi/doi/10.1101/gad.1884710

7. Lim LP, Glasner ME, Yekta S, Burge CB, Bartel DP. Vertebrate microRNA genes. Science [Internet]. 2003 [cited 2017 Dec 12];299:1540. Available from: http://www.sciencemag.org/cgi/doi/10.1126/science.1080372

8. Bartel DP. MicroRNAs: Target Recognition and Regulatory Functions. Cell [Internet]. 2009 [cited 2017 Dec 12];136:215–33. Available from: http://www.ncbi.nlm.nih.gov/pubmed/19167326

9. Ambros V, Bartel B, Bartel DP, Burge CB, Carrington JC, Chen X, et al. A uniform system for microRNA annotation. RNA [Internet]. 2003 [cited 2017 Dec 12];9:277–9. Available from: http://www.ncbi.nlm.nih.gov/pubmed/12592000

10. Inui M, Martello G, Piccolo S. MicroRNA control of signal transduction. Nat Rev Mol Cell Biol [Internet]. 2010 [cited 2017 Dec 12];11:252–63. Available from: http://www.nature.com/doifinder/10.1038/nrm2868

11. Filipowicz W, Bhattacharyya SN, Sonenberg N. Mechanisms of post-transcriptional regulation by microRNAs: are the answers in sight? Nat Rev Genet [Internet]. 2008 [cited 2017 Dec 12];9:102–14. Available from: http://www.nature.com/doifinder/10.1038/nrg2290

12. Krol J, Loedige I, Filipowicz W. The widespread regulation of microRNA biogenesis, function and decay. Nat Rev Genet [Internet]. 2010 [cited 2017 Dec 12];11:597–610. Available from: http://www.ncbi.nlm.nih.gov/pubmed/20661255

13. Winter J, Jung S, Keller S, Gregory RI, Diederichs S. Many roads to maturity: microRNA biogenesis pathways and their regulation. Nat Cell Biol [Internet]. 2009 [cited 2017 Dec 12];11:228–34. Available from: http://www.nature.com/doifinder/10.1038/ncb0309-228

14. Kiriakidou M, Tan GS, Lamprinaki S, De Planell-Saguer M, Nelson PT, Mourelatos Z. An mRNA m7G Cap Binding-like Motif within Human Ago2 Represses Translation. Cell [Internet]. 2007 [cited 2017 Dec 12];129:1141–51. Available from: http://www.ncbi.nlm.nih.gov/pubmed/17524464

15. Meister G, Landthaler M, Patkaniowska A, Dorsett Y, Teng G, Tuschl T. Human Argonaute2 mediates RNA cleavage targeted by miRNAs and siRNAs. Mol Cell [Internet]. 2004 [cited 2017 Dec 12];15:185–97. Available from: http://linkinghub.elsevier.com/retrieve/pii/S1097276504004150

16. Lin S, Gregory RI. MicroRNA biogenesis pathways in cancer. Nat Rev Cancer [Internet]. 2015 [cited 2017 Dec 14];15:321–33. Available from: http://www.ncbi.nlm.nih.gov/pubmed/25998712

17. Liu J, Valencia-Sanchez MA, Hannon GJ, Parker R. MicroRNA-dependent localization of targeted mRNAs to mammalian P-bodies. Nat Cell Biol [Internet]. 2005 [cited 2017 Dec 12];7:719–23. Available from: http://www.ncbi.nlm.nih.gov/pubmed/15937477

18. Poliseno L, Salmena L, Zhang J, Carver B, Haveman WJ, Pandolfi PP. A coding-independent function of gene and pseudogene mRNAs regulates tumour biology. Nature [Internet]. 2010 [cited 2017 Dec 12];465:1033–8. Available from: http://www.ncbi.nlm.nih.gov/pubmed/20577206

19. Meola N, Gennarino V, Banfi S. microRNAs and genetic diseases. Pathogenetics [Internet]. 2009 [cited 2017 Dec 12];2:7. Available from: http://www.ncbi.nlm.nih.gov/pubmed/19889204

20. Abelson JF, Kwan KY, O'Roak BJ, Baek DY, Stillman AA, Morgan TM, et al. Sequence variants in SLITRK1 are associated with Tourette's syndrome. Science [Internet]. 2005 [cited 2017 Dec 12];310:317–20. Available from: http://www.sciencemag.org/cgi/doi/10.1126/science.1116502

21. Cheever A, Blackwell E, Ceman S. Fragile X protein family member FXR1P is regulated by microRNAs. RNA [Internet]. 2010 [cited 2017 Dec 12];16:1530–9. Available from: http://rnajournal.cshlp.org/cgi/doi/10.1261/rna.2022210

22. Zhao Y, Samal E, Srivastava D. Serum response factor regulates a muscle-specific microRNA that targets Hand2 during cardiogenesis. Nature [Internet]. 2005 [cited 2017 Dec 12];436:214–20. Available from: http://www.nature.com/articles/nature03817

23. Thum T, Galuppo P, Wolf C, Fiedler J, Kneitz S, van Laake LW, et al. MicroRNAs in the human heart: a clue to fetal gene reprogramming in heart failure. Circulation [Internet]. 2007 [cited 2017 Dec 12];116:258–67. Available from: http://circ.ahajournals.org/cgi/doi/10.1161/CIRCULATIONAHA.107.687947

24. Zhao Y, Ransom JF, Li A, Vedantham V, von Drehle M, Muth AN, et al. Dysregulation of cardiogenesis, cardiac conduction, and cell cycle in mice lacking miRNA-1-2. Cell [Internet]. 2007 [cited 2017 Dec 12];129:303–17. Available from: http://linkinghub.elsevier.com/retrieve/pii/S0092867407003984

25. Thum T, Catalucci D, Bauersachs J. MicroRNAs: novel regulators in cardiac development and disease. Cardiovasc Res [Internet]. 2008 [cited 2017 Dec 12];79:562–70. Available from: http://www.ncbi.nlm.nih.gov/pubmed/18511432

26. Chen J-F, Mandel EM, Thomson JM, Wu Q, Callis TE, Hammond SM, et al. The role of microRNA-1 and microRNA-133 in skeletal muscle proliferation and differentiation. Nat Genet [Internet]. 2006 [cited 2017 Dec 12];38:228–33. Available from: http://www.nature.com/articles/ng1725

27. van Rooij E, Sutherland LB, Qi X, Richardson JA, Hill J, Olson EN. Control of stress-dependent cardiac growth and gene expression by a microRNA. Science [Internet]. 2007 [cited 2017 Dec 12];316:575–9. Available from: http://www.sciencemag.org/cgi/doi/10.1126/science.1139089

28. Carè A, Catalucci D, Felicetti F, Bonci D, Addario A, Gallo P, et al. MicroRNA-133 controls cardiac hypertrophy. Nat Med [Internet]. 2007 [cited 2017 Dec 12];13:613–8. Available from: http://www.nature.com/doifinder/10.1038/nm1582

29. Yang B, Lin H, Xiao J, Lu Y, Luo X, Li B, et al. The muscle-specific microRNA miR-1 regulates cardiac arrhythmogenic potential by targeting GJA1 and KCNJ2. Nat Med [Internet]. 2007 [cited 2017 Dec 12];13:486–91. Available from: http://www.nature.com/doifinder/10.1038/nm1569

30. Schratt G. microRNAs at the synapse. Nat Rev Neurosci [Internet]. 2009 [cited 2017 Dec 12];10:842–9. Available from: http://www.ncbi.nlm.nih.gov/pubmed/19888283

31. Miska EA, Alvarez-Saavedra E, Townsend M, Yoshii A, Sestan N, Rakic P, et al. Microarray analysis of microRNA expression in the developing mammalian brain. Genome Biol [Internet]. 2004 [cited 2017 Dec 12];5:R68. Available from: http://genomebiology.biomedcentral.com/articles/10.1186/gb-2004-5-9-r68

32. Martins M, Rosa A, Guedes LC, Fonseca B V, Gotovac K, Violante S, et al. Convergence of miRNA expression profiling, α-synuclein interacton and GWAS in Parkinson's disease. Banfi S, editor. PLoS One [Internet]. 2011 [cited 2017 Dec 12];6:e25443. Available from: http://dx.plos.org/10.1371/journal.pone.0025443

33. Hébert SS, Horré K, Nicolaï L, Papadopoulou AS, Mandemakers W, Silahtaroglu AN, et al. Loss of microRNA cluster miR-29a/b-1 in sporadic Alzheimer's disease correlates with increased BACE1/beta-secretase expression. Proc Natl Acad Sci U S A [Internet]. 2008 [cited 2017 Dec 12];105:6415–20. Available from: http://www.pnas.org/cgi/doi/10.1073/pnas.0710263105

34. Willem M, Garratt AN, Novak B, Citron M, Kaufmann S, Rittger A, et al. Control of peripheral nerve myelination by the beta-secretase BACE1. Science [Internet]. 2006 [cited 2017 Dec 12];314:664–6. Available from: http://www.sciencemag.org/cgi/doi/10.1126/science.1132341

35. Jopling CL, Yi M, Lancaster AM, Lemon SM, Sarnow P. Modulation of Hepatitis C Virus RNA Abundance by a Liver-Specific MicroRNA. Science (80-) [Internet]. 2005 [cited 2017 Dec 12];309:1577–81. Available from: http://www.ncbi.nlm.nih.gov/pubmed/16141076

36. Jopling CL, Schütz S, Sarnow P. Position-dependent function for a tandem microRNA miR-122-binding site located in the hepatitis C virus RNA genome. Cell Host Microbe [Internet]. 2008 [cited 2017 Dec 12];4:77–85. Available from:

http://linkinghub.elsevier.com/retrieve/pii/S193131280800173X

37. Machlin ES, Sarnow P, Sagan SM. Masking the 5' terminal nucleotides of the hepatitis C virus genome by an unconventional microRNA-target RNA complex. Proc Natl Acad Sci U S A [Internet]. 2011 [cited 2017 Dec 12];108:3193–8. Available from: http://www.pnas.org/cgi/doi/10.1073/pnas.1012464108

38. Henke JI, Goergen D, Zheng J, Song Y, Schüttler CG, Fehr C, et al. microRNA-122 stimulates translation of hepatitis C virus RNA. EMBO J [Internet]. 2008 [cited 2017 Dec 12];27:3300–10. Available from: http://www.ncbi.nlm.nih.gov/pubmed/19020517

39. Li Y, Masaki T, Yamane D, McGivern DR, Lemon SM. Competing and noncompeting activities of miR-122 and the 5' exonuclease Xrn1 in regulation of hepatitis C virus replication. Proc Natl Acad Sci U S A [Internet]. 2013 [cited 2017 Dec 12];110:1881–6. Available from: http://www.pnas.org/cgi/doi/10.1073/pnas.1213515110

40. Sedano CD, Sarnow P. Hepatitis C virus subverts liver-specific miR-122 to protect the viral genome from exoribonuclease Xrn2. Cell Host Microbe [Internet]. 2014 [cited 2017 Dec 12];16:257–64. Available from: http://linkinghub.elsevier.com/retrieve/pii/S1931312814002601

41. Shimakami T, Yamane D, Jangra RK, Kempf BJ, Spaniel C, Barton DJ, et al. Stabilization of hepatitis C virus RNA by an Ago2-miR-122 complex. Proc Natl Acad Sci U S A [Internet]. 2012 [cited 2017 Dec 12];109:941–6. Available from: http://www.pnas.org/cgi/doi/10.1073/pnas.1112263109

42. Nakasa T, Miyaki S, Okubo A, Hashimoto M, Nishida K, Ochi M, et al. Expression of microRNA-146 in rheumatoid arthritis synovial tissue. Arthritis Rheum [Internet]. 2008 [cited 2017 Dec 12];58:1284–92. Available from: http://doi.wiley.com/10.1002/art.23429

43. Dai Y, Huang Y-S, Tang M, Lv T-Y, Hu C-X, Tan Y-H, et al. Microarray analysis of microRNA expression in peripheral blood cells of systemic lupus erythematosus patients. Lupus [Internet]. 2007 [cited 2017 Dec 12];16:939–46. Available from: http://journals.sagepub.com/doi/10.1177/0961203307084158

44. Ng R, Song G, Roll GR, Frandsen NM, Willenbring H. A microRNA-21 surge facilitates rapid cyclin D1 translation and cell cycle progression in mouse liver regeneration. J Clin Invest [Internet]. 2012 [cited 2017 Dec 12];122:1097–108. Available from: http://www.jci.org/articles/view/46039

45. Rayner KJ, Esau CC, Hussain FN, McDaniel AL, Marshall SM, van Gils JM, et al. Inhibition of miR-33a/b in non-human primates raises plasma HDL and lowers VLDL triglycerides. Nature [Internet]. 2011 [cited 2017 Dec 12];478:404–7. Available from: http://www.nature.com/doifinder/10.1038/nature10486

46. Taganov KD, Boldin MP, Chang K-J, Baltimore D. NF-kappaB-dependent induction of microRNA miR-146, an inhibitor targeted to signaling proteins of innate immune responses. Proc Natl Acad Sci U S A [Internet]. 2006 [cited 2017 Dec 12];103:12481–6. Available from: http://www.pnas.org/cgi/doi/10.1073/pnas.0605298103

47. Png KJ, Halberg N, Yoshida M, Tavazoie SF. A microRNA regulon that mediates endothelial recruitment and metastasis by cancer cells. Nature [Internet]. 2011 [cited 2017 Dec 12];481:190–4. Available from: http://www.nature.com/doifinder/10.1038/nature10661

48. Hanahan D, Weinberg RA. Hallmarks of Cancer: The Next Generation. Cell [Internet]. 2011 [cited 2017 Dec 12];144:646–74. Available from: http://www.ncbi.nlm.nih.gov/pubmed/21376230

49. Fidler IJ. The pathogenesis of cancer metastasis: the "seed and soil" hypothesis revisited. Nat Rev Cancer [Internet]. 2003 [cited 2017 Dec 12];3:453–8. Available from: http://www.nature.com/doifinder/10.1038/nrc1098

50. Ventura A, Jacks T. MicroRNAs and cancer: short RNAs go a long way. Cell [Internet]. 2009 [cited 2017 Dec 12];136:586–91. Available from: http://linkinghub.elsevier.com/retrieve/pii/S009286740900141X

51. Croce CM. Causes and consequences of microRNA dysregulation in cancer. Nat Rev Genet [Internet]. 2009 [cited 2017 Dec 12];10:704–14. Available from: http://www.ncbi.nlm.nih.gov/pubmed/19763153

52. MacFarlane L-A, R. Murphy P. MicroRNA: Biogenesis, Function and Role in Cancer. Curr Genomics [Internet]. 2010 [cited 2017 Dec 12];11:537–61. Available from: http://www.ncbi.nlm.nih.gov/pubmed/21532838

53. Hayes J, Peruzzi PP, Lawler S. MicroRNAs in cancer: biomarkers, functions and therapy. Trends Mol Med [Internet]. 2014 [cited 2017 Dec 12];20:460–9. Available from: http://linkinghub.elsevier.com/retrieve/pii/S1471491414001014

54. Calin GA, Sevignani C, Dumitru CD, Hyslop T, Noch E, Yendamuri S, et al. Human microRNA genes are frequently located at fragile sites and genomic regions involved in cancers. Proc Natl Acad Sci U S A [Internet]. 2004 [cited 2017 Dec 12];101:2999–3004. Available from: http://www.pnas.org/cgi/doi/10.1073/pnas.0307323101

55. Calin GA, Dumitru CD, Shimizu M, Bichi R, Zupo S, Noch E, et al. Frequent deletions and down-regulation of micro- RNA genes miR15 and miR16 at 13q14 in chronic lymphocytic leukemia. Proc Natl Acad Sci U S A [Internet]. 2002 [cited 2017 Dec 12];99:15524–9. Available from: http://www.pnas.org/cgi/doi/10.1073/pnas.242606799

56. Cummins JM, Velculescu VE. Implications of micro-RNA profiling for cancer diagnosis. Oncogene [Internet]. 2006 [cited 2017 Dec 12];25:6220–7. Available from: http://www.ncbi.nlm.nih.gov/pubmed/17028602

57. Roldo C, Missiaglia E, Hagan JP, Falconi M, Capelli P, Bersani S, et al. MicroRNA expression abnormalities in pancreatic endocrine and acinar tumors are associated with distinctive pathologic features and clinical behavior. J Clin Oncol [Internet]. 2006 [cited 2017 Dec 12];24:4677–84. Available from: http://ascopubs.org/doi/10.1200/JCO.2005.05.5194

58. Zhang W, Edwards A, Fan W, Flemington EK, Zhang K. miRNA-mRNA correlation-network modules in human prostate cancer and the differences between primary and metastatic tumor subtypes. Chiariotti L, editor. PLoS One [Internet]. 2012 [cited 2017 Dec 12];7:e40130. Available from: http://dx.plos.org/10.1371/journal.pone.0040130

59. Lui W-O, Pourmand N, Patterson BK, Fire A. Patterns of known and novel small RNAs in human cervical cancer. Cancer Res [Internet]. 2007 [cited 2017 Dec 12];67:6031–43. Available from: http://cancerres.aacrjournals.org/cgi/doi/10.1158/0008-5472.CAN-06-0561

60. Zhang L, Volinia S, Bonome T, Calin GA, Greshock J, Yang N, et al. Genomic and

epigenetic alterations deregulate microRNA expression in human epithelial ovarian cancer. Proc Natl Acad Sci U S A [Internet]. 2008 [cited 2017 Dec 12];105:7004–9. Available from: http://www.pnas.org/cgi/doi/10.1073/pnas.0801615105

61. Subramanian S, Lui WO, Lee CH, Espinosa I, Nielsen TO, Heinrich MC, et al. MicroRNA expression signature of human sarcomas. Oncogene [Internet]. 2008 [cited 2017 Dec 12];27:2015–26. Available from: http://www.ncbi.nlm.nih.gov/pubmed/17922033

62. Bray I, Bryan K, Prenter S, Buckley PG, Foley NH, Murphy DM, et al. Widespread dysregulation of MiRNAs by MYCN amplification and chromosomal imbalances in neuroblastoma: association of miRNA expression with survival. Jones C, editor. PLoS One [Internet]. 2009 [cited 2017 Dec 12];4:e7850. Available from: http://dx.plos.org/10.1371/journal.pone.0007850

63. Peng Y, Dai Y, Hitchcock C, Yang X, Kassis ES, Liu L, et al. Insulin growth factor signaling is regulated by microRNA-486, an underexpressed microRNA in lung cancer. Proc Natl Acad Sci U S A [Internet]. 2013 [cited 2017 Dec 12];110:15043–8. Available from: http://www.pnas.org/cgi/doi/10.1073/pnas.1307107110

64. Li C, Hashimi SM, Good DA, Cao S, Duan W, Plummer PN, et al. Apoptosis and microRNA aberrations in cancer. Clin Exp Pharmacol Physiol [Internet]. 2012 [cited 2017 Dec 12];39:739–46. Available from: http://www.ncbi.nlm.nih.gov/pubmed/22409455

65. Pichiorri F, Suh S-S, Rocci A, De Luca L, Taccioli C, Santhanam R, et al. Downregulation of p53-inducible microRNAs 192, 194, and 215 Impairs the p53/MDM2 Autoregulatory Loop in Multiple Myeloma Development. Cancer Cell [Internet]. 2010 [cited 2017 Dec 12];18:367–81. Available from: http://www.ncbi.nlm.nih.gov/pubmed/20951946

66. Fornari F, Gramantieri L, Giovannini C, Veronese A, Ferracin M, Sabbioni S, et al. MiR-122/cyclin G1 interaction modulates p53 activity and affects doxorubicin sensitivity of human hepatocarcinoma cells. Cancer Res [Internet]. 2009 [cited 2017 Dec 12];69:5761–7. Available from: http://cancerres.aacrjournals.org/cgi/doi/10.1158/0008-5472.CAN-08-4797

67. Hermeking H. The miR-34 family in cancer and apoptosis. Cell Death Differ [Internet]. 2010 [cited 2017 Dec 12];17:193–9. Available from: http://www.ncbi.nlm.nih.gov/pubmed/19461653

68. Misso G, Di Martino MT, De Rosa G, Farooqi AA, Lombardi A, Campani V, et al. Mir-34: a new weapon against cancer? Mol Ther Nucleic Acids [Internet]. 2014 [cited 2017 Dec 12];3:e194. Available from: http://linkinghub.elsevier.com/retrieve/pii/S2162253116303341

69. Ma L, Weinberg RA. Micromanagers of malignancy: role of microRNAs in regulating metastasis. Trends Genet [Internet]. 2008 [cited 2017 Dec 12];24:448–56. Available from: http://linkinghub.elsevier.com/retrieve/pii/S0168952508001972

70. Voorhoeve PM, le Sage C, Schrier M, Gillis AJM, Stoop H, Nagel R, et al. A Genetic Screen Implicates miRNA-372 and miRNA-373 As Oncogenes in Testicular Germ Cell Tumors. Cell [Internet]. 2006 [cited 2017 Dec 12];124:1169–81. Available from: http://www.ncbi.nlm.nih.gov/pubmed/16564011

71. Gregory PA, Bert AG, Paterson EL, Barry SC, Tsykin A, Farshid G, et al. The miR-200 family and miR-205 regulate epithelial to mesenchymal transition by targeting ZEB1 and SIP1. Nat Cell Biol [Internet]. 2008 [cited 2017 Dec 12];10:593–601. Available from: http://www.nature.com/doifinder/10.1038/ncb1722

72. Ma L, Young J, Prabhala H, Pan E, Mestdagh P, Muth D, et al. miR-9, a MYC/MYCN-activated microRNA, regulates E-cadherin and cancer metastasis. Nat Cell Biol [Internet]. 2010 [cited 2017 Dec 12];12:247–56. Available from: http://www.nature.com/doifinder/10.1038/ncb2024

73. Almeida MI, Reis RM, Calin GA. MYC-microRNA-9-metastasis connection in breast cancer. Cell Res [Internet]. 2010 [cited 2017 Dec 12];20:603–4. Available from: http://www.nature.com/doifinder/10.1038/cr.2010.70

74. Meng X, Wu J, Pan C, Wang H, Ying X, Zhou Y, et al. Genetic and epigenetic down-regulation of microRNA-212 promotes colorectal tumor metastasis via dysregulation of MnSOD. Gastroenterology [Internet]. 2013 [cited 2017 Dec 12];145:426-36-6. Available from: http://linkinghub.elsevier.com/retrieve/pii/S0016508513004976

75. Tavazoie SF, Alarcón C, Oskarsson T, Padua D, Wang Q, Bos PD, et al. Endogenous human microRNAs that suppress breast cancer metastasis. Nature [Internet]. 2008 [cited 2017 Dec 12];451:147–52. Available from: http://www.ncbi.nlm.nih.gov/pubmed/18185580

76. Bemis LT, Chen R, Amato CM, Classen EH, Robinson SE, Coffey DG, et al. MicroRNA-137 targets microphthalmia-associated transcription factor in melanoma cell lines. Cancer Res [Internet]. 2008 [cited 2017 Dec 12];68:1362–8. Available from: http://cancerres.aacrjournals.org/cgi/doi/10.1158/0008-5472.CAN-07-2912

77. Lu J, Getz G, Miska EA, Alvarez-Saavedra E, Lamb J, Peck D, et al. MicroRNA expression profiles classify human cancers. Nature [Internet]. 2005 [cited 2017 Dec 12];435:834–8. Available from: http://www.ncbi.nlm.nih.gov/pubmed/15944708

78. Penna E, Orso F, Cimino D, Tenaglia E, Lembo A, Quaglino E, et al. microRNA-214 contributes to melanoma tumour progression through suppression of TFAP2C. EMBO J [Internet]. 2011 [cited 2017 Dec 12];30:1990–2007. Available from: http://emboj.embopress.org/cgi/doi/10.1038/emboj.2011.102

79. Bennett PE, Bemis L, Norris DA, Shellman YG. miR in melanoma development: miRNAs and acquired hallmarks of cancer in melanoma. Physiol Genomics [Internet]. 2013 [cited 2017 Dec 12];45:1049–59. Available from: http://physiolgenomics.physiology.org/cgi/doi/10.1152/physiolgenomics.00116.2013

80. Luo C, Weber CEM, Osen W, Bosserhoff A-K, Eichmüller SB. The role of microRNAs in melanoma. Eur J Cell Biol [Internet]. 2014 [cited 2017 Dec 12];93:11–22. Available from: http://www.ncbi.nlm.nih.gov/pubmed/24602414

81. Raimo M, Orso F, Grassi E, Cimino D, Penna E, De Pittà C, et al. miR-146a Exerts Differential Effects on Melanoma Growth and Metastatization. Mol Cancer Res [Internet]. American Association for Cancer Research; 2016 [cited 2018 Jan 16];14:548–62. Available from: http://www.ncbi.nlm.nih.gov/pubmed/27311960

82. Iorio M V, Ferracin M, Liu C-G, Veronese A, Spizzo R, Sabbioni S, et al. MicroRNA gene expression deregulation in human breast cancer. Cancer Res [Internet]. 2005 [cited 2017 Dec 12];65:7065–70. Available from: http://cancerres.aacrjournals.org/lookup/doi/10.1158/0008-5472.CAN-05-1783

83. Cimino D, De Pittà C, Orso F, Zampini M, Casara S, Penna E, et al. miR148b is a major coordinator of breast cancer progression in a relapse-associated microRNA signature by targeting ITGA5, ROCK1, PIK3CA, NRAS, and CSF1. FASEB J [Internet]. 2013 [cited

2017 Dec 12];27:1223–35. Available from: http://www.fasebj.org/cgi/doi/10.1096/fj.12-214692

84. Pinatel EM, Orso F, Penna E, Cimino D, Elia AR, Circosta P, et al. miR-223 is a coordinator of breast cancer progression as revealed by bioinformatics predictions. PLoS One [Internet]. Public Library of Science; 2014 [cited 2018 Jan 16];9:e84859. Available from: http://www.ncbi.nlm.nih.gov/pubmed/24400121

85. Juliano R, Bauman J, Kang H, Ming X. Biological Barriers to Therapy with Antisense and siRNA Oligonucleotides. Mol Pharm [Internet]. 2009 [cited 2017 Dec 12];6:686–95. Available from: http://www.ncbi.nlm.nih.gov/pubmed/19397332

86. Henry JC, Azevedo-Pouly ACP, Schmittgen TD. microRNA Replacement Therapy for Cancer. Pharm Res [Internet]. 2011 [cited 2017 Dec 12];28:3030–42. Available from: http://www.ncbi.nlm.nih.gov/pubmed/21879389

87. Saumet A, Mathelier A, Lecellier C-H. The Potential of MicroRNAs in Personalized Medicine against Cancers. Biomed Res Int [Internet]. 2014 [cited 2017 Dec 12];2014:1–10. Available from: http://www.ncbi.nlm.nih.gov/pubmed/25243170

88. Zhang S, Chen L, Jung EJ, Calin GA. Targeting microRNAs with small molecules: from dream to reality. Clin Pharmacol Ther [Internet]. 2010 [cited 2017 Dec 12];87:754–8. Available from: http://doi.wiley.com/10.1038/clpt.2010.46

89. Ebert MS, Sharp PA. Emerging Roles for Natural MicroRNA Sponges. Curr Biol [Internet]. 2010 [cited 2017 Dec 12];20:R858–61. Available from: http://www.ncbi.nlm.nih.gov/pubmed/20937476

90. van der Ree MH, de Vree JM, Stelma F, Willemse S, van der Valk M, Rietdijk S, et al. Safety, tolerability, and antiviral effect of RG-101 in patients with chronic hepatitis C: a phase 1B, double-blind, randomised controlled trial. Lancet [Internet]. Elsevier; 2017 [cited 2018 Jan 16];389:709–17. Available from: http://www.sciencedirect.com/science/article/pii/S0140673616317159?via%3Dihub

91. van der Ree MH, van der Meer AJ, van Nuenen AC, de Bruijne J, Ottosen S, Janssen HL, et al. Miravirsen dosing in chronic hepatitis C patients results in decreased microRNA-122 levels without affecting other microRNAs in plasma. Aliment Pharmacol Ther [Internet]. 2016 [cited 2018 Jan 16];43:102–13. Available from: http://doi.wiley.com/10.1111/apt.13432

92. Liu YP, Berkhout B. miRNA cassettes in viral vectors: Problems and solutions. Biochim Biophys Acta - Gene Regul Mech [Internet]. 2011 [cited 2017 Dec 12];1809:732–45. Available from: http://www.ncbi.nlm.nih.gov/pubmed/21679781

93. Kortylewski M, Nechaev S. How to train your dragon: targeted delivery of microRNA to cancer cells in vivo. Mol Ther [Internet]. 2014 [cited 2017 Dec 12];22:1070–1. Available from: http://linkinghub.elsevier.com/retrieve/pii/S1525001616306931

94. Bozzuto G, Molinari A. Liposomes as nanomedical devices. Int J Nanomedicine [Internet]. 2015 [cited 2017 Dec 12];10:975. Available from: http://www.ncbi.nlm.nih.gov/pubmed/25678787

95. Doh K-O, Yeo Y. Application of polysaccharides for surface modification of nanomedicines. Ther Deliv [Internet]. 2012 [cited 2017 Dec 12];3:1447–56. Available from:

http://www.ncbi.nlm.nih.gov/pubmed/23323561

96. Peer D, Florentin A, Margalit R. Hyaluronan is a key component in cryoprotection and formulation of targeted unilamellar liposomes. Biochim Biophys Acta [Internet]. 2003 [cited 2017 Dec 12];1612:76–82. Available from: http://www.ncbi.nlm.nih.gov/pubmed/12729932

97. Ando H, Asai T, Koide H, Okamoto A, Maeda N, Tomita K, et al. Advanced cancer therapy by integrative antitumor actions via systemic administration of miR-499. J Control Release [Internet]. 2014 [cited 2017 Dec 12];181:32–9. Available from: http://linkinghub.elsevier.com/retrieve/pii/S0168365914001199

98. Liu X-Q, Song W-J, Sun T-M, Zhang P-Z, Wang J. Targeted delivery of antisense inhibitor of miRNA for antiangiogenesis therapy using cRGD-functionalized nanoparticles. Mol Pharm [Internet]. 2011 [cited 2017 Dec 12];8:250–9. Available from: http://pubs.acs.org/doi/abs/10.1021/mp100315q

99. Anand S, Majeti BK, Acevedo LM, Murphy EA, Mukthavaram R, Scheppke L, et al. MicroRNA-132-mediated loss of p120RasGAP activates the endothelium to facilitate pathological angiogenesis. Nat Med [Internet]. 2010 [cited 2017 Dec 12];16:909–14. Available from: http://www.nature.com/doifinder/10.1038/nm.2186

100. Beg MS, Brenner AJ, Sachdev J, Borad M, Kang Y-K, Stoudemire J, et al. Phase I study of MRX34, a liposomal miR-34a mimic, administered twice weekly in patients with advanced solid tumors. Invest New Drugs [Internet]. Springer US; 2017 [cited 2018 Jan 16];35:180–8. Available from: http://link.springer.com/10.1007/s10637-016-0407-y

101. Ochiya T, Nagahara S, Sano A, Itoh H, Terada M. Biomaterials for gene delivery: atelocollagen-mediated controlled release of molecular medicines. Curr Gene Ther [Internet]. 2001 [cited 2017 Dec 12];1:31–52. Available from: http://www.ncbi.nlm.nih.gov/pubmed/12109137

102. Samal SK, Dash M, Van Vlierberghe S, Kaplan DL, Chiellini E, van Blitterswijk C, et al. Cationic polymers and their therapeutic potential. Chem Soc Rev [Internet]. 2012 [cited 2017 Dec 12];41:7147. Available from: http://www.ncbi.nlm.nih.gov/pubmed/22885409

103. DANG J, LEONG K. Natural polymers for gene delivery and tissue engineering☆. Adv Drug Deliv Rev [Internet]. 2006 [cited 2017 Dec 12];58:487–99. Available from: http://www.ncbi.nlm.nih.gov/pubmed/16762443

104. Boussif O, Lezoualc'h F, Zanta MA, Mergny MD, Scherman D, Demeneix B, et al. A versatile vector for gene and oligonucleotide transfer into cells in culture and in vivo: polyethylenimine. Proc Natl Acad Sci U S A [Internet]. 1995 [cited 2017 Dec 12];92:7297–301. Available from: http://www.ncbi.nlm.nih.gov/pubmed/7638184

105. Calarco A, Bosetti M, Margarucci S, Fusaro L, Nicolì E, Petillo O, et al. The genotoxicity of PEI-based nanoparticles is reduced by acetylation of polyethylenimine amines in human primary cells. Toxicol Lett [Internet]. 2013 [cited 2017 Dec 12];218:10–7. Available from: http://www.ncbi.nlm.nih.gov/pubmed/23296103

106. Chou Y-T, Lin H-H, Lien Y-C, Wang Y-H, Hong C-F, Kao Y-R, et al. EGFR Promotes Lung Tumorigenesis by Activating miR-7 through a Ras/ERK/Myc Pathway That Targets the Ets2 Transcriptional Repressor ERF. Cancer Res [Internet]. 2010 [cited 2017 Dec 12];70:8822–31. Available from: http://www.ncbi.nlm.nih.gov/pubmed/20978205

107. Bouissou C, Rouse JJ, Price R, van der Walle CF. The Influence of Surfactant on PLGA Microsphere Glass Transition and Water Sorption: Remodeling the Surface Morphology to Attenuate the Burst Release. Pharm Res [Internet]. 2006 [cited 2017 Dec 12];23:1295–305. Available from: http://www.ncbi.nlm.nih.gov/pubmed/16715359

108. Zhou J, Shum K-T, Burnett J, Rossi J. Nanoparticle-Based Delivery of RNAi Therapeutics: Progress and Challenges. Pharmaceuticals [Internet]. 2013 [cited 2017 Dec 12];6:85–107. Available from: http://www.ncbi.nlm.nih.gov/pubmed/23667320

109. Ellington AD, Szostak JW. In vitro selection of RNA molecules that bind specific ligands. Nature [Internet]. 1990 [cited 2017 Dec 12];346:818–22. Available from: http://www.ncbi.nlm.nih.gov/pubmed/1697402

110. Tuerk C, Gold L. Systematic evolution of ligands by exponential enrichment: RNA ligands to bacteriophage T4 DNA polymerase. Science [Internet]. 1990 [cited 2017 Dec 12];249:505–10. Available from: http://www.ncbi.nlm.nih.gov/pubmed/2200121

111. Gelinas AD, Davies DR, Janjic N. Embracing proteins: structural themes in aptamer-protein complexes. Curr Opin Struct Biol [Internet]. 2016 [cited 2017 Dec 12];36:122–32. Available from: http://linkinghub.elsevier.com/retrieve/pii/S0959440X16000129

112. LEE J, STOVALL G, ELLINGTON A. Aptamer therapeutics advance. Curr Opin Chem Biol [Internet]. 2006 [cited 2017 Dec 12];10:282–9. Available from: http://www.ncbi.nlm.nih.gov/pubmed/16621675

113. Bless NM, Smith D, Charlton J, Czermak BJ, Schmal H, Friedl HP, et al. Protective effects of an aptamer inhibitor of neutrophil elastase in lung inflammatory injury. Curr Biol [Internet]. 1997 [cited 2017 Dec 12];7:877–80. Available from: http://www.ncbi.nlm.nih.gov/pubmed/9382799

114. Ulrich H. RNA aptamers: from basic science towards therapy. Handb Exp Pharmacol [Internet]. 2006 [cited 2017 Dec 12];305–26. Available from: http://www.ncbi.nlm.nih.gov/pubmed/16594622

115. McCauley TG, Hamaguchi N, Stanton M. Aptamer-based biosensor arrays for detection and quantification of biological macromolecules. Anal Biochem [Internet]. 2003 [cited 2017 Dec 12];319:244–50. Available from: http://www.ncbi.nlm.nih.gov/pubmed/12871718

116. Ulrich H, Martins AHB, Pesquero JB. RNA and DNA aptamers in cytomics analysis. Cytometry [Internet]. 2004 [cited 2017 Dec 12];59A:220–31. Available from: http://www.ncbi.nlm.nih.gov/pubmed/15170601

117. Davis KA, Lin Y, Abrams B, Jayasena SD. Staining of cell surface human CD4 with 2'-F-pyrimidine-containing RNA aptamers for flow cytometry. Nucleic Acids Res [Internet]. 1998 [cited 2017 Dec 12];26:3915–24. Available from: http://www.ncbi.nlm.nih.gov/pubmed/9705498

118. Bagalkot V, Zhang L, Levy-Nissenbaum E, Jon S, Kantoff PW, Langer R, et al. Quantum dot-aptamer conjugates for synchronous cancer imaging, therapy, and sensing of drug delivery based on bi-fluorescence resonance energy transfer. Nano Lett [Internet]. 2007 [cited 2017 Dec 12];7:3065–70. Available from: http://pubs.acs.org/doi/abs/10.1021/nl071546n

119. Gold L, Ayers D, Bertino J, Bock C, Bock A, Brody EN, et al. Aptamer-Based Multiplexed

Proteomic Technology for Biomarker Discovery. Gelain F, editor. PLoS One [Internet]. 2010 [cited 2017 Dec 12];5:e15004. Available from: http://www.ncbi.nlm.nih.gov/pubmed/21165148

120. Lee JW, Kim HJ, Heo K. Therapeutic aptamers: developmental potential as anticancer drugs. BMB Rep [Internet]. 2015 [cited 2017 Dec 12];48:234–7. Available from: http://www.ncbi.nlm.nih.gov/pubmed/25560701

121. Yoon S, Rossi JJ. Emerging cancer-specific therapeutic aptamers. Curr Opin Oncol [Internet]. 2017 [cited 2017 Dec 12];29:366–74. Available from: http://insights.ovid.com/crossref?an=00001622-201709000-00010

122. Lupold SE, Hicke BJ, Lin Y, Coffey DS. Identification and characterization of nuclease-stabilized RNA molecules that bind human prostate cancer cells via the prostate-specific membrane antigen. Cancer Res [Internet]. 2002 [cited 2018 Jan 16];62:4029–33. Available from: http://www.ncbi.nlm.nih.gov/pubmed/12124337

123. Chu TC, Twu KY, Ellington AD, Levy M. Aptamer mediated siRNA delivery. Nucleic Acids Res [Internet]. Oxford University Press; 2006 [cited 2018 Jan 16];34:e73. Available from: http://www.ncbi.nlm.nih.gov/pubmed/16740739

124. Lai W-Y, Wang W-Y, Chang Y-C, Chang C-J, Yang P-C, Peck K. Synergistic inhibition of lung cancer cell invasion, tumor growth and angiogenesis using aptamer-siRNA chimeras. Biomaterials [Internet]. 2014 [cited 2018 Jan 16];35:2905–14. Available from: http://www.ncbi.nlm.nih.gov/pubmed/24397988

125. Kruspe S, Giangrande P. Aptamer-siRNA Chimeras: Discovery, Progress, and Future Prospects. Biomedicines [Internet]. 2017 [cited 2018 Jan 16];5:45. Available from: http://www.ncbi.nlm.nih.gov/pubmed/28792479

126. Dai F, Zhang Y, Zhu X, Shan N, Chen Y. The anti-chemoresistant effect and mechanism of MUC1 aptamer-miR-29b chimera in ovarian cancer. Gynecol Oncol [Internet]. 2013 [cited 2017 Dec 12];131:451–9. Available from: http://linkinghub.elsevier.com/retrieve/pii/S0090825813010779

127. Rohde J-H, Weigand JE, Suess B, Dimmeler S. A Universal Aptamer Chimera for the Delivery of Functional microRNA-126. Nucleic Acid Ther [Internet]. 2015 [cited 2017 Dec 12];25:141–51. Available from: http://online.liebertpub.com/doi/10.1089/nat.2014.0501

128. Rankin E, Giaccia A. The Receptor Tyrosine Kinase AXL in Cancer Progression. Cancers (Basel) [Internet]. 2016 [cited 2017 Dec 12];8:103. Available from: http://www.ncbi.nlm.nih.gov/pubmed/27834845

129. Esposito CL, Catuogno S, de Franciscis V. Aptamer-mediated selective delivery of short RNA therapeutics in cancer cells. J RNAi Gene Silencing [Internet]. 2014 [cited 2017 Dec 12];10:500–6. Available from: http://www.ncbi.nlm.nih.gov/pubmed/25414727

130. Catuogno S, Rienzo A, Di Vito A, Esposito CL, de Franciscis V. Selective delivery of therapeutic single strand antimiRs by aptamer-based conjugates. J Control Release [Internet]. 2015 [cited 2017 Dec 12];210:147–59. Available from: http://linkinghub.elsevier.com/retrieve/pii/S0168365915005751

131. Iaboni M, Russo V, Fontanella R, Roscigno G, Fiore D, Donnarumma E, et al. Aptamer-miRNA-212 Conjugate Sensitizes NSCLC Cells to TRAIL. Mol Ther Nucleic Acids

[Internet]. 2016 [cited 2017 Dec 12];5:e289. Available from: http://linkinghub.elsevier.com/retrieve/pii/S2162253117300835

132. Esposito CL, Nuzzo S, Kumar SA, Rienzo A, Lawrence CL, Pallini R, et al. A combined microRNA-based targeted therapeutic approach to eradicate glioblastoma stem-like cells. J Control Release [Internet]. 2016 [cited 2017 Dec 12];238:43–57. Available from: http://www.ncbi.nlm.nih.gov/pubmed/27448441

133. Cerchia L, Esposito CL, Camorani S, Rienzo A, Stasio L, Insabato L, et al. Targeting Axl With an High-affinity Inhibitory Aptamer. Mol Ther [Internet]. 2012 [cited 2017 Dec 12];20:2291–303. Available from: http://www.ncbi.nlm.nih.gov/pubmed/22910292

134. Kim JK, Choi K-J, Lee M, Jo M, Kim S. Molecular imaging of a cancer-targeting theragnostics probe using a nucleolin aptamer- and microRNA-221 molecular beacon-conjugated nanoparticle. Biomaterials [Internet]. 2012 [cited 2017 Dec 12];33:207–17. Available from: http://linkinghub.elsevier.com/retrieve/pii/S0142961211010647

135. Perepelyuk M, Maher C, Lakshmikuttyamma A, Shoyele SA. Aptamer-hybrid nanoparticle bioconjugate efficiently delivers miRNA-29b to non-small-cell lung cancer cells and inhibits growth by downregulating essential oncoproteins. Int J Nanomedicine [Internet]. 2016 [cited 2017 Dec 12];11:3533–44. Available from: https://www.dovepress.com/aptamer-hybrid-nanoparticle-bioconjugate-efficiently-delivers-mirna-29-peer-reviewed-article-IJN

136. Xu L, Shen SS, Hoshida Y, Subramanian A, Ross K, Brunet J-P, et al. Gene expression changes in an animal melanoma model correlate with aggressiveness of human melanoma metastases. Mol Cancer Res [Internet]. 2008 [cited 2017 Dec 12];6:760–9. Available from: http://mcr.aacrjournals.org/cgi/doi/10.1158/1541-7786.MCR-07-0344

137. Penna E, Orso F, Cimino D, Vercellino I, Grassi E, Quaglino E, et al. miR-214 coordinates melanoma progression by upregulating ALCAM through TFAP2 and miR-148b downmodulation. Cancer Res [Internet]. 2013 [cited 2017 Dec 12];73:4098–111. Available from: http://cancerres.aacrjournals.org/lookup/doi/10.1158/0008-5472.CAN-12-3686

138. Minn AJ, Gupta GP, Siegel PM, Bos PD, Shu W, Giri DD, et al. Genes that mediate breast cancer metastasis to lung. Nature [Internet]. 2005 [cited 2017 Dec 12];436:518–24. Available from: http://www.ncbi.nlm.nih.gov/pubmed/16049480

139. Bookout AL, Mangelsdorf DJ. Quantitative real-time PCR protocol for analysis of nuclear receptor signaling pathways. Nucl Recept Signal [Internet]. 2003 [cited 2017 Dec 12];1:e012. Available from: http://www.nursa.org/article.cfm?doi=10.1621/nrs.01002

140. Curtis C, Shah SP, Chin S-F, Turashvili G, Rueda OM, Dunning MJ, et al. The genomic and transcriptomic architecture of 2,000 breast tumours reveals novel subgroups. Nature [Internet]. 2012 [cited 2017 Dec 14];486:346–52. Available from: http://www.ncbi.nlm.nih.gov/pubmed/22522925

141. Dvinge H, Git A, Gräf S, Salmon-Divon M, Curtis C, Sottoriva A, et al. The shaping and functional consequences of the microRNA landscape in breast cancer. Nature [Internet]. 2013 [cited 2017 Dec 14];497:378–82. Available from: http://www.ncbi.nlm.nih.gov/pubmed/23644459

142. Segura MF, Belitskaya-Lévy I, Rose AE, Zakrzewski J, Gaziel A, Hanniford D, et al. Melanoma MicroRNA signature predicts post-recurrence survival. Clin Cancer Res [Internet]. 2010 [cited 2017 Dec 12];16:1577–86. Available from:

http://clincancerres.aacrjournals.org/cgi/doi/10.1158/1078-0432.CCR-09-2721

143. Worley LA, Long MD, Onken MD, Harbour JW. Micro-RNAs associated with metastasis in uveal melanoma identified by multiplexed microarray profiling. Melanoma Res [Internet]. 2008 [cited 2017 Dec 12];18:184–90. Available from: http://content.wkhealth.com/linkback/openurl?sid=WKPTLP:landingpage&an=00008390-200806000-00004

144. Volinia S, Calin GA, Liu C-G, Ambs S, Cimmino A, Petrocca F, et al. A microRNA expression signature of human solid tumors defines cancer gene targets. Proc Natl Acad Sci U S A [Internet]. 2006 [cited 2017 Dec 12];103:2257–61. Available from: http://www.pnas.org/cgi/doi/10.1073/pnas.0510565103

145. Blenkiron C, Goldstein LD, Thorne NP, Spiteri I, Chin S-F, Dunning MJ, et al. MicroRNA expression profiling of human breast cancer identifies new markers of tumor subtype. Genome Biol [Internet]. 2007 [cited 2017 Dec 12];8:R214. Available from: http://genomebiology.biomedcentral.com/articles/10.1186/gb-2007-8-10-r214

146. Ueda T, Volinia S, Okumura H, Shimizu M, Taccioli C, Rossi S, et al. Relation between microRNA expression and progression and prognosis of gastric cancer: a microRNA expression analysis. Lancet Oncol [Internet]. 2010 [cited 2017 Dec 12];11:136–46. Available from: http://www.ncbi.nlm.nih.gov/pubmed/20022810

147. Yang H, Kong W, He L, Zhao J-J, O'Donnell JD, Wang J, et al. MicroRNA expression profiling in human ovarian cancer: miR-214 induces cell survival and cisplatin resistance by targeting PTEN. Cancer Res [Internet]. 2008 [cited 2017 Dec 12];68:425–33. Available from: http://cancerres.aacrjournals.org/cgi/doi/10.1158/0008-5472.CAN-07-2488

148. Wang Z, Cai H, Lin L, Tang M, Cai H. Upregulated expression of microRNA-214 is linked to tumor progression and adverse prognosis in pediatric osteosarcoma. Pediatr Blood Cancer [Internet]. 2014 [cited 2017 Dec 12];61:206–10. Available from: http://doi.wiley.com/10.1002/pbc.24763

149. Wang M, Zhao C, Shi H, Zhang B, Zhang L, Zhang X, et al. Deregulated microRNAs in gastric cancer tissue-derived mesenchymal stem cells: novel biomarkers and a mechanism for gastric cancer. Br J Cancer [Internet]. 2014 [cited 2017 Dec 12];110:1199–210. Available from: http://www.nature.com/doifinder/10.1038/bjc.2014.14

150. Yang T-S, Yang X-H, Wang X-D, Wang Y-L, Zhou B, Song Z-S. MiR-214 regulate gastric cancer cell proliferation, migration and invasion by targeting PTEN. Cancer Cell Int [Internet]. 2013 [cited 2017 Dec 12];13:68. Available from: http://cancerci.biomedcentral.com/articles/10.1186/1475-2867-13-68

151. Xu Z, Wang T. miR-214 promotes the proliferation and invasion of osteosarcoma cells through direct suppression of LZTS1. Biochem Biophys Res Commun [Internet]. 2014 [cited 2017 Dec 12];449:190–5. Available from: http://linkinghub.elsevier.com/retrieve/pii/S0006291X14008031

152. Deng M, Ye Q, Qin Z, Zheng Y, He W, Tang H, et al. miR-214 promotes tumorigenesis by targeting lactotransferrin in nasopharyngeal carcinoma. Tumour Biol [Internet]. 2013 [cited 2017 Dec 12];34:1793–800. Available from: http://link.springer.com/10.1007/s13277-013-0718-y

153. Mueller DW, Rehli M, Bosserhoff AK. miRNA expression profiling in melanocytes and

melanoma cell lines reveals miRNAs associated with formation and progression of malignant melanoma. J Invest Dermatol [Internet]. 2009 [cited 2017 Dec 12];129:1740–51. Available from: http://linkinghub.elsevier.com/retrieve/pii/S0022202X15344006

154. Bloomston M, Frankel WL, Petrocca F, Volinia S, Alder H, Hagan JP, et al. MicroRNA expression patterns to differentiate pancreatic adenocarcinoma from normal pancreas and chronic pancreatitis. JAMA [Internet]. 2007 [cited 2017 Dec 12];297:1901–8. Available from: http://jama.jamanetwork.com/article.aspx?doi=10.1001/jama.297.17.1901

155. Zhang Z, Zheng W, Hai J. MicroRNA-148b expression is decreased in hepatocellular carcinoma and associated with prognosis. Med Oncol [Internet]. 2014 [cited 2017 Dec 12];31:984. Available from: http://link.springer.com/10.1007/s12032-014-0984-6

156. Zhao G, Zhang J-G, Liu Y, Qin Q, Wang B, Tian K, et al. miR-148b functions as a tumor suppressor in pancreatic cancer by targeting AMPKα1. Mol Cancer Ther [Internet]. 2013 [cited 2017 Dec 12];12:83–93. Available from: http://mct.aacrjournals.org/cgi/doi/10.1158/1535-7163.MCT-12-0534-T

157. Song Y-X, Yue Z-Y, Wang Z-N, Xu Y-Y, Luo Y, Xu H-M, et al. MicroRNA-148b is frequently down-regulated in gastric cancer and acts as a tumor suppressor by inhibiting cell proliferation. Mol Cancer [Internet]. 2011 [cited 2017 Dec 12];10:1. Available from: http://molecular-cancer.biomedcentral.com/articles/10.1186/1476-4598-10-1

158. Liu G-L, Liu X, Lv X-B, Wang X-P, Fang X-S, Sang Y. miR-148b functions as a tumor suppressor in non-small cell lung cancer by targeting carcinoembryonic antigen (CEA). Int J Clin Exp Med [Internet]. 2014 [cited 2017 Dec 12];7:1990–9. Available from: http://www.ncbi.nlm.nih.gov/pubmed/25232379

159. Li X, Zhang J, Gao L, McClellan S, Finan MA, Butler TW, et al. MiR-181 mediates cell differentiation by interrupting the Lin28 and let-7 feedback circuit. Cell Death Differ [Internet]. 2012 [cited 2017 Dec 12];19:378–86. Available from: http://www.nature.com/doifinder/10.1038/cdd.2011.127

160. Tao T, Wang Y, Luo H, Yao L, Wang L, Wang J, et al. Involvement of FOS-mediated miR-181b/miR-21 signalling in the progression of malignant gliomas. Eur J Cancer [Internet]. 2013 [cited 2017 Dec 12];49:3055–63. Available from: http://linkinghub.elsevier.com/retrieve/pii/S0959804913004073

161. Martello G, Rosato A, Ferrari F, Manfrin A, Cordenonsi M, Dupont S, et al. A MicroRNA Targeting Dicer for Metastasis Control. Cell [Internet]. 2010 [cited 2017 Dec 12];141:1195–207. Available from: http://www.ncbi.nlm.nih.gov/pubmed/20603000

162. Cuiffo BG, Campagne A, Bell GW, Lembo A, Orso F, Lien EC, et al. MSC-regulated microRNAs converge on the transcription factor FOXP2 and promote breast cancer metastasis. Cell Stem Cell [Internet]. 2014 [cited 2017 Dec 12];15:762–74. Available from: http://linkinghub.elsevier.com/retrieve/pii/S1934590914004524

163. Kasinski AL, Kelnar K, Stahlhut C, Orellana E, Zhao J, Shimer E, et al. A combinatorial microRNA therapeutics approach to suppressing non-small cell lung cancer. Oncogene [Internet]. 2015 [cited 2017 Dec 12];34:3547–55. Available from: http://www.nature.com/doifinder/10.1038/onc.2014.282

164. Swart GWM, Lunter PC, Kilsdonk JWJ van, Kempen LCLT van. Activated leukocyte cell adhesion molecule (ALCAM/CD166): signaling at the divide of melanoma cell clustering

and cell migration? Cancer Metastasis Rev [Internet]. 2005 [cited 2017 Dec 12];24:223–36. Available from: http://link.springer.com/10.1007/s10555-005-1573-0

165. Valastyan S, Benaich N, Chang A, Reinhardt F, Weinberg RA. Concomitant suppression of three target genes can explain the impact of a microRNA on metastasis. Genes Dev [Internet]. 2009 [cited 2017 Dec 12];23:2592–7. Available from: http://www.ncbi.nlm.nih.gov/pubmed/19875476

166. Liu S, Goldstein RH, Scepansky EM, Rosenblatt M. Inhibition of rho-associated kinase signaling prevents breast cancer metastasis to human bone. Cancer Res [Internet]. 2009 [cited 2017 Dec 12];69:8742–51. Available from: http://cancerres.aacrjournals.org/cgi/doi/10.1158/0008-5472.CAN-09-1541

167. Lane J, Martin TA, Watkins G, Mansel RE, Jiang WG. The expression and prognostic value of ROCK I and ROCK II and their role in human breast cancer. Int J Oncol [Internet]. 2008 [cited 2017 Dec 12];33:585–93. Available from: http://www.ncbi.nlm.nih.gov/pubmed/18695890

168. Renner O, Blanco-Aparicio C, Grassow M, Cañamero M, Leal JFM, Carnero A. Activation of phosphatidylinositol 3-kinase by membrane localization of p110alpha predisposes mammary glands to neoplastic transformation. Cancer Res [Internet]. 2008 [cited 2017 Dec 12];68:9643–53. Available from: http://cancerres.aacrjournals.org/cgi/doi/10.1158/0008-5472.CAN-08-1539

169. Weidle UH, Eggle D, Klostermann S, Swart GWM. ALCAM/CD166: cancer-related issues. Cancer Genomics Proteomics [Internet]. [cited 2017 Dec 12];7:231–43. Available from: http://www.ncbi.nlm.nih.gov/pubmed/20952758

170. Masedunskas A, King JA, Tan F, Cochran R, Stevens T, Sviridov D, et al. Activated leukocyte cell adhesion molecule is a component of the endothelial junction involved in transendothelial monocyte migration. FEBS Lett [Internet]. 2006 [cited 2017 Dec 12];580:2637–45. Available from: http://doi.wiley.com/10.1016/j.febslet.2006.04.013

171. van Kilsdonk JWJ, Wilting RH, Bergers M, van Muijen GNP, Schalkwijk J, van Kempen LCLT, et al. Attenuation of melanoma invasion by a secreted variant of activated leukocyte cell adhesion molecule. Cancer Res [Internet]. 2008 [cited 2017 Dec 12];68:3671–9. Available from: http://cancerres.aacrjournals.org/cgi/doi/10.1158/0008-5472.CAN-07-5767

172. Kuphal S, Bauer R, Bosserhoff A-K. Integrin signaling in malignant melanoma. Cancer Metastasis Rev [Internet]. 2005 [cited 2017 Dec 12];24:195–222. Available from: http://www.ncbi.nlm.nih.gov/pubmed/15986132

173. Mierke CT, Frey B, Fellner M, Herrmann M, Fabry B. Integrin α5β1 facilitates cancer cell invasion through enhanced contractile forces. J Cell Sci [Internet]. 2011 [cited 2017 Dec 12];124:369–83. Available from: http://jcs.biologists.org/cgi/doi/10.1242/jcs.071985

174. Sawada K, Mitra AK, Radjabi AR, Bhaskar V, Kistner EO, Tretiakova M, et al. Loss of E-cadherin promotes ovarian cancer metastasis via alpha 5-integrin, which is a therapeutic target. Cancer Res [Internet]. 2008 [cited 2017 Dec 12];68:2329–39. Available from: http://cancerres.aacrjournals.org/cgi/doi/10.1158/0008-5472.CAN-07-5167

175. McKenzie JA, Liu T, Goodson AG, Grossman D. Survivin enhances motility of melanoma cells by supporting Akt activation and {alpha}5 integrin upregulation. Cancer Res [Internet]. 2010 [cited 2017 Dec 12];70:7927–37. Available from:

http://cancerres.aacrjournals.org/cgi/doi/10.1158/0008-5472.CAN-10-0194

176. McKenzie JA, Liu T, Jung JY, Jones BB, Ekiz HA, Welm AL, et al. Survivin promotion of melanoma metastasis requires upregulation of α5 integrin. Carcinogenesis [Internet]. 2013 [cited 2017 Dec 12];34:2137–44. Available from: https://academic.oup.com/carcin/article-lookup/doi/10.1093/carcin/bgt155

177. Mitra AK, Sawada K, Tiwari P, Mui K, Gwin K, Lengyel E. Ligand-independent activation of c-Met by fibronectin and α(5)β(1)-integrin regulates ovarian cancer invasion and metastasis. Oncogene [Internet]. 2011 [cited 2017 Dec 12];30:1566–76. Available from: http://www.nature.com/doifinder/10.1038/onc.2010.532

178. Arpaia E, Blaser H, Quintela-Fandino M, Duncan G, Leong HS, Ablack A, et al. The interaction between caveolin-1 and Rho-GTPases promotes metastasis by controlling the expression of alpha5-integrin and the activation of Src, Ras and Erk. Oncogene [Internet]. 2012 [cited 2017 Dec 12];31:884–96. Available from: http://www.nature.com/doifinder/10.1038/onc.2011.288

179. Esposito CL, Cerchia L, Catuogno S, De Vita G, Dassie JP, Santamaria G, et al. Multifunctional Aptamer-miRNA Conjugates for Targeted Cancer Therapy. Mol Ther [Internet]. 2014 [cited 2017 Dec 12];22:1151–63. Available from: http://linkinghub.elsevier.com/retrieve/pii/S1525001616307031

180. Iaboni M, Russo V, Fontanella R, Roscigno G, Fiore D, Donnarumma E, et al. Aptamer-miRNA-212 Conjugate Sensitizes NSCLC Cells to TRAIL. Mol Ther - Nucleic Acids [Internet]. 2016 [cited 2017 Dec 12];5:e289. Available from: http://www.ncbi.nlm.nih.gov/pubmed/27111415

181. Amarzguioui M, Lundberg P, Cantin E, Hagstrom J, Behlke MA, Rossi JJ. Rational design and in vitro and in vivo delivery of Dicer substrate siRNA. Nat Protoc [Internet]. Nature Publishing Group; 2006 [cited 2018 Jan 22];1:508–17. Available from: http://www.nature.com/doifinder/10.1038/nprot.2006.72

182. Orso F, Quirico L, Virga F, Penna E, Dettori D, Cimino D, et al. miR-214 and miR-148b Targeting Inhibits Dissemination of Melanoma and Breast Cancer. Cancer Res [Internet]. 2016 [cited 2017 Dec 12];76:5151–62. Available from: http://cancerres.aacrjournals.org/cgi/doi/10.1158/0008-5472.CAN-15-1322

183. Boyer DS, Goldbaum M, Leys AM, Starita C, V.I.S.I.O.N. Study Group. Effect of pegaptanib sodium 0.3 mg intravitreal injections (Macugen) in intraocular pressure: posthoc analysis from V.I.S.I.O.N. study. Br J Ophthalmol [Internet]. 2014 [cited 2017 Dec 12];98:1543–6. Available from: http://bjo.bmj.com/lookup/doi/10.1136/bjophthalmol-2013-304075

184. Reyes-Reyes EM, Teng Y, Bates PJ. A new paradigm for aptamer therapeutic AS1411 action: uptake by macropinocytosis and its stimulation by a nucleolin-dependent mechanism. Cancer Res [Internet]. 2010 [cited 2017 Dec 12];70:8617–29. Available from: http://cancerres.aacrjournals.org/cgi/doi/10.1158/0008-5472.CAN-10-0920

185. Bates PJ, Laber DA, Miller DM, Thomas SD, Trent JO. Discovery and development of the G-rich oligonucleotide AS1411 as a novel treatment for cancer. Exp Mol Pathol [Internet]. 2009 [cited 2017 Dec 12];86:151–64. Available from: http://linkinghub.elsevier.com/retrieve/pii/S0014480009000069

186. Waldschmidt JM, Simon A, Wider D, Müller SJ, Follo M, Ihorst G, et al. CXCL12 and CXCR7 are relevant targets to reverse cell adhesion-mediated drug resistance in multiple myeloma. Br J Haematol [Internet]. 2017 [cited 2018 Jan 19];179:36–49. Available from: http://www.ncbi.nlm.nih.gov/pubmed/28670693

187. Esposito CL, Cerchia L, Catuogno S, De Vita G, Dassie JP, Santamaria G, et al. Multifunctional Aptamer-miRNA Conjugates for Targeted Cancer Therapy. Mol Ther [Internet]. 2014 [cited 2017 Dec 12];22:1151–63. Available from: http://www.ncbi.nlm.nih.gov/pubmed/24441398

188. Zhou J, Li H, Li S, Zaia J, Rossi JJ. Novel dual inhibitory function aptamer-siRNA delivery system for HIV-1 therapy. Mol Ther [Internet]. 2008 [cited 2017 Dec 12];16:1481–9. Available from: http://linkinghub.elsevier.com/retrieve/pii/S1525001616322845

189. Wargalla UC, Reisfeld RA. Rate of internalization of an immunotoxin correlates with cytotoxic activity against human tumor cells. Proc Natl Acad Sci U S A [Internet]. 1989 [cited 2017 Dec 12];86:5146–50. Available from: http://www.ncbi.nlm.nih.gov/pubmed/2544891

190. Ritchie M, Tchistiakova L, Scott N. Implications of receptor-mediated endocytosis and intracellular trafficking dynamics in the development of antibody drug conjugates. MAbs [Internet]. 2013 [cited 2017 Dec 12];5:13–21. Available from: http://www.tandfonline.com/doi/abs/10.4161/mabs.22854

191. Wahba HA, El-Hadaad HA. Current approaches in treatment of triple-negative breast cancer. Cancer Biol Med [Internet]. 2015 [cited 2017 Dec 12];12:106–16. Available from: http://www.ncbi.nlm.nih.gov/pubmed/26175926

192. Benedetto G, Hamp TJ, Wesselman PJ, Richardson C. Identification of epithelial ovarian tumor-specific aptamers. Nucleic Acid Ther [Internet]. Mary Ann Liebert, Inc.; 2015 [cited 2018 Jan 20];25:162–72. Available from: http://www.ncbi.nlm.nih.gov/pubmed/25894736

193. CHEN X, BO L, LU W, ZHOU G, CHEN Q. MicroRNA-148b targets Rho-associated protein kinase 1 to inhibit cell proliferation, migration and invasion in hepatocellular carcinoma. Mol Med Rep [Internet]. 2016 [cited 2018 Jan 20];13:477–82. Available from: http://www.ncbi.nlm.nih.gov/pubmed/26530325

194. Zhang J, Shi Y, Hong D, Song M, Huang D, Wang C, et al. MiR-148b suppresses cell proliferation and invasion in hepatocellular carcinoma by targeting WNT1/β-catenin pathway. Sci Rep [Internet]. 2015 [cited 2017 Dec 12];5:8087. Available from: http://www.nature.com/articles/srep08087

195. Nie F, Liu T, Zhong L, Yang X, Liu Y, Xia H, et al. MicroRNA-148b enhances proliferation and apoptosis in human renal cancer cells via directly targeting MAP3K9. Mol Med Rep [Internet]. 2016 [cited 2017 Dec 12];13:83–90. Available from: https://www.spandidos-publications.com/

196. Xiang D, Zheng C, Zhou S-F, Qiao S, Tran PH-L, Pu C, et al. Superior Performance of Aptamer in Tumor Penetration over Antibody: Implication of Aptamer-Based Theranostics in Solid Tumors. Theranostics [Internet]. 2015 [cited 2017 Dec 13];5:1083–97. Available from: http://www.ncbi.nlm.nih.gov/pubmed/26199647

197. Kreso A, Dick JE. Evolution of the cancer stem cell model. Cell Stem Cell [Internet]. Elsevier; 2014 [cited 2017 Dec 13];14:275–91. Available from:

http://www.ncbi.nlm.nih.gov/pubmed/24607403

198. Liu Q, Xu Y, Wei S, Gao W, Chen L, Zhou T, et al. miRNA-148b suppresses hepatic cancer stem cell by targeting neuropilin-1. Biosci Rep [Internet]. Portland Press Ltd; 2015 [cited 2017 Dec 13];35. Available from: http://www.ncbi.nlm.nih.gov/pubmed/25997710

199. Mou Z, Xu X, Dong M, Xu J. MicroRNA-148b Acts as a Tumor Suppressor in Cervical Cancer by Inducing G1/S-Phase Cell Cycle Arrest and Apoptosis in a Caspase-3-Dependent Manner. Med Sci Monit [Internet]. 2016 [cited 2017 Dec 12];22:2809–15. Available from: http://www.ncbi.nlm.nih.gov/pubmed/27505047

200. He W, Huang L, Li M, Yang Y, Chen Z, Shen X. MiR-148b, MiR-152/ALCAM Axis Regulates the Proliferation and Invasion of Pituitary Adenomas Cells. Cell Physiol Biochem [Internet]. 2017 [cited 2017 Dec 12];44:792–803. Available from: https://www.karger.com/Article/FullText/485342

201. Kang S-A, Hasan N, Mann AP, Zheng W, Zhao L, Morris L, et al. Blocking the Adhesion Cascade at the Premetastatic Niche for Prevention of Breast Cancer Metastasis. Mol Ther [Internet]. 2015 [cited 2018 Jan 20];23:1044–54. Available from: http://www.ncbi.nlm.nih.gov/pubmed/25815697

202. Tucker CE, Chen LS, Judkins MB, Farmer JA, Gill SC, Drolet DW. Detection and plasma pharmacokinetics of an anti-vascular endothelial growth factor oligonucleotide-aptamer (NX1838) in rhesus monkeys. J Chromatogr B Biomed Sci Appl [Internet]. 1999 [cited 2017 Dec 12];732:203–12. Available from: http://www.ncbi.nlm.nih.gov/pubmed/10517237

203. Catuogno S, Rienzo A, Di Vito A, Esposito CL, de Franciscis V. Selective delivery of therapeutic single strand antimiRs by aptamer-based conjugates. J Control Release [Internet]. 2015 [cited 2017 Dec 12];210:147–59. Available from: http://www.ncbi.nlm.nih.gov/pubmed/25998051

204. Agrawal S, Joshi M, Christoforidis JB. Vitreous Inflammation Associated with Intravitreal Anti-VEGF Pharmacotherapy. Mediators Inflamm [Internet]. 2013 [cited 2017 Dec 12];2013:1–6. Available from: http://www.ncbi.nlm.nih.gov/pubmed/24307762

205. Ghasemi Falavarjani K, Nguyen QD. Adverse events and complications associated with intravitreal injection of anti-VEGF agents: a review of literature. Eye [Internet]. 2013 [cited 2017 Dec 12];27:787–94. Available from: http://www.ncbi.nlm.nih.gov/pubmed/23722722

206. Henry SP, Giclas PC, Leeds J, Pangburn M, Auletta C, Levin AA, et al. Activation of the alternative pathway of complement by a phosphorothioate oligonucleotide: potential mechanism of action. J Pharmacol Exp Ther [Internet]. 1997 [cited 2017 Dec 12];281:810–6. Available from: http://www.ncbi.nlm.nih.gov/pubmed/9152389

207. Swayze EE, Siwkowski AM, Wancewicz E V, Migawa MT, Wyrzykiewicz TK, Hung G, et al. Antisense oligonucleotides containing locked nucleic acid improve potency but cause significant hepatotoxicity in animals. Nucleic Acids Res [Internet]. 2007 [cited 2017 Dec 12];35:687–700. Available from: https://academic.oup.com/nar/article-lookup/doi/10.1093/nar/gkl1071

208. Behlke MA. Chemical Modification of siRNAs for *In Vivo* Use. Oligonucleotides [Internet]. 2008 [cited 2017 Dec 12];18:305–20. Available from: http://www.ncbi.nlm.nih.gov/pubmed/19025401

209. Zhang R, Sun X, Niu B. The importance of pegaptanib sodium treatment for patients with vascular active vitreoretinopathy. Exp Ther Med [Internet]. 2017 [cited 2018 Jan 19];14:6002–6. Available from: http://www.ncbi.nlm.nih.gov/pubmed/29285149